ISTANBUL TECHNICAL UNIVERSITY ★ GRADUATE SCHOOL OF SCIENCE ENGINEERING AND TECHNOLOGY

SET-UP OF A 2-COLOR PYROMETER AND DESIGN OF A RADIATIVE CALIBRATION CELL

M.Sc. THESIS

Kaan ERDEM

Department of Mechanical Engineering

Heat-Fluid Programme

JULY 2012

ISTANBUL TECHNICAL UNIVERSITY ★ GRADUATE SCHOOL OF SCIENCE ENGINEERING AND TECHNOLOGY

SET-UP OF A 2-COLOR PYROMETER AND DESIGN OF A RADIATIVE CALIBRATION CELL

M.Sc. THESIS

Kaan ERDEM
(503101112)

Department of Mechanical Engineering

Heat-Fluid Programme

Thesis Advisor: Prof. Dr. Abdurrahman KILIÇ

JULY 2012

İSTANBUL TEKNİK ÜNİVERSİTESİ ★ FEN BİLİMLERİ ENSTİTÜSÜ

2 RENKLİ PİROMETRE KURULUMU VE IŞINIMSAL KALİBRASYON HÜCRESİ TASARIMI

YÜKSEK LİSANS TEZİ

Kaan ERDEM
(503101112)

Makine Mühendisliği Anabilim Dalı

Isı-Akışkan Programı

Tez Danışmanı: Prof. Dr. Abdurrahman KILIÇ

TEMMUZ 2012

Kaan Erdem, a **M.Sc.** student of ITU **Graduate School of. Science, Engineering and Technology** student ID **503101112**, successfully defended the **thesis** entitled "Set-up of a 2-color pyrometer and design of a radiative calibration cell", which he prepared after fulfilling the requirements specified in the associated legislations, before the jury whose signatures are below.

Thesis Advisor :	**Prof. Dr. Abdurrahman KILIÇ** Istanbul Technical University	.....
Jury Members :	**Prof. Dr. Abdurrahman KILIÇ** Istanbul Technical University	.....
	Prof. Dr. A. Feridun ÖZGÜÇ Istanbul Technical University	.....
	Yrd. Doç. Dr. Sevilay HACIYAKUPOĞLU Istanbul Technical University	.....

Date of Submission : 14 June 2012
Date of Defense : 30 July 2012

To my grandmother,

FOREWORD

I have been in Technical University of Munich for eight months via an exchange program. I had the opportunity to conclude my master thesis. I enjoyed every moment I spent there.

First of all, I would like to thank my supervisor, *Prof. Dr. Abdurrahman Kılıç* for letting me take this great chance. I am also very grateful to *M.Sc. Federico Botteghi* for patience and supervision along the whole process, and *Dipl. Ing. Gundula Balan* for all the help and consideration during experiments.

Finally, I could not accomplish to finish my master degree without support of my family and friends, whom I am lucky to have.

July 2012 Kaan ERDEM

TABLE OF CONTENTS

Page

ABBREVIATIONS

DC	:Direct Current
FOV	:Field of View
HNA	:Half Noise Amplitude
IR	:Infrared
ITS	:International Temperature Scale
NIST	:National Institute of Standards and Technology
NPL	:National Physical Laboratory
PC	:Personal Computer
PDP	:Particle Discrimination Procedure
Std. Dev.	:Standard Deviation
TUM	:Technical University of Munich
US	:United States
WMR	:Wire Mesh Reactor

LIST OF TABLES

Page

LIST OF FIGURES

Page

SET-UP OF A 2-COLOR PYROMETER AND DESIGN OF A RADIATIVE CALIBRATION CELL

SUMMARY

The 2-color pyrometer is an optical measurement instrument which enables non-contact temperature detection using the ratio of monochromatic radiation signals from the object at two different wavelengths determined as visible and infrared. A built in-house instrument has been set up to obtain the surface temperature of the individual fuel particles and then calculate the pyrometric diameter (fixed emissivity, perfect spheres). The emitted radiation from the surface of reacting fuel particle is collected and filtered by an optic system (lenses, optic fibers and bandpass filters). The radiation is then detected and quantified using silicon photodiodes in main and reference channels. The electric signals are eventually amplified and sent to a computer for evaluation and post-processing after getting converted into digital form. By running iterative routines, one can determine the surface temperature of a particle with respect to calibration results obtained in advance. Then the size of a particle can be computed based on the measured surface temperature with spherical particle assumption. Thus, calibration of the instrument is required. The pyrometer was calibrated against a black body radiator and calibration curve were extrapolated for higher temperature levels (>1200°C). To increase the level of precision at elevated temperature levels, a self-design method enforcing electrical heating of a thin tungsten sheet in Argon purge was developed. As the results were not satisfying enough to acceps as valid calibration, extrapolation curves have been hence chosen to perform the measurement campaign in an entrained flow combustion reactor with various combustion conditions such as air-fuel ratio, optical port level, filter cleaning, sulfur and Kaolin addition into Caliro type straw. The instrument has been successfully tested during this campaign delivering precious information about the reacting particles and combustion kinetics being able to provide additional information about the status of the reactor (e.g. non-constant mass feeding) served the purpose of checking the applicability of the pyrometer. Aim of this work was, further to the calibration, to test and prove the reliability of the instrument and the reproducibility of the results.

2 RENKLİ PİROMETRE KURULUMU VE IŞINIMSAL KALİBRASYON HÜCRESİ TASARIMI

ÖZET

2 renkli pirometre, temassız sıcaklık tespitinde kullanılan, radyasyon, optik yasalarına ve cisimlerin yayınırlık katsayılarına dayanan optik bir ölçüm cihazı olup hedef objenin yüzeyinden iki farklı dalga boyunda ölçülen monokromatik ışınım sinyallerinin oranı yardımı ile sıcaklık ölçümü gerçekleştirilmesi temeline dayanır. Gazlaştırma ve yanma işlemlerinde pirometre kullanımı, hareket halinde küçük objeleri ölçebilme kabiliyetinden ötürü oldukça yaygındır. Hareket halinde veya durgun katı yakıt parçacıklarının tek tek yüzey sıcaklıklarının ölçülüp, pirometrik yarıçaplarının (sabit yayınırlık ve küresel şekil kabulü) hesaplanması amacıyla pirometre cihazının kurulumu gerçekleştirilmiştir.

Reaksiyon halindeki katı yakıt parçacığının yüzeyinden neşredilen ışınım, bir optik düzenek (lensler, optik fiber, ve filtreler) yardımı ile algılanıp filtrelenir. Dürbün prensibi ile çalışan bir optik prob aracılığı ile sinyal optik probun öbür ucuna sabitlenen optik fiber girişine odaklanır. Daha sonra optik fiber, ana ve referans olmak üzere iki kanala ayrılır. Referans kanalında sinyal, lensler yardımı ile kızılötesi dalgaboyunda çalışan foto algılayıcıya iletilir. Ana kanala ulaşan sinyalin ise bir kısmı görünen (kırmızı) dalgaboyunu hissetme yetisi olan foto algılayıcıya yansıtılırken sinyalin geri kalanı yine kızılötesi bir foto algılayıcıya yansıtılmadan iletilir. Foto algılayıcılara varmadan sinyaller filtre elemanları ile belli ve dar dalgaboylarında filtrelenir. Filtreleme sonrasında ışınım değerleri silikon foto algılayıcılarda algılanır ve elektrik sinyalleri üretilir. Bu elektrik sinyalleri çok küçük büyüklüklerde olduklarından, üretilen bu elektrik sinyalleri ölçüm kolaylığı için kuvvetlendirilir. Kuvvetlendirilen bu sinyaller analog formdan, dijital formda çevrilerek bilgisayara aktarılır. Bilgisayarda ise ölçümler Lab-view 9.0 programında geliştirilen yazılım yardımı ile sonuçlar kayıt edilir ve elde edilen veriler amaca yönelik olarak işlenir.

Kurulumu tamamlandıktan sonra, uygulamaya konmadan önce pirometre cihazının kalibre edilmesi gerekmektedir. Bu sebepten pirometre cihazı siyah cisim ısı kaynağına karşı 800-1200°C arasında kalibre edilmiştir. Bu işlem 50°C artmak koşuluyla her sıcaklıkta beşer kere tekrarlanıp, kabul edilir küçüklükte sapmalarla elde edilen ortalama veriler sıcaklık tespitinde kullanılmıştır. Siyah cisim ısı kaynağı limitli sıcaklıklarda referans değerler sağladığından 1200°C üstü sıcaklıklar için kalibrasyon eğrisi Wien yasası kullanılarak ekstrapole edilmiştir. Yüksek sıcaklıklarda daha kesin veriler elde etmek adına ticari metodlar incelenmiştir. Bu tip uygulamalarda en sık kullanılan, önceden kalibre edilmiş tungsten filament lambasının üretimi durduruluğu için yeni bir yöntem geliştirme yoluna gidilmiştir.

Siyah cisim kapasitesinin yetmediği yüksek sıcaklarda daha doğru sonuçlar almak adına ince bir tungsten levhanın elektriksel ısıtılmasına dayalı yeni bir yöntem geliştirilmiştir. Bu yöntemde enstitü dahilinde mevcut ve kullanıma hazır olan kapalı bir elektrot sisteminden yararlanılmıştır. Elektrotlar arasına yerleştirilen ince tungsten levha elektrik ile ısıtılıp yüzeyinin yüksek sıcaklıklara çıkması sağlanmıştır. İstenmeyen reaksiyonların önüne geçmek için sistem, deneyler esnasında bir inert gaz olan Argon gazı ile doldurulmuştur. Bir diğer yandan da C tipi termokapıl ile levhanın alt tarafından yüzey sıcaklığına bağlı olarak voltaj değerleri okunup, okunan

bu değerlerin sıcaklık olarak karşılıkları C tipi termokapıla ait referans tablosundan elde edilmiştir. Sinyal iletim kayıplarını önlemek için de kompensazyon kablosu kullanılmıştır.

Yeni geliştirilen bu yöntemin sonuçları ile siyah cisim kalibrasyon çizgileri aynı trende sahip olmalarına rağmen birbirleri ile yeterli tutarlık göstermemiştir. Bu duruma sebep olarak görüş açısı, yayınırlık katsayısı gibi faktörlerin yanında Argon gazının yarattığı soğutma etkisi ve en önemli olarak eski ve zayıf thermokapıl bağlantıları düşünülmüştür. Ayrıca uzun deney zamanlarında tungsten buharlaşması meydana gelmiştir. Bu durum levhanın kesitinin daralmasına ve aynı koşullarda farklı sonuçlar alınmasına yol açmıştır. Bu problem tungsten levhanın belirli zaman aralıklarında değiştirilmesi ile ortadan kaldırılabilmiştir. Zaman kısıtlaması olduğundan siyah cisim kalibrasyonundan ve Wien yasası ile yürütülen ektrapolasyondan elde edilen değerler ile deneyler gerçekleştirerek cihazın uygulanabilirliği, verdiği sonuçların güvenilirliği ve tutarlılığının test edilmesi amaçlanmıştır. Yeni geliştirilen metod hala geçerli bir yöntemdir. Gerekli iyileştirmeler yapılarak yöntemin daha da geliştirilmesi ve yüksek sıcaklıklarda kalibrasyon uygulamalarında kullanılması mümkündür.

Deneyler enstitüye ait sürüklemeli akış yanma reaktöründe gerçekleştirilmiştir. Set sıcaklığı her zaman 1100°C olarak ayarlanmış olup yakıt olarak Caliro tipi saman taneleri kullanılmıştır. Reaktör üzerinde mevcut özel gözlem pencerelerinden pirometre ile yanmakta olan taneler izlenmiştir. Pirometrenin, taneleri rahatlıkla tanıyabilmesi için reaktör penceresinin karşının soğuk arka plan olmasına dikkat edilmiştir. Gözlenen ve yanan katı yakıt tanelerinden alınan sinyaller bilgisayar programında değerlendirilmiştir. Alınan sinyal değerleri yardımı ile, önceden elde edilen kalibrasyon eğrileri üzerinde iteratif yöntemler uygulayarak katı yakıt tanelerinin yüzey sıcaklıkları ölçülmüş, daha sonra bu ölçülen yüzey sıcaklıkları uygun denklemlerde yerine konarak tam küresel çaplı tanecik ve sabit yayınırlık kabulu ile tanelerin pirometrik boyutları hesaplanmıştır. Her foto algılayıcıya ait sinyal grafiklerinde, yanmakta olan tanenin gözlenmesi anında meydana gelen tepe noktaların zaman düzleminde yerlerini temel alan kriterler yardımı ile hatalı ölçümlerin olabildiğince aza indirgenmesi hedeflenmiştir.

Pirometre cihazı ile hava/yakıt oranı, gözlem penceresi yüksekliği, reaktör filtresinin temizliği, katı yakıta sülfür ve Kaolin ilavesi gibi etkenlerin, tanelerin yüzey sıcaklıkları ve pirometrik çapları üzerindeki etkileri incelenmiştir. Hava yakıt oranı, reaktörün optimum değerine yaklaştıkça tanelerin ortalama sıcaklık dağılımında artış görünürken ortalama pirometrik çap değerleri azalmakta ve bu durum yanma işleminin iyileştiğini göstermektedir. Ayrıca farklı tarihlerde ama aynı koşullarda yapılan deney sonuçları pirometre cihazının tutarlı ve tekrarlanabilir sonuçlar sağladığını kanıtlamıştır. Gözlem penceresinin yüksekliğinin değiştirilmesi yanma işleminin farklı aşamaları hakkında fikir verirken, reaktör filtresinin temizlenmesi ile tespit edilen yanan tane sayısında artış meydana gelmiştir. Katı saman yakıtına sülfür eklenmesi önemli değişiklere yol açmazken, Kaolin ilavesi sonucu tespit edilen tanecik sayısı iki katına çıkmış, ortalama pirometrik çap büyük ölçüde azalmış ve ortalama yüzey sıcaklığı artmıştır. Bu durum pirometrenin Kaolin tanelerini de saman tanesi olarak tespit etmesi ile açıklanabilmektedir. Yapılan deneyler pirometre cihazının uygulanabilir olduğunu göstermiş ve ayrıca reaktör çalışma koşullarının daha uygun biçimde düzenlenmesine de fayda sağlamıştır.

Bu proje, bazı ek çalışmalarla desteklenebilir ve geliştirilebilir. Yanma sonu gazları ve yanma öncesi saman taneciklerinin laboratuvar analizleri, sonuçların değerlendirilmesi büyük fayda sağlayacaktır. Ayrıca analog-dijital dönüştürücünün 1500-1600°C üstünde doyuma ulaşması daha yüksek sıcaklıklarda ölçüm yapılmasını mümkün kılamamaktadır. Bu sorun, foto algılayıcıların öncül sinyal büyütme oranları küçültülerek giderilebilir. Bu durumda kalibrasyon işlemi en baştan tekrarlanmalıdır. Yeni geliştirilen kalibrasyon metodu daha iyi sistem elemanları kullanılarak yüksek sıcaklıklarda güvenilir ve net veriler sağlayabilir. Pirometre, uzun deney saatleri sonucunda ısınmakta ve bu da foto algılayıcıların hassasiyetini etkileyip yanlış sonuçlar elde edilmesine yol açmaktadır. Bu etki de bir fan soğutma sistemi ilavesi ile kolaylıkla giderilebilir.

Sonuç olarak pirometre kurulumu yapılmış ve siyah cisim ısı kaynağında kalibrasyonu gerçekleştirilmiştir. Daha sonra yüksek sıcaklıklarda, elde edilmiş olan kalibrasyon değerleri ekstrapole edilmiştir. Kalibre edilmiş pirometre başarılı bir şekilde uygulamaya konarak ölçümler alınmış ve bu ölçümler sonucu yanma işlemi hakkında değerli sonuçlar elde edilmiştir. Biyokütle yakıtlarının yanma kinetikleri hakkında aydınlatıcı veriler sağlamıştır. Ayrıca reaktör çalışması hakkında yardımcı bilgi sağlanarak (örn. düzensiz yakıt besleme) cihazın uygulanabilirliği kontrol edilmiştir. Bu projenin genel amacı pirometre kalibrasyonuna ek olarak cihazın güvenilirliğinin ve ölçüm sonuçlarının tekrar gerçekleştirilebilirliğinin test edilmesi olmuştur.

1. INTRODUCTION

Temperature is one of the most common measured physical quantities in many fields such as engineering, medicine and astronomy since ages. In most of the industrial application it is required to control over process temperature. In order to manage control over temperature, many methods were tried so far. First, temperature was distinguished as cold or hot relating to human body fever. Then glow of metal surfaces were taken into account to determine temperature level. The temperature metering trials started with Galileo's air thermometer which was based upon expansion of air by heating. With time, air was substituted by materials with higher density and wider detectable temperature range. The thermometers were needed to be calibrated for sake of applicability. Following that, the Celsius temperature scale was developed by using the boiling and freezing point of water. Precision in the temperature measurement field became greater and greater with the invention of new temperature scales, devising thermocouple, thermistors and resistance thermometers, discovering radiation laws and using them to measure the temperatures. After 20th century, fiber-optic temperature sensors were developed. As a result of all these developments, updated standards in this area were collected together in the newest version of International Temperature Scale (ITS-90), which has been established to harmonize the world wide practical temperature measurement.

The concept of temperature, underlies energy calculations, expresses the kinetic energy of the vibrating atoms and molecules of matter. This energy can be measured by secondary phenomena, e.g., change of volume or pressure, electrical resistance, electromagnetic force, electron surface charge or emission of electromagnetic radiation [1]. Temperature plays an important role in both every day and scientific processes. Accurate temperature measurements can remarkably increase the value of effectiveness and quality of a product. Temperature detection methods can be classified into two groups; direct contact or non-contact. The direct contact method,

which is applied by the help of the thermocouple, has a low response-time. The heating rates are very high to heat small particles like coal, which results in conduction errors of thermocouple measurement [2]. Therefore, this method is not suitable to measure locally high temperature gradients. On the other hand, the non-contact method determines the temperature of a body by measuring the emitted radiation from the surface of an object. Every object with a temperature above absolute zero (-273.15 °C) emits radiation that transports energy used to determine the temperature of the object.

Radiation thermometry is a general concept, which depends on a lot of parameters, is based on Planck's law of thermal radiation. Radiation pyrometry has been successfully applied over a wide temperature range from 730 K up to 3200 K. With technical developments, it is possible today to measure temperatures under 0°C from a distance and without making contact with the object to be measured [19]. Also radiation thermometers do not come in contact with the object and it does not need thermal equilibrium. Hence, it can measure very rapidly distant objects or moving objects at very elevated temperatures. Furthermore, it does not interfere with the object temperature distribution [1, 3-4].

'Pyrometer' linguistically comes from the Greek words pyr means "fire" and metron means "measure". Pyrometry is the non-contact method which was originally used by blacksmiths and steel workers to accurately gauge the temperature of metals by observing the brightness and coloration while forging [5]. Pyrometry is the process of measurement by a pyrometer which is a device that intercepts and remotely measures thermal radiation of a surface. How the pyrometer basically works is that the emitted heat radiation from an object is received by an optical fiber and transmitted to the detector where radiation converted into electric signals. With convenient correlation between temperature and electric signals, the surface temperature of an object can be determined. There are three main types of optical pyrometer, which are commercially in use, monochromatic (one-color), two-color and multi-color (multi-wavelength) pyrometers. As the fuel particles are conveyed by a gas stream in entrained flow reactors, the pyrometry technique is the only practical

method to measure the surface temperature of reacting fuel particles in motion [1-2, 6-21].

Temperature measurement in gasification and combustion has a significant role to comprehend the kinetics of combustion and gasification. Due to these advantages mentioned above, pyrometry is now standard procedure in combustion, gasification, etc. and the method was studied several times in that area [1-2, 6-21]. As the radiation intensity from a surface depends on the emissivity, ratio pyrometers with at least two wavelengths are mostly applied to eliminate the emissivity issue during measurements. During thermal conversion of the coal particle, the temperature varies due to the surrounding gas by hundreds of Kelvin due to transient heating and chemical reactions. The surface temperature determines the combustion/gasification rate of the particles. Thus, knowing the surface temperature and size of individual burning fuel particles is important to understand chemical and physical processes. These parameters are required for studies over solid fuel conversion systems and kinetics. The temporal behavior of the temperature of combusting particles is significantly assistive to control the formation of combustion/gasification products and to enhance the thermal efficiency of the process [1]. Furthermore, the temperature influences the design and operation of reactors. For investigation of technical problems such as corrosion, slagging, etc., temperature is significant parameter. Hence knowing temperature can help to design durable reactors.

The main purpose of this study was to set-up a 2-color pyrometer with optical probe and to test its applicability and reliability in combustion and gasification researches. Hence it was aimed to calibrate the pyrometer for temperature range as wide as possible in order to measure the temperature of fuel particles from pyrometric signals accurately and calculate the pyrometric size individually by using relevant formulas. The tests of 2-color pyrometer were conducted at the entrained flow combustion reactor of the Institute for Energy Systems in TU München.

2. THEORY

Radiation can be evakated as a fluxing energy with the velocity of light in space. Radiation is not in a heat form. It can only be absorbed by an object and be converted into heat. The rest of radiation is also absorbed by other objects later. Materials emit radiation by means of temperature that they possess. This kind of radiation is called "Thermal radiation" and is evaluated under heat transfer subject. To understand thermal radiation phenomena precisely, following terms should be introduced first. Radiation can be partially or wholly reflected, absorbed or transmitted while coming across particles on its way. The ratio of reflected radiation over total radiation states reflectivity, "ρ". By following the same rule, absorptivity is denoted with "α" and transmissivity is denoted as "τ". Summation of ρ, α and τ always equals to one. The radiation at one wavelength is stated as monochromatic radiation. Net radiation is occurred by bunch of monochromatic radiation.

Wavelength can vary from zero to infinity. In heat transfer calculations, only electromagnetic spectrum is important. Electromagnetic radiation has a very large spectrum between 10^{-13}m (cosmic ray) and 1000m. It includes visible spectrum (0.38-0.78 μm). Infrared wavelength band is the spectrum which is mostly used in industrial applications.

Monochromatic energy that emitted from a radiative surface depends on the surface temperature and radiation wavelength. When the temperature is fixed, emissivity is a function of wavelength. Otherwise is also applicable.

The basic equations mentioned in the fundamental resources of heat and mass transfer are used in this section [22-23].

2.1 Thermal Radiation

The mechanism of emission is related to energy released as a result of oscillations or transitions of the electrons. These oscillations are sustained by the temperature of the matter. All forms of matter over 0K emit radiation. For gases and for semitransparent solids, emission is a volumetric phenomenon. In most liquids and solids, radiation is a surface phenomenon. For this case, radiation emerging throughout the surface is studied.

One theory states radiation as the propagation of a collection of particles termed photons and quanta (quantum mechanics). On the other hand, thermal radiation energy may be viewed as the consisting of electromagnetic waves (electromagnetic wave theory). Neither point of view is able to describe completely radiation phenomena. Radiative properties of liquids, solids and their interfaces are easily predicted using electromagnetic wave theory, while radiative properties of gases are obtained from quantum mechanics. In both ways, radiation can be attributed to the standard wave properties of frequency ν and wavelength, λ. The two properties are related by

$$\lambda = \frac{c}{\nu} \qquad \textbf{(2.1)}$$

Where c is the speed of light in the medium. In a vacuum, $c_0 = 2.998\,x\,10^8\ m/s$. The unit of wavelength is commonly the micrometer, μm. The unit of frequency is Hz.

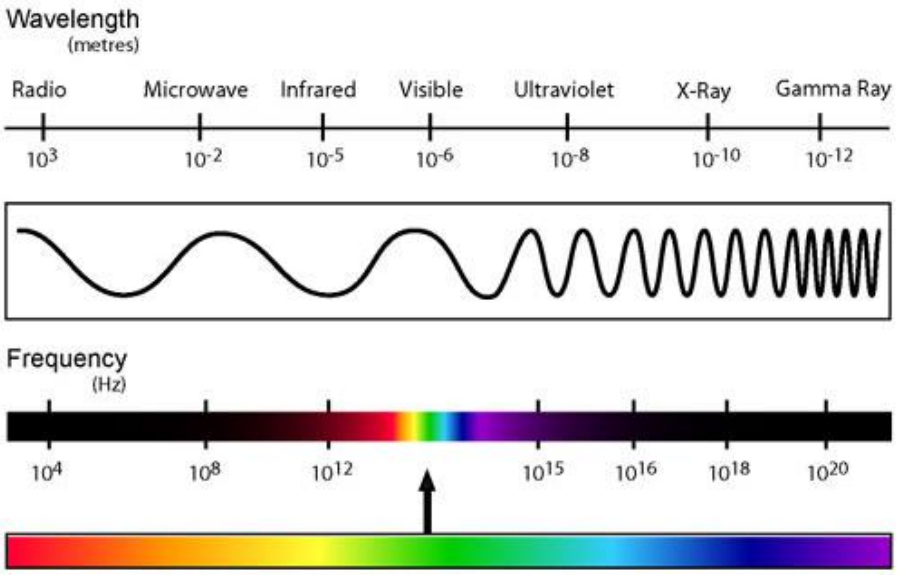

Figure 2.1 : Electromagnetic wave spectrum [24].

The complete electromagnetic spectrum is delineated in Fig.2.1. The short wavelength gamma rays, X rays and ultraviolet (UV) radiation are primarily utilized in the fields of study like high-energy physics and the nuclear energy applications, while the long wavelength microwaves and radio waves are subjects of the electrical engineering. It is the intermediate portion of the spectrum, which extends from approximately 0.1 to 100μm and includes a portion of the UV and all of the visible and infrared (IR), are termed thermal radiation applications such as pyrometry. The magnitude of the thermal radiation varies with wavelength, temperature and direction. The term spectral is used to refer to the dependence of wavelength. Directional distribution of radiation can affect the net radiative heat transfer rate and the concept of solid angle (Fig.2.2) is introduced at this point;

$$d\omega = \frac{dA_n}{r^2} \qquad \textbf{(2.2)}$$

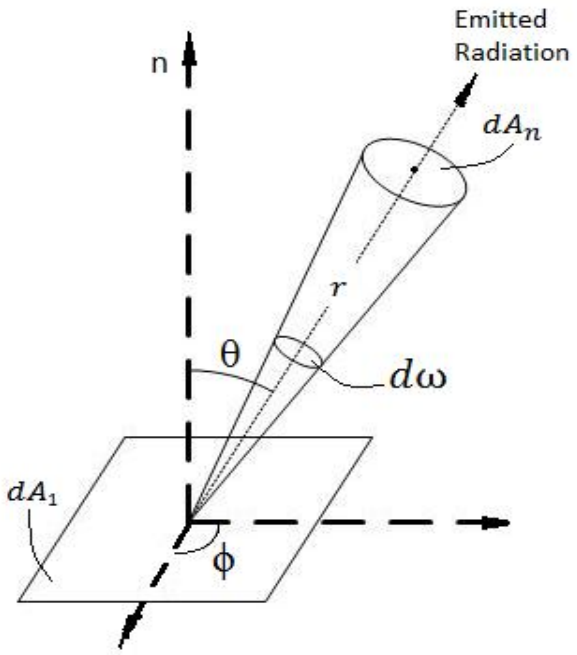

Figure 2.2 : Emission of a radiation from a differential area dA_1 into a solid angle dω corresponded by dA_n at a point on dA_1.

The unit of solid angle is the steradian (sr), analogous to radians for plane angles.

2.2 Black Body Radiation

Black body absorbs all incident radiation regardless of wavelength and direction; however, it emits radiation as a function of wavelength and temperature. Black body surface radiates more energy than any other surface at same temperature without any reflection or transmissivity. Thus, black body absorbs all incidents of light and reflects none of incoming and outgoing electromagnetic waves, is recognized as a standard to compare the emission from real surfaces. Although there is no surface precisely exhibits blackbody behavior, the closest approximation is achieved by a cavity with an inner surface at constant temperature. The spectral radiance of a blackbody is denoted as $I_{\lambda,b}$ with unit of $W/m^2.\mu m.sr$.

2.2.1 Planck's distribution law

Max Planck first has determined the frequency spectrum of black body radiation in a cavity in 1900 [10]. Planck has deduced the analytic formula for the density and

spectral distribution of the radiant energy and developed the law, called Planck's Radiation Law;

$$I_{\lambda,b}(T) = \frac{2hc_0{}^2}{\lambda^5\left[\exp\left(\frac{hc_0}{\lambda k_B T}\right)-1\right]} \quad \textbf{(2.3)}$$

where

λ is the wavelength[μm],

T is the absolute temperature of the blackbody [T],

I is the spectral radiance [W/m^2.μm.sr],

h is the Planck constant = 6.624 x 10^{-34} [J.s],

c_0 is the speed of light = 2.9978 x 10^8 [m/s],

k_B is the Boltzmann constant = 1.3805 x 10^{-23} [J/K],

Spectral emissive power is, $E_{\lambda,b}$;

$$E_{\lambda,b}(\lambda,T) = \pi . I_{\lambda,b}(\lambda,T) = \frac{C_1}{\lambda^5[\exp(C_2/\lambda T)-1]} \quad \textbf{(2.4)}$$

where

$E_{\lambda,b}$ is the spectral emissive power of a blackbody [W/m^2. μm],

C_1 is constant = 3.742 x 10^8 [W. μm^4/m^2],

C_2 is constant = 1.439 x 10^4 [μm. K],

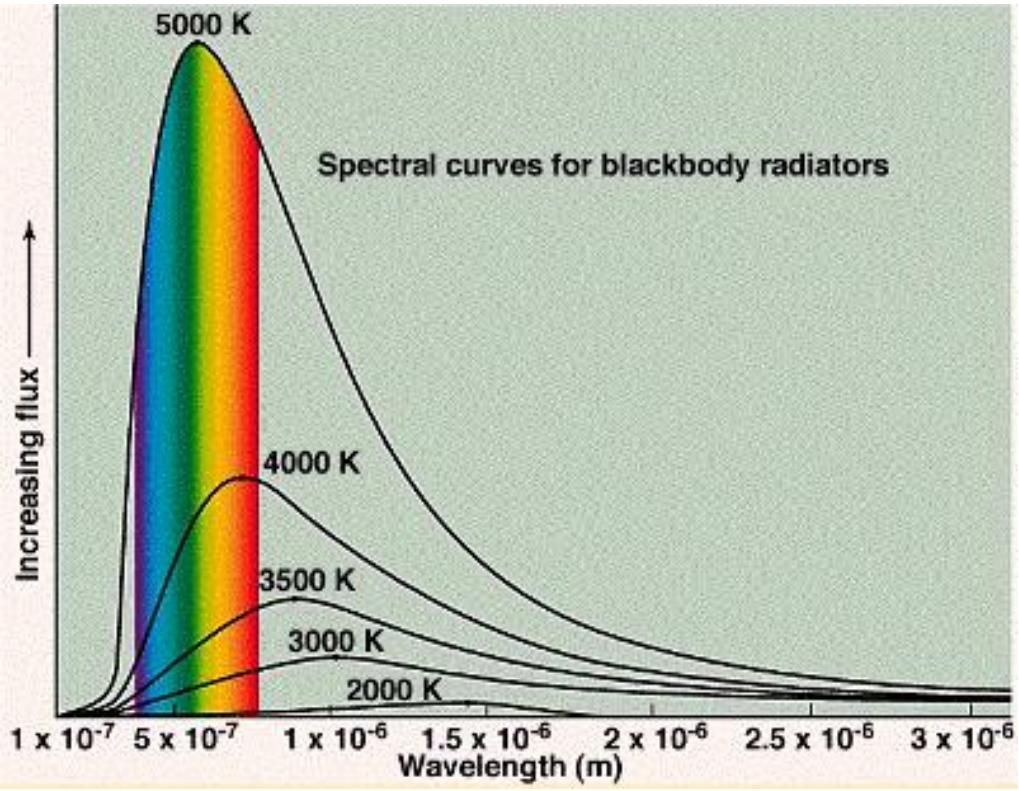

Figure 2.3 : Spectral blackbody emissive power [25].

2.2.2 The Stefan-Boltzman law

The Stefan-Boltzman law is deduced by integrating the eq.2.5 over the all spectrum:

$$E_b(T) = \int_0^\infty E_{\lambda,b}(\lambda, T)\, d\lambda \qquad \textbf{(2.5)}$$

E_b [W/m^2] expresses the total emissive power of a blackbody. After performing the integration, eq.2.6 may be shown as:

$$E_b(T) = \sigma . T^4 \qquad \textbf{(2.6)}$$

where σ is the Stefan-Boltzmann constant, is a product of C_1 and C_2 constants. ($\sigma = 5.67x10^{-8} W/m^2K^4$)

2.2.3 Wien's displacement law

According to Wien's displacement law, the wavelength at the peak point of intensity that is emitted gets shorter while the temperature is increasing. When the maximum radiation energy is evaluated by the Planck's radiation law, the multiplication of

temperature and peak wavelength gives a constant value. With this finding, it is possible to obtain the temperature of hot bodies by applying extrapolation.

$$\lambda_{max}.\,T = C \qquad \textbf{(2.7)}$$

where λ_{max} is the peak wavelength, T is the absolute temperature of the black body, and C is the Wien's displacement constant, equals to 2.898 x 10^{-3} m.K.

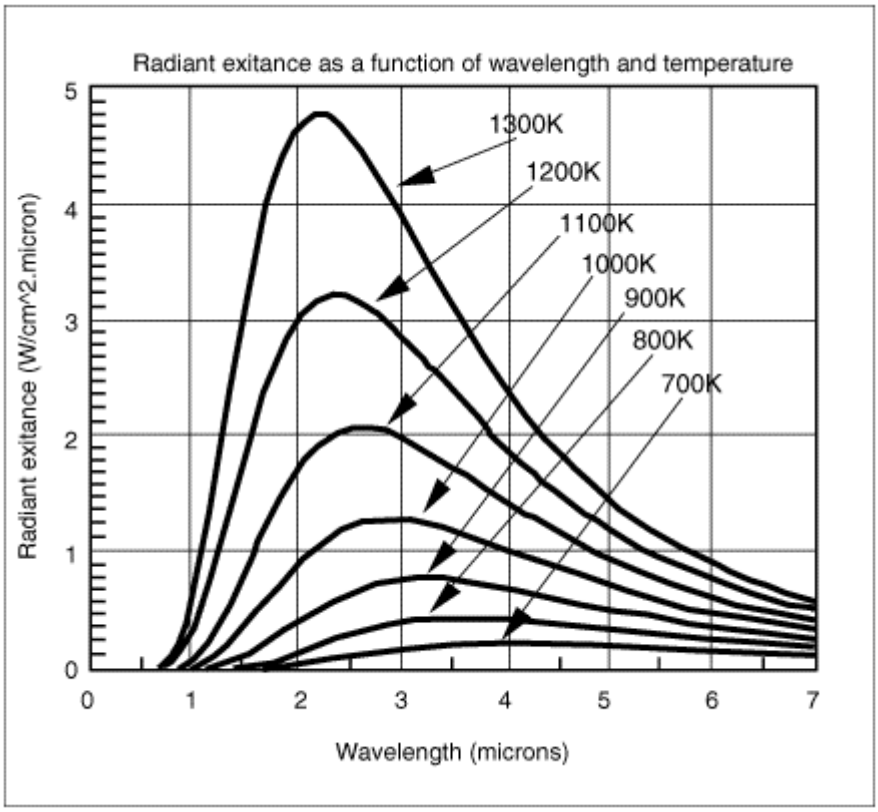

Figure 2.4 : Wien's displacement law [26].

2.2.4 Emissive power

All surfaces above 0 K emit electromagnetic radiation into the surroundings. This radiative heat flux emerging from the surface, is called the emissive power E, depends on the temperature and on the material. The heat flux emitted over the entire spectrum represents total emissive power, when the spectral emissive power, which is also called monochromatic radiation, is the power at a given wavelength. The total and spectral emissive powers are related by;

$$E(T) = \int_0^\infty E_\lambda\,(T,\lambda)d\lambda \qquad \textbf{(2.8)}$$

Where E is total emissive power, E_λ is spectral emissive power.

2.3 Emission From Real Surfaces

Planck's radiation law could not yield the results correctly for real surfaces. At this point, a dimensionless quantity called the "spectral emissivity" of the real body, a function of both wavelength and temperature, should be introduced. The emissivity is defined as the ratio of the total radiance emitted per unit of area of a real body at the temperature T to the emitted radiance of an ideal blackbody at the same temperature. It can also be defined as the ratio of the luminance of the body to that of an ideal black body at the same temperature, T. Based on the laws of thermodynamics, the spectral emissivity is always between zero and unity (unity corresponding to a black body, and zero corresponding to a perfectly reflecting body).

Basically, the methods used for the experimental determination of the spectral emissivity of metals can be classified into two groups; indirect method and direct or comparison method.

- Indirect Methods

  According to Kirchhoff's laws of thermal radiation, the absorptivity and the emissivity of any surface are equal at all wavelengths. Also, since the sum of the absorptivity and the reflectivity equals unity for a lightproof body.

$$\varepsilon_\lambda \text{ (emissivity)} = \alpha_\lambda \text{ (absorptivity)} = 1 - \rho_\lambda \text{ (reflectivity)} \qquad \textbf{(2.9)}$$

  It can be used when either the absorptivity or the reflectivity is known.

- Direct, or Comparison, Methods

  Emissivity can be computed by evaluating the ratio of the radiant intensity from a real surface to the intensity from an approximate blackbody at the same temperature. A direct comparison method is utilized to measure the spectral emissivity of a real surface at incandescent temperatures. In that method, the spectral emissivity is computed from the basic relation;

$$\varepsilon(\lambda, T) = \frac{I(T)}{I_b(T)} = \frac{I(T)}{\sigma . T^4} \qquad \textbf{(2.10)}$$

where $\varepsilon(\lambda, T)$ is the spectral emissivity at temperature T and wavelength λ, S is the radiant intensity of a source, I is the radiant intensity of the approximate black body.

2.4 Radiative Heat Transfer

In this study, calibration at high temperature is performed in vacuum conditions. Hence, convective heat transfer is neglected. Net radiation exchange at a surface represents the net rate at which energy would have to be transferred to the surface in order to maintain it at a constant temperature. It may be expressed as:

$$q_i = A_i(J_i - G_i) \tag{2.11}$$

$$J_i \equiv E_i + \rho_i G_i \tag{2.12}$$

By substituting eq.2.12 into eq.2.11, one can obtain the net radiative transfer from the surface in terms of the surface emissive power and the absorbed irradiation:

$$q_i = A_i(E_i - \alpha_i G_i) \tag{2.13}$$

where α_i equals to $1 - \rho_i$ for an opaque surface. By substituting eq.1, following expressions may be deducted for an opaque, diffuse, gray surface:

$$J_i = \varepsilon_i E_i + G_i(1 - \varepsilon_i) \tag{2.14}$$

$$q_i = \frac{E_{bi} - J_i}{(1-\varepsilon_i)/\varepsilon_i A_i} \tag{2.15}$$

To determine the radiation exchange between two facing surfaces in enclosure, this equation is used.

$$q_{12} = q_1 = -q_2 = \frac{(T_1^4 - T_2^4)}{\frac{1-\varepsilon_1}{\varepsilon_1 A_1} + \frac{1}{A_1 F_{12}} + \frac{1-\varepsilon_2}{\varepsilon_2 A_2}} \tag{2.16}$$

2.4.1 The view factor

The view factor is defined as the fraction of the radiation emitted by one surface (A_i) that is intercepted by other surface (A_j). The maximum view angle is defined as half sphere, which is equal to 2π radian. Two parallel surfaces are in their 2π-radian wide

sights. The view factor between these surfaces is expressed as F_{ij} or F_{ji}, depending on which one is emitting radiation.

$$F_{ij} = \frac{1}{A_i}\int_{A_i}\int_{A_j}\frac{\cos\theta_i \cos\theta_j}{\pi R^2} dA_i dA_j \quad \textbf{(2.17)}$$

From the view factor integral (eq.2.17), following relations are obtained:

$$A_i F_{ij} = A_j F_{ji} \quad \textbf{(2.18)}$$

$$\sum_{j=1}^{N} F_{ij} = 1 \quad \textbf{(2.19)}$$

Finally, net radiative heat transfer between surfaces can be calculated with following formula:

$$Q_{ij} = \frac{F_{ij}A_i\left(T_i^4 - T_j^4\right)}{\frac{1-\varepsilon_i}{\varepsilon_i A_i} + \frac{1}{A_i F_{ij}} + \frac{1-\varepsilon_j}{\varepsilon_j A_j}} \quad \textbf{(2.20)}$$

2.5 Pyrometry

2.5.1 2-color pyrometer

The spectral radiation from a real body at one wavelength is derived by multiplying eq 2.4 with the emissivity factor:

$$I_\lambda(T) = \varepsilon_\lambda \frac{\lambda^{-5}}{exp[C_2/(\lambda T)]} \quad \textbf{(2.21)}$$

Since the surface emissivity is unknown, the best approach of computing the temperature is to take the ratio of temperature readings at two discrete wavelengths. On the other hand, emissivity varies with the wavelength for real surfaces. Accordingly, coal particles that are target of 2-color pyrometer are considered as a gray body ($\varepsilon_{gb} = constant$). The pyrometer is calibrated against a black body ($\varepsilon_b = 1$). Thus small deviation occurs while evaluating the temperature of a real surface with an emissivity factor different than one. With the following formula, true temperature of the object can be attained.

$$\frac{1}{T_r} = \frac{1}{T} + \frac{\lambda}{C_2} ln\left(\frac{\varepsilon_b}{\varepsilon_r}\right) \quad \textbf{(2.22)}$$

where ε_r is the emissivity of real surface, $\varepsilon_b$is the emissivity of blackbody, T is the temperature measured by recorded signal, λ is wavelength, C_2 is the constant from eq.2.5 and T_r is the true temperature.

By measuring the intensities at both narrow wavelength band around λ_1 and λ_2 with eq.2.21 and dividing them, following expression for ratio temperature can be obtained:

$$T_R = C_2 \left(\frac{1}{\lambda_1} - \frac{1}{\lambda_2}\right) ln \left[\left(\frac{I_1}{I_2}\right)\left(\frac{\lambda_1}{\lambda_2}\right)^5 \left(\frac{\varepsilon_2}{\varepsilon_1}\right)\right] \quad \textbf{(2.23)}$$

Since $\varepsilon_1 = \varepsilon_2$ for a grey body, the last term on the right hand side in eq.2.23 will be zero and the measured ratio temperature will be equal to the true temperature T. (eq.2.22)

3. INSTRUMENTATION

The two-colour pyrometer, which was used during this project, has been developed by Federico Botteghi at Energy Systems Institute of TUM, Germany. The pyrometer will be described briefly in the following section.

The 2-color pyrometry system consists of chassis, optic fiber, optic probe, shutter, bandwidth filters, plano-convex lenses, photodiodes, cage system, analogue to digital A/D converter card (detection box) and PC with Lab-view software installed. The pyrometry system generally looks as in the Fig.3.1.

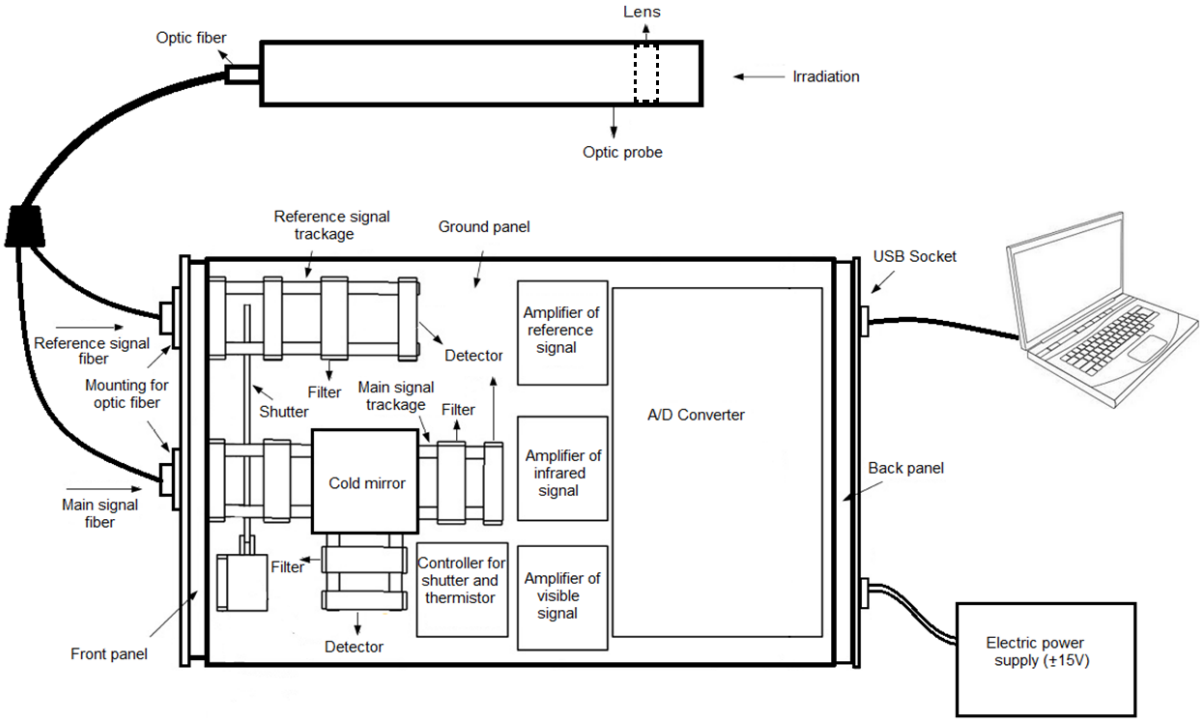

Figure 3.1 : Overall appearance of the 2-color pyrometer [27].

Components of the device can be classified into three groups such as optical, electrical and the rest. They all are explained briefly in the following segment.

3.1 Optical Components

An optical fiber, which transmits signals of the emitted radiation from the object to the system, takes place at the first stage of the pyrometer's functionality. Optical fiber alignment with the source of intensity is maintained by the help of cylindrical probe including achromatic lens to focus the light coming from the target onto surface of fiber. Optical probe is positioned at one end of probe, while achromatic lens is positioned at the other end. This lens helps fiber to detect the intensity of an object at specific distance by adjusting magnification ratio.

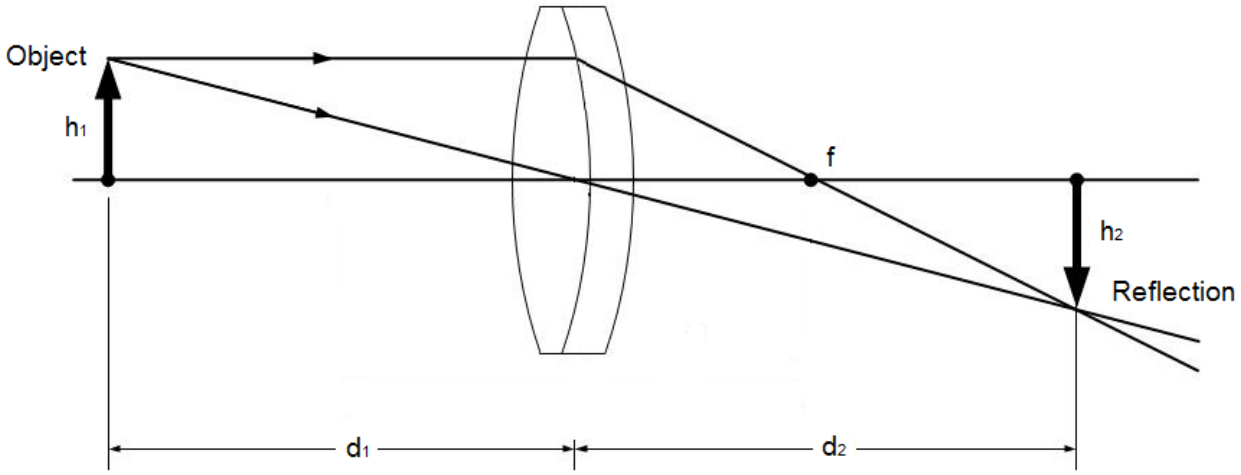

Figure 3.2 : Magnification ratio.

Magnification ratio can simply computed by the following formula:

$$MR = \frac{h_2}{h_1} = \frac{d_2}{d_1} \qquad \textbf{(3.1)}$$

With the aid of magnification ratio, probe alignment is done at particular distance from the source, which is the FOV at the center of a reactor in this case. Also, The optical magnification has been selected as 3 , so the size of the FOV at the center of the reactor is 3 times the optical fiber diameter; 1 mm. The optical magnification can be arranged pursuant to readjust ability of distance between optic fiber and achromatic lens.

Once the signal reaches to the tip of optical fiber, it is separated into two ways. One way gathers signals onto the ratio detectors. This channel, which is called main fiber, has only one fiber and constitutes a circular area in the FOV. The other way, reference fiber, concentrates light signals into the reference detector. Reference fiber actually consists of a bundle of thin optical fibers surrounding the main fiber that are patterned on a circular plane and reflects as small circles around the main fiber's projection in the FOV. That is how particles are discriminated. Two peaks in reference channel represent FOV entry and exit of a particle. On the other hand, one peak in main channels between two peaks of reference signals proves that a good particle is detected. The fiber, which is made of a fluorine fused silica, has a diameter of 1 mm with 12.7°; half cone angle of signal transmission. It can transmit the light in all visible and near infrared wavelength regions.

In main fiber channel, the radiation coming from the fiber is parallelized through plano-convex lens with focal length of 35 mm. Then the light at visible wavelengths is reflected by 45° cold mirror while the light at infrared wavelengths is transmitted. After that, the light in both channels are filtered by bandwidth filters at around 650 nm and 1050 nm. In reference channel, the light is received by a photodiode without splitting. When the radiation is filtered at particular wavelengths, it is concentrated on the surface of detectors. Since the detectors detect light, they are also called photodiodes. The ray of light coming from the source is shown in the following figure.

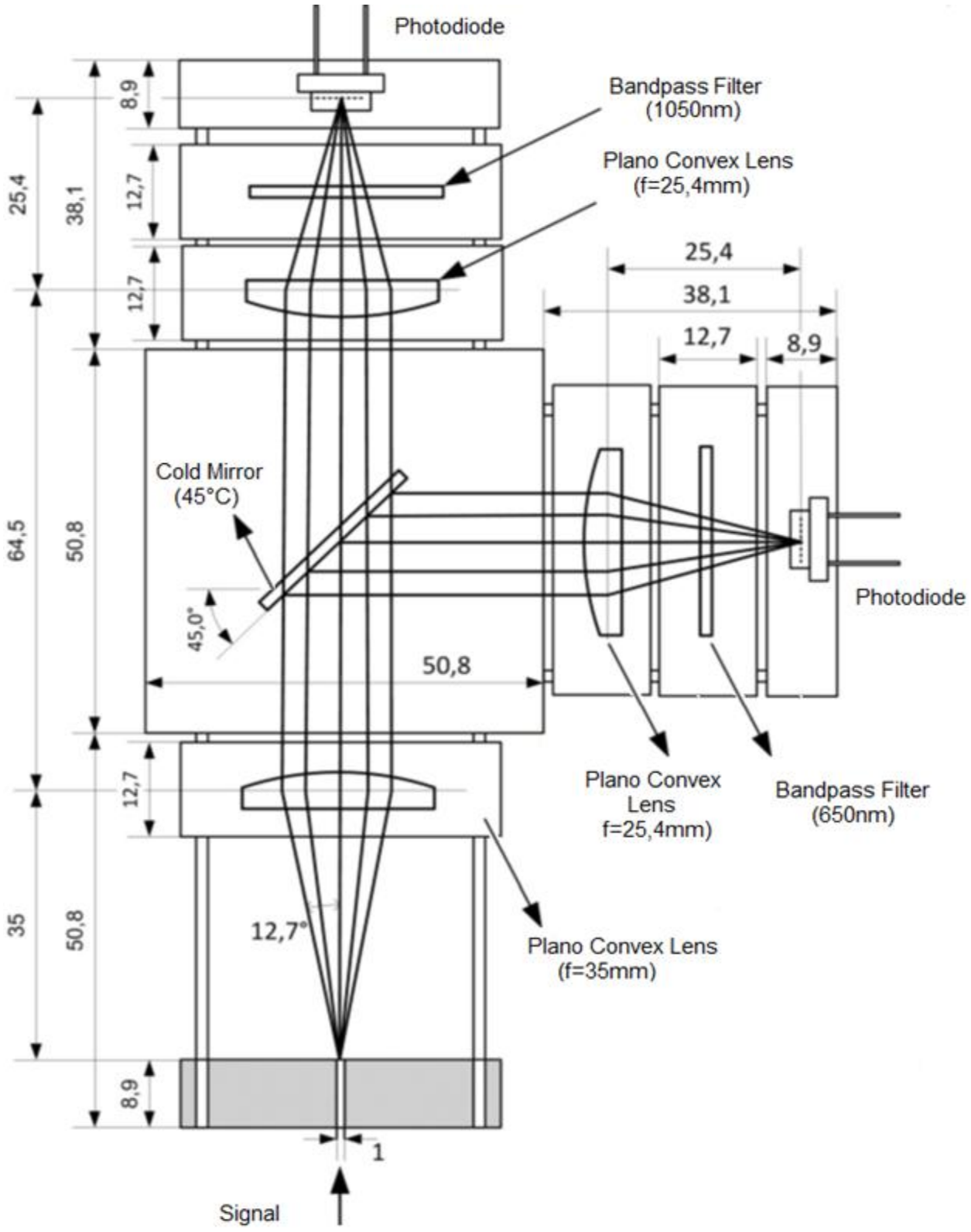

Figure 3.3 : Ray of light coming from the source [27].

3.2 Electronic Components

When signals are transmitted to the photodiodes, the radiation is converted into electric voltage with the help of a resistance. After conversion, the electrical signals should be amplified, because signals are too low to provide precise detection of emitted radiation. There is also secondary 10-times-amplification implemented for more precise measurement. Then the electric signals are transmitted by an analogue-to-digital converter to the computer. In the computer, records are transferred into the software, Lab-view 2009 for data acquisition. For all electric power requirements, power supply ($\pm 15V$) is put to use.

3.3 Other Components

The chassis of the pyrometer is made of aluminum and covered with black paint to prevent interference of light reflection inside of the chassis. The cage system of the optical part forms from rods to align filters, lenses and detectors in order. Special mounts are utilized in order to place and fix optical components. This mounting mechanism also enables to easily adjust the distance between optical components through rods.

The fiber is fixed to the system by a connector with a screw to fix. With the help of a closure “shutter”, the incoming radiation to the system can be blocked in order to allow measurement of the pyrometer electronic part’s noise. These measurements are useful for zeroing the device before start. The aperture also helps to perform the subtraction of the noise from the measured data during the measurement process. The shutter is controlled and shifted occasionally by a specific magnet.

4. CALIBRATION

4.1 Black Body Calibration

4.1.1 Procedure and instrumentation

The black body emits specific amount of radiation intensity at each temperature. This intensity from the interior of black body can be viewed through a small aperture. The intensity basically comes from a heated isothermal spherical cavity. The emissivity of the black body is assumed close to 1 regardless the material used inside. The spherical black body source from *Isotechna* has been utilized in this work. The black body is spherical shaped with 425mm diameter and 25 kilograms heavy. It can heat up to 1200°C in 3 hours. The warm-up time reduces to 1 hour for lower temperatures. Black body operates in an ambience at 0 to 50°C, when relative humidity is lover than 70%.

Before starting calibration, a basic program is created in Lab-view for data acquisition as in the following figure (Fig.4.1). The developed program allows determining amount of sample for each channel to record and rate of recording. It is also possible to turn on the secondary amplification (10 times). Essentially, the program helps to demonstrate continuously the equivalent voltage of detected radiation at both channels. The voltage values are shown in form of numeric indicator and graph. Beside, minimum, maximum and mean voltage values at both channels are indicated for ease. Since the photodiodes have restrictions over their working ambient temperature, thermistor has been implemented into the pyrometer to control the inside temperature. The change in inner temperature can also be observed from the current program. Finally, as it is required to calculate the fraction of voltage values recorded by infrared and visible photodiodes, the ratio between these values is both indicated and plotted simultaneously.

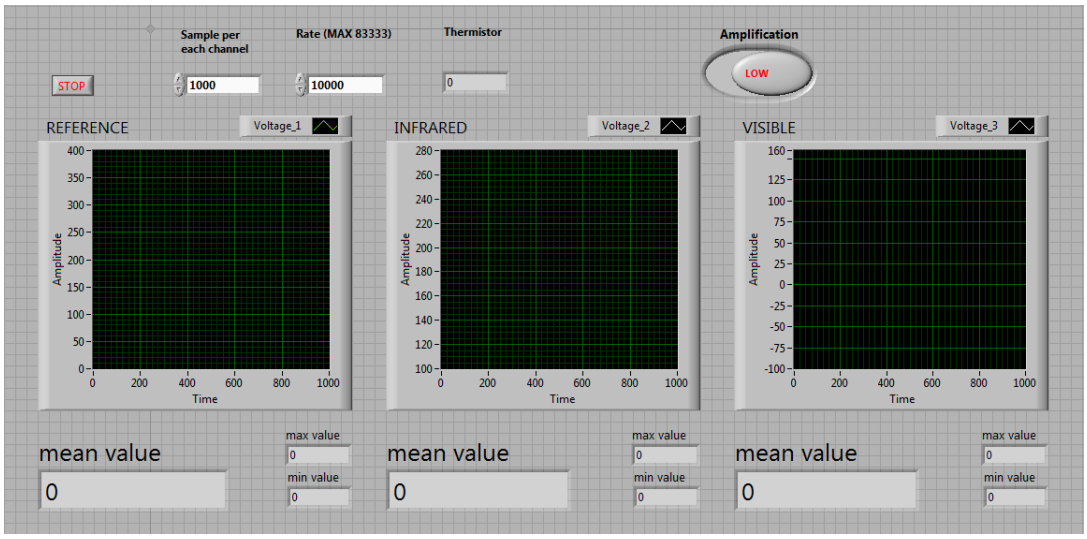

Figure 4.1 : Scheme of Lab-view program for calibration procedure.

The 2-color pyrometer- built up in house- was calibrated against black body, calibration reference. After the optic fiber was aligned coaxially with the centre of the black body, measurements were recorded in terms of mV for temperature range between 800°C-1200°C. This temperature range could not have been exceeded due the limitations of the blackbody.

After Lab-view program was ready to operate, the black body was first set to temperature of 800 °C. The temperature was measured by the help of type K control thermocouple in order to validate the temperature shown on the screen of blackbody. Then Labview program, written for calibration procedure, was run in order to measure the radiation intensity in terms of electric voltage. This measurement was repeated five times at each temperature starting from 800°C up to 1200°C. The reason beyond five times measurement is to provide the opportunity of calculating mean value and standard deviation. Since reaching to the thermal equilibrium lasts a lot of time, it took approximately one day to complete one cycle of calibration between 800°C-1200°C. The measured data were recorded in Microsoft Excel 2010 to create calibration curve for temperature as a function of voltage. Hence, it is possible to calculate the temperature of any object with known emissivity value. The curve fitting has been completed for each of reference, visible and infrared channels and these curve functions were implemented into the program that is designed for measurement campaign.

After completing several measurements, the oscillation around the consistent mean value of recording has been noticed. Later this problem is solved by providing a proper grounding to the system.

4.1.2 Results

When the calibration was completed for five times at intervals of 50 °C, the results were recorded in Excel. Then average voltage values and standard deviations were calculated for each of set temperatures. Final results are listed in the following table. As it is easily interpreted from the table, standard deviation at each point is very low. This indicates that results are consistent.

Table 4.1 : Results of calibration against the black body.

	Reference		Infrared (Ch2)		Visible (Ch1)	
T(°C)	Average(mV)	Std. Dev.	Average(mV)	Std. Dev.	Average(mV)	Std. Dev.
849	285.838	*0.070*	301.687	*0.090*	9.234	*0.020*
901	486.137	*0.130*	516.646	*0.149*	26.792	*0.008*
950	781.411	*0.097*	834.908	*0.119*	61.152	*0.011*
999	1216.993	*0.155*	1306.125	*0.172*	127.254	*0.014*
1049	1833.813	*0.222*	1976.378	*0.283*	246.527	*0.038*
1100	2699.473	*0.373*	2920.965	*0.480*	456.893	*0.062*
1149	3836.558	*0.539*	4166.605	*0.713*	798.650	*0.132*
1198	5283.880	*0.612*	5756.058	*0.578*	1326.650	*0.136*

It is possible to extrapolate the available data for higher temperature. At this point, auxiliary equation is needed. In general, one can extrapolate at the end of data

boundary of the table above by inserting Wien's displacement law (Section 2.1.6) as well as in this project.

Firstly, Wien formula was integrated along the lower and upper limits of wavelength band at both channels for temperatures that were considered to be useful in measurements. Then the constant values of Wien's law were computed for infrared and visible channels by using the last datum in extrapolation wise. By multiplying the obtained constant with the data from Wien's formula, necessary data for extrapolation were acquired. After that, correlation curve between temperature and voltage was established with the aid of curve-fit option in Microsoft Excel. The plot and function of extrapolation curve is shown in Figure 4.2.

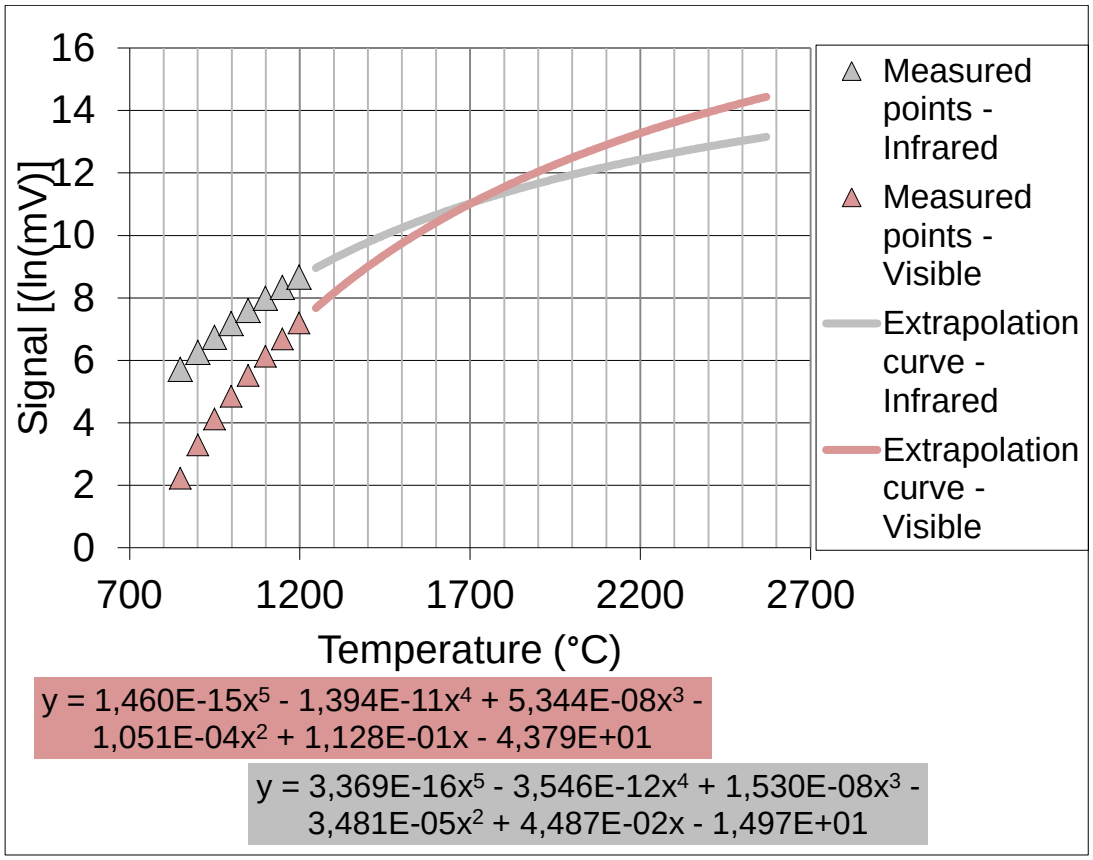

Figure 4.2 : Extrapolation curves and functions for infrared and visible channels.

These derived functions are implemented into Lab-view program written for measurement campaign. They enable the pyrometer to link the ratio of detected radiation signals to the temperature from calibration data.

4.2 Calibration At Elevated Temperatures

The black body is limited to provide temperatures higher than 1200 °C. On the other hand, temperature reaches up to higher values than 1200 °C in combustion processes. Thus, calibration at high temperature is required for more precise results. By utilizing black body calibration data, results were expanded by applying Wien's integral extrapolation. The commercial methods were investigated in order to extrapolation at elevated temperatures [28].

Although the blackbody is considered as an appropriate source of radiation, it has disadvantages. The heating equipment should be large to minimize temperature gradients. Therefore, the blackbody is hard to manage and considerably expensive. Especially in the ultraviolet spectral region, it is hard to generate detectable quantity of radiation at high temperatures due to oxidation and evaporation of the hollow body. The last but not least disadvantage is that it is difficult to keep the temperature constant during the time required for accurate detection, when the temperature is getting higher.

4.2.1 Commercial method

The most common ways to provide reference source for higher temperature are using metals or metal alloys with high melting point and using pre-calibrated lamps or pyrometers. For all methods, it is required to use certified current vs. temperature relation tables prepared in accordance with the ITS-90 from national laboratories such as NIST, NPL, etc.

One of the widely-used methods is to calibrate the device against certified tungsten ribbon filament lamp. As a substitution of blackbody cavities, tungsten ribbon filament lamps are widely applied as standard reference sources. [7, 14] In the light of national laboratories' statements, tungsten lamps are highly reproducible radiance sources and can be accurately calibrated and be continuously used between 800°C to 2300°C. Recently there are offers of calibrated pyrometric lamps, traceable to the ITS-90, operating over the range 700 °C to 2600 °C with low uncertainty and high stability. Even though this kind of calibration lamps must be pre-calibrated, the certified correlation between electric current of the tungsten filament lamp and the temperature is always provided by the producer.

The lamps utilized in this method are electrically rated at particular voltage and amperage. Schematic diagram of electrical system for a tungsten ribbon filament lamp can be seen in the Figure 4.3. These lamps are constructed as ribbon filament with a notch in the middle of its length to provide reproducibility of facing the same point each time. The length is much higher than the width. They are mounted in a tubular glass envelope which may be vacuumed or gas-filled. Vacuum filament lamps are generally more stable than gas-filled lamps below 1400°C and should be used preferably to gas-filled lamps under this temperature if possible [29].

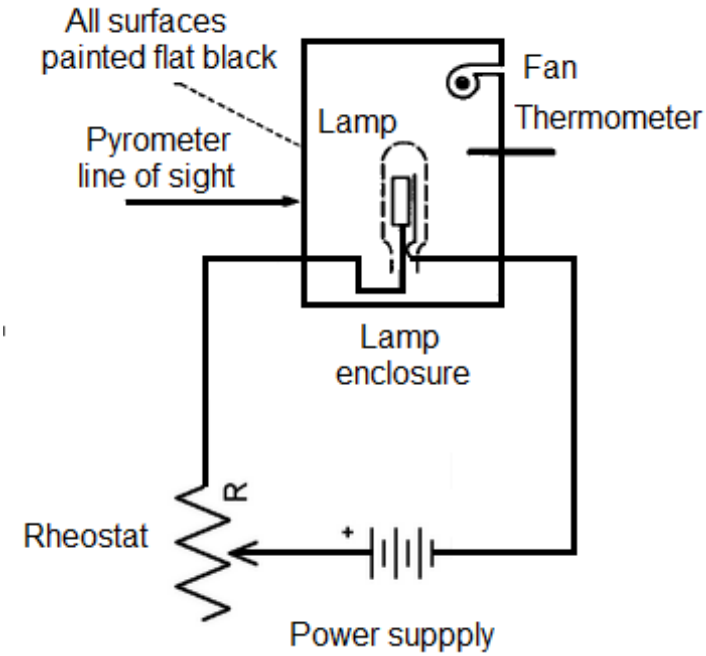

Figure 4.3 : Schematic diagram of electrical system for tungsten ribbon filament lamp.

A typical certificate (Table 4.2) shows accuracy estimation and operating instructions as follows. These values apply when the lamp is operated base down at room temperature, 25 °C and the sighting is made on the center of the filament. For best accuracy, certified reference pyrometers should be recalibrated (as a function of pyrometer current) after about 200 hours of use [5].

Table 4.2 : Brightness temperature vs. lamp current table from a typical certificate of a particular tungsten strip lamp from US National Bureau of Standards [5].

Brightness Temperature (at 0.653 µm) versus Lamp Current			
Temperature (°C)	**Current (A)**	**Temperature (°C)**	**Current (A)**
800	*11.26*	1600	*23.53*
900	*12.12*	1700	*25.78*
1000	*13.17*	1800	*28.13*
1100	*14.44*	1900	*30.58*
1200	*15.92*	2000	*33.12*
1300	*17.59*	2100	*35.75*
1400	*19.43*	2200	*38.48*
1500	*21.41*	2300	*41.3*
The maximum uncertainties of the values at 1000-1100 °C correspond to about ±3 °C. At lower and higher temperatures the maximum uncertainties are increasing up to ±5 °C for 800 °C. and up to ±7 °C for 2300 °C.			

Firstly the temperature is set to the highest point desired in the current method unlike calibration against the black body. Temperature setting is easily done by adjusting the rheostat electrical current passing through the lamp based on the certificate of calibration data. The current is controlled by an ammeter or potentiometer. Once the electrical signal is received from a detector, it is converted into an equivalent readout in temperature units by using the certified temperature vs. current table. Using reference tables, correlation between temperature and signal of the pyrometer at the required calibration point can be determined by matching the temperature corresponding to the current of the tungsten ribbon filament lamp with the electrical

output of the pyrometer. Calibration generally takes place at intervals of 100°C. Some time is required between points to allow the lamp to reach equilibrium after each set temperature change. While the set temperature is decreasing, the waiting period required for thermal equilibrium of the lamp is increasing.

In some cases, it is also possible to use a pyrometer (ratio, disappearing-filament, etc.) readily calibrated. Since it was not probable for this study, the tungsten ribbon filament lamp was investigated and the construction of calibration cell was studied. In consequence of the fact that producers do not offer that kind of lamp any more, this idea has been suspended. As the tungsten ribbon filament lamps are out of stock and are not produced at that moment, a solution has been invented regarding the working principle of tungsten filament ribbon lamp.

4.2.2 Self-design solution- WMR

4.2.2.1 Concept

Since the tungsten ribbon filament is heated by an electrical current, this method provides an accurate adjustment and high stableness. The ribbon filament mounted in vacuum or in an inert atmosphere also attains high temperatures. In comparison with other metals or carbon, tungsten has advantages by means of high purity, reproducibility, and easy maintenance, constancy of temperature and ability of annealing exposure for several hours. In consideration of facts above, self-design calibration control method has been developed. In this method, a thin tungsten sheet is placed between electrodes in a reactor with vacuuming or gas-streaming options. The sheet is cut very thin in order to create higher electrical resistance than the electrodes. Then the sheet is electrified in order to heat up to high temperatures. The temperature is observed by type C thermocouple while the 2-color pyrometer is aligned with 15-30° angles to the line of sight facing the surface of the sheet. In this method, WMR of the Institute for energy systems at TUM is utilized.

4.2.2.2 Sheet material

As tungsten is non-black body, emission factor varying 0 and 1, called the normal spectral emissivity, is required. For abbreviation, this factor will be denoted as the emissivity. The emissivity of metals varies non-uniformly with the wavelength. On

the other hand, the variation with the temperature is relatively smaller, regular and mostly linear. So it does not strongly depend on the temperature [30].

At higher temperatures optical pyrometers, calibrated for brightness temperatures, are usually applied. The true temperature can be determined directly by the help of the calibrated optical pyrometer and the equation below. It is important to know the emissivity at one wavelength as a function of temperature from earlier measurements.

$$\frac{1}{T} = \frac{1}{T_B} + \frac{\lambda}{c_2} \ln[\tau . \varepsilon(\lambda, T)] \qquad \textbf{(4.1)}$$

where T is the true temperature in K, T_B is the brightness temperature in K, $\varepsilon(\lambda, T)$ is the spectral emissivity of tungsten, τ is the transmission factor of the window, λ is the wavelength in μm, $c_2 = 14380$ μm.K. When the source and the detector are not parallel to each other, the angle factor should be introduced into the term inside natural logarithm at equation above.

Several determinations for the emissivity of tungsten have been performed so far. As one of the most common investigators in this field, DeVos [30] developed a new determination of the spectral emissivity of tungsten to procure more reliable data in wide range of temperature (1600K - 2800K, at intervals of 200K) and wavelength (0.23μm – 2.7μm) instead of using extrapolation or combination of computed results of previous investigations. He aimed to provide a standard source of radiation as a function of the wavelength and the temperature for photometry and pyrometry. The main data about earlier measurements of tungsten emissivity at 2900K are gathered in Appendix B and Appendix C. For the spectral emissivity at lower temperatures, The document in Appendix E, which is published by from NASA Astrophysics data system, is referred.

As a result of DeVos' measurements, the graph (Appendix A) is prepared [30]. There are many other studies carried through the previous century to detect experimentally the spectral emissivity of tungsten. Larrabee compared his results with the data obtained by DeVos before, which can be seen in Appendix D. DeVos measured the spectral emissivity of tungsten with the same method excluding the scattered light correction (eq.4.2) that reasonably lowered the measured emissivity values approximately 2.5 per cent [31].

$$\varepsilon(\lambda, T) = \frac{S-\alpha}{I-\alpha} \quad \textbf{(4.2)}$$

where $\varepsilon(\lambda, T)$ is the spectral emissivity at temperature T and wavelength λ, S is the uncorrected radiant intensity of the tungsten source, I is the uncorrected radiant intensity of the approximate black body and α is the scattered component of radiation for both blackbody and tungsten source readings [31]. Radiance in the line of sight varies because of multiple reflections between the sheet and the window. In the concept developed, there is no reflection problem since the housing is not made of glass. Additionally apertures on the reactor housing except the one used for pyrometric detection should be covered.

4.2.2.3 WMR – Wire Mesh Reactor

The WMR basically enables heat generation from the electrical resistivity of an object that is positioned between the electrodes (Fig. 4.4a). The object in this case is thin tungsten sheet. The release of heat is constitutively provided by electric current passing through the tungsten sheet. With the adjustment of amperage, one can achieve high temperatures in a heating process. That kind of heating is called Joule heating or resistive heating in literature. The reactor has relatively small housing and this allows the ambient conditions inside to be arranged easily. By the help of pump facility, gas suction or vacuuming are doable treatments for prevention of undesired chemical reactions (Fig.4.4b).

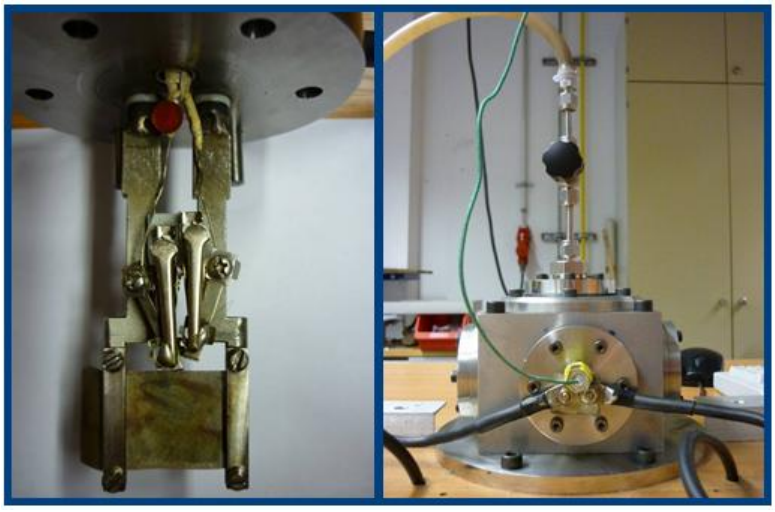

Figure 4.4 : a) Electrodes of the WMR, b) Side view of the WMR including gas suction facility and electrode mounting with cable connection [32].

The parts that WMR consists of are listed in a table as follows:

Table 4.3 : Components of WMR in the Institute for Energy Systems, TUM.

Component	Features	Function
Reactor housing	- made of steel - dimensions of 120 mm x 120 mm x 90 mm - 1 aperture for mounting electrodes - 3 aperture with quartz glass - 1 gas inlet hole - 1 gas outlet hole	-Preservation of ambient conditions during calibration -Enabling the pyrometer alignment with the sheet
DC Power supply	- SM 15-200 D from *Delta Electronics* - rated voltage of 15V - rated amperage of 200A	-Supply of required electric current to the tungsten sheet
A high pressure gas container and a vacuum pump	- 50 lt. Argon(Ar) gas tank - AEG pump 1.4 kW 200V	-Control of calibration atmosphere inside the housing -Avoiding unwanted reactions
Electrodes	- made of heat resistant steel - effective dimensions of 4mm x 5 mm x 20 mm - 2 screws for each electrode - cable connection for power supply and thermocouple - heated area of 22mm x 20mm	-Positioning and fixing the tungsten sheet -Heating the tungsten sheet by electric current -Transmission of signals from type C thermocouple to the PC
PC	- Lab-view software installed - control board module plugged	-Data acquisition

4.2.2.4 Theoretical calculations

4.2.2.4.1 Heat transfer calculation

The calibration up to 1200°C is achieved by black body cell. For calibrating the 2-color pyrometer against higher temperatures, the tungsten sheet heating method (Fig.4.5) is developed. In this method, 0.1 mm thick tungsten sheet between electrodes is heated by passing electric current through inside stainless steel housing with a circular fused quartz glass for pyrometric detection. On the other hand, the temperature of metal sheet is obtained by the help of high-temperature thermocouple. When the sheet reaches to the desired temperature, the pyrometric measurement is performed. Afterwards, the calibration procedure is concluded with the data obtained.

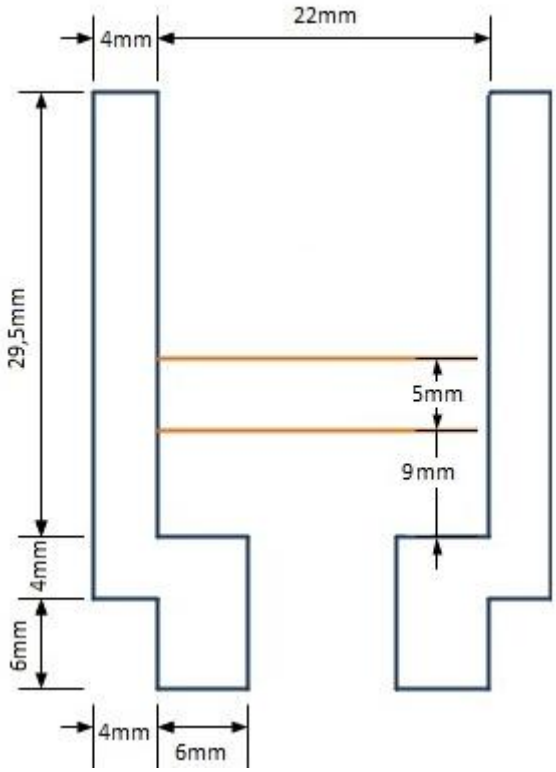

Figure 4.5 : The scheme of tungsten sheet heating method without housing.

For calibration control, the temperature of the sheet must be constant. In case of thermal equilibrium, the constancy of the temperature is provided. By calculating radiation emitted from the surface of the sheet, required electrical current can be

found. Before starting radiation heat transfer analysis, the following assumptions should be taken into consideration:

- In vacuum, convection affects are not being considered.
- Reactor housing has diffuse-gray surface.
- Effect of electrode handler is neglected.
- Tungsten sheet is considered parallel to the floor and in the middle of the housing.
- Since the housing shape of the reactor is not in a simple. It is considered as a cylinder. (It was also investigated as a sphere, but it did not make any drastic changes in calculations)

Calibration at high temperature is performed in vacuum conditions. Hence, convective heat transfer is neglected. However the conductive and convective heat losses depend on the ambient temperature, the heat loss at elevated temperatures is mostly radiative. Hence the heat losses other than radiative loss are negligible. [28]

Since very thin metal is electrically heated, the temperature gradient along the sheet is not taken into account. From the heat balance, the power generated electrically by the sheet is equal to the total radiative energy leaving the surface to the upper part of housing ($q_{rad,1}$), to the window aperture ($q_{rad,2}$) and to the lower part of housing ($q_{rad,3}$) and in case of gas-filling, convective energy to the ambience (q_{conv}) inside the housing. By calculating the total energy radiated from the both surfaces of the sheet, the required current and voltage can be determined. Electrical part will be explained in detail later.

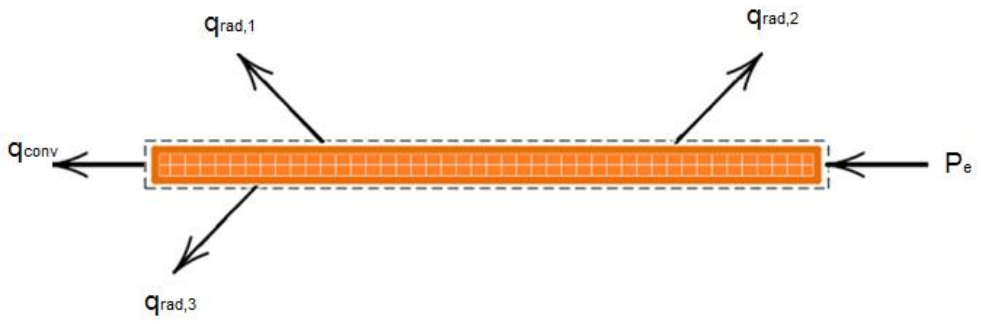

Figure 4.6 : Heat balance of the tungsten sheet.

From that point, emitted radiation calculations are carried out by considering the reactor housing cylinder. The metal sheet stands in the center of the housing. For

easiness in calculations, the sheet is assumed as disk-shaped with respect to circular shape of the window aperture on the housing. Based on width and length dimensions of the sheet, the diameter of the sheet is determined with the aid of equivalent area approach. In this case, view factor formula for coaxial parallel disks is applied as follows:

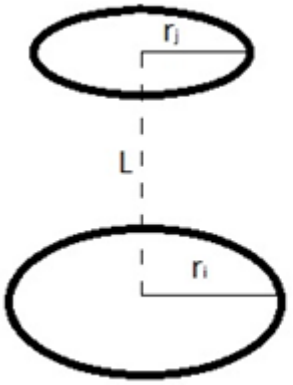

$$R_i = {}^{r_i}/_{L}, R_j = {}^{r_j}/_{L}$$

$$S = 1 + \frac{1+R_j^2}{R_i^2}$$

$$F_{ij} = \frac{1}{2}\left\{S - \left[S^2 - 4\left({}^{r_j}/_{r_i}\right)^2\right]^{1/2}\right\}$$

Figure 4.7 : The view factor calculation between coaxial parallel disks.

The tungsten sheet is aligned in the center of the cylindrical housing and then, the housing is separated into two from the middle section for simplicity in calculation (Fig.4.8). Here, 0 represents tungsten sheet, while 2 indicates fused quartz glass. 1 and 3 signify the housing made of stainless steel.

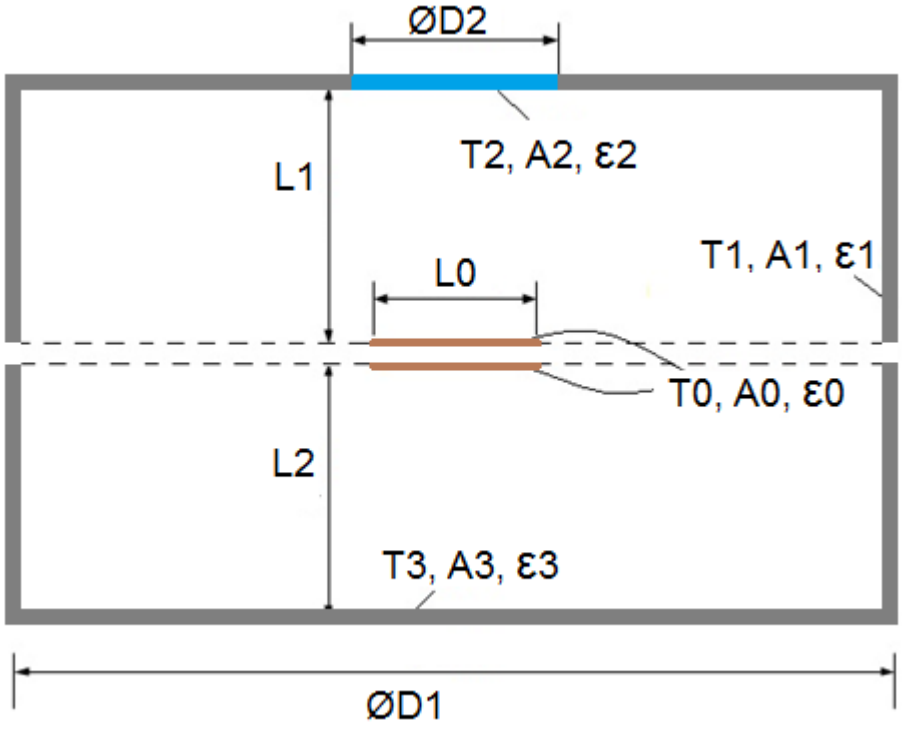

Figure 4.8 : The cylindrical housing.

Some useful parameters for radiative heat transfer calculations are tabulated as:

Table 4.4 : Emissivity and view factor values for radiative heat transfer calculations.

F_{00}	0.000
F_{01}	0.863
F_{02}	0.137
F_{03}	1.000
$\varepsilon_{tungsten}$	0.40
$\varepsilon_{stainless\ steel}$	0.59
$\varepsilon_{fused\ quartz}$	1.00

4.2.2.4.2 Electrical resistance calculation

The instantaneous power consumed/created by every circuit element equals the product of its voltage and current. By applying Ohm's law to evaluate the dissipated power, the following formula can be written:

$$P = VI = IR^2 = {}^{V^2}/_{R} \quad \textbf{(4.3)}$$

where I is the electric current [A], R is the electrical resistance [Ω)] and V is the voltage [V]. The unit of the dissipated power [P] is W or J/s.

A physical sheet has a resistance and hence dissipates power. The sheet behaves like a resistor in a circuit and warms while current passing through. In fact, the quantity *R* presents the resistance of a unit-length of material. Most materials have a positive resistivity value. The electrical resistances of the sheet and electrodes are required to compute the dissipated power from the sheet. The resistance R is obtained by the formula:

$$R = \rho \frac{l}{A} \quad \textbf{(4.4)}$$

where l is the length of the conductor (in this case : sheet) [m], A is the cross-sectional area of the conductor [m²], ρ is the electrical resistivity (also called *specific*

electrical resistance) of the material [Ω·m]. The longer the sheet is, the greater the resistance and thus the power dissipated. Besides the thinner the sheet is, the greater the resistance and relatedly the power dissipation.

The electrical circuit of the reactor must be formed in order to obtain the power dissipation of the sheet. Firstly electrical resistances are calculated by using eq.4.4. As the electrical resistivity is a temperature-dependent quantity, the linear approximation is generally used:

$$\rho(T) = \rho_0[1 + \alpha(T - T_0)] \quad \textbf{(4.5)}$$

where α is called the *temperature coefficient of resistivity*, T_0 is a fixed reference temperature (usually room temperature), and ρ_0 is the resistivity at temperature T_0. α depends on the material of sheet. All the dimensional and physical information, required to calculate the resistances and create the electrical circuit of system, are given in the Table 4.5. Since the temperature of the tungsten sheet is higher than room temperature, electrical resistivity of the sheet is computed using eg.4.5.

Table 4.5 : Electrical and dimensional properties of electrodes and tungsten sheet.

		Electrodes	***Tungsten***
Electrical resistance	ρ[Ω. mm]	2.15 x 10^{-3}	24.2 x 10^{-3}
Thickness	t[mm]	5	0.1
Length(width)	L[mm] (w[mm])	16 (4) + 10 (6)	22 (5)

From eq. 4.4, resistances can be calculated for each electrodes and metal sheet. The electrical circuit is formed as in the Fig.4.9. R_1 symbolizes the resistance of tungsten sheet between electrodes. R_2 and R_3 symbolizes the resistances of parts of electrodes, differs from width.

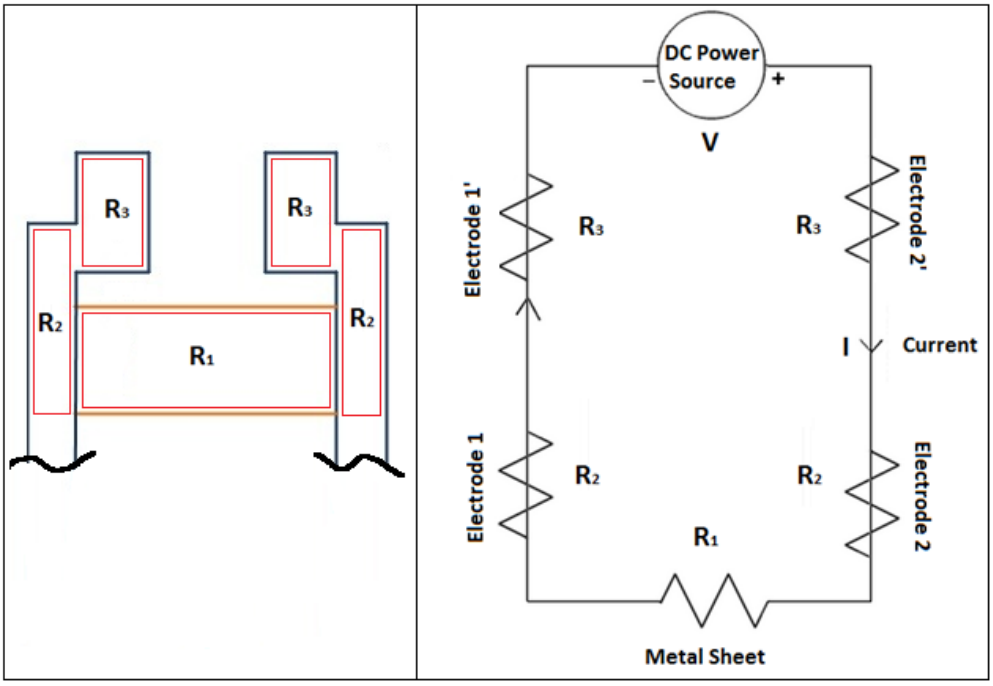

Figure 4.9 : The electrical circuit of the reactor.

As a result, it has been proved that available power supply covers the power requirement for that method.

4.2.2.5 Setup

Type C thermocouple, made of Tungsten-Rhenium with melting point of 2480 °C, was selected considering working temperature range of 0°C to 2310°C. The thermocouple was not welded to the sheet in order to prevent composition change of the sheet because of excessive heat exposure. Then it was reclined upon the bottom surface of tungsten sheet. It was placed lower part of the sheet in direction of detection to eliminate interference of the thermocouple in results. Contact between the thermocouple and the sheet was substantial. Because when the circuit remains open, it yields erroneous measurement. The experiments were carried under Argon gas in order to prevent unwanted reactions such as tungsten oxidation. The cooling effect of inert gas is negligible since irradiative heat release from the hot surface is greater than convective heat loss.

The magnification ratio was lowered from 3 to 1 for this application. So the diameter of FOV dropped to 1mm. In order to provide sufficient area for detection, the width of the tungsten sheet was determined as 5 mm. The sheet was placed 9mm further from the end of the electrodes to prevent high thermal effects on thermocouple and

enable the sheet surface directly seen from the window on the reactor. Due to the construction of the reactor, it was not possible to position the tungsten sheet surface parallel to the window aperture. This view angle factor was also taken into consideration in the calculations.

In the first stage of the calibration, the Lab-view software, which is programming software used for the black body calibration as well, was launched. A code has been developed in order to observe the measurements simultaneously and document the results. After the software was ready, the sheet was fixed in between the electrodes. With the thermocouple on the lower side, the sheet was positioned between electrodes. When the sheet is positioned properly, the electric current was supplied to the system. For connection between electrodes and computer board, special type of compensating cable for thermocouple type C was used in order to eliminate signal losses during transmission and to get more precise results. After each run, signals from visible and infrared channels of pyrometer were recorded beside signal from type C thermocouple.

4.2.3 Results

As it is explained before, the self solution method was aimed to check the accuracy of Wien's integral extrapolation as a product of black body calibration. Before starting the test, a relation between thermoelectric voltage and temperature was required. Between thermocouple signal and temperature, 6^{th} order polynomial curve was fitted between 750°C and 2310°C with respect to ITS-90 terms. Specifications about the correlation curve can be seen in the following figure.

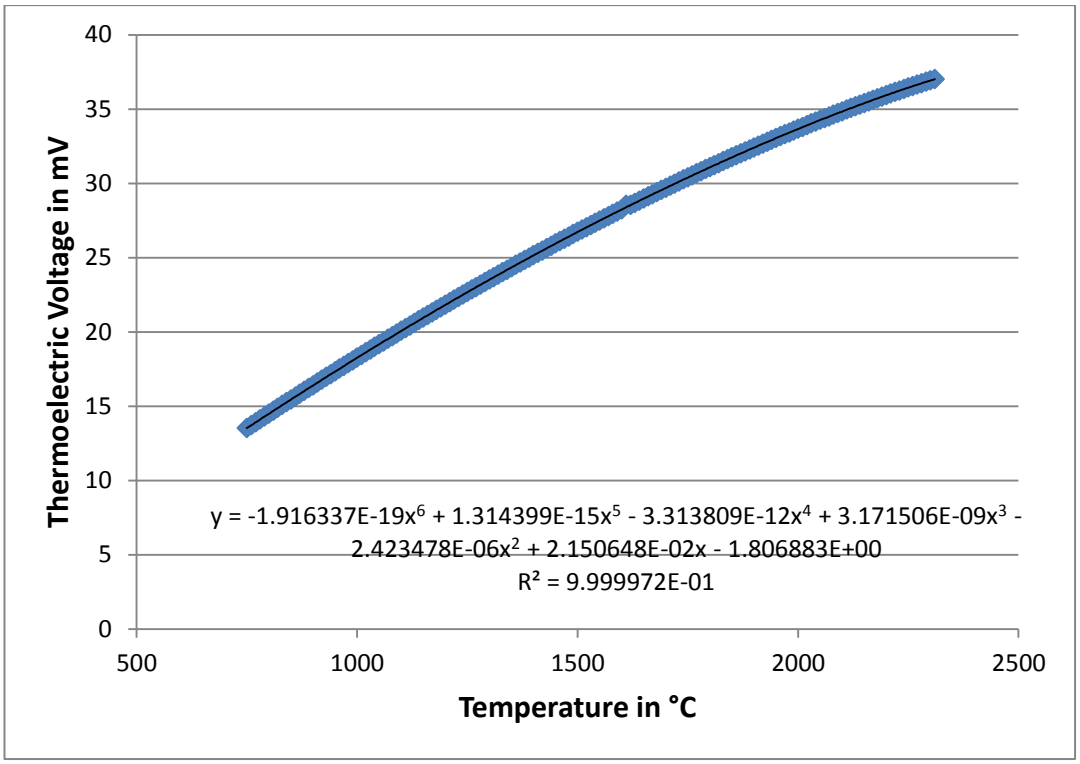

Figure 4.10 : Correlation curve between thermoelectric voltage in mV and temperature in °C.

Since the tungsten sheet is not a black body and the emissivity factor varies with temperature and wavelength, the radiant/brightness temperature changes at visible and infrared detection channels for every temperature level. Furthermore transmissivity of window aperture and the viewing angle factor are influences on measurements. By taking all these factors into account, radiation signals from pyrometer were divided by emissivity, transmissivity and angle factor to convert measured signals into black body radiation values. For each temperature level, thermoelectric voltage, retrieved from reference table of type C thermocouple, was matched with black body radiation signals at both channels. Then calculated results were compared with the extrapolation data in the following graph.

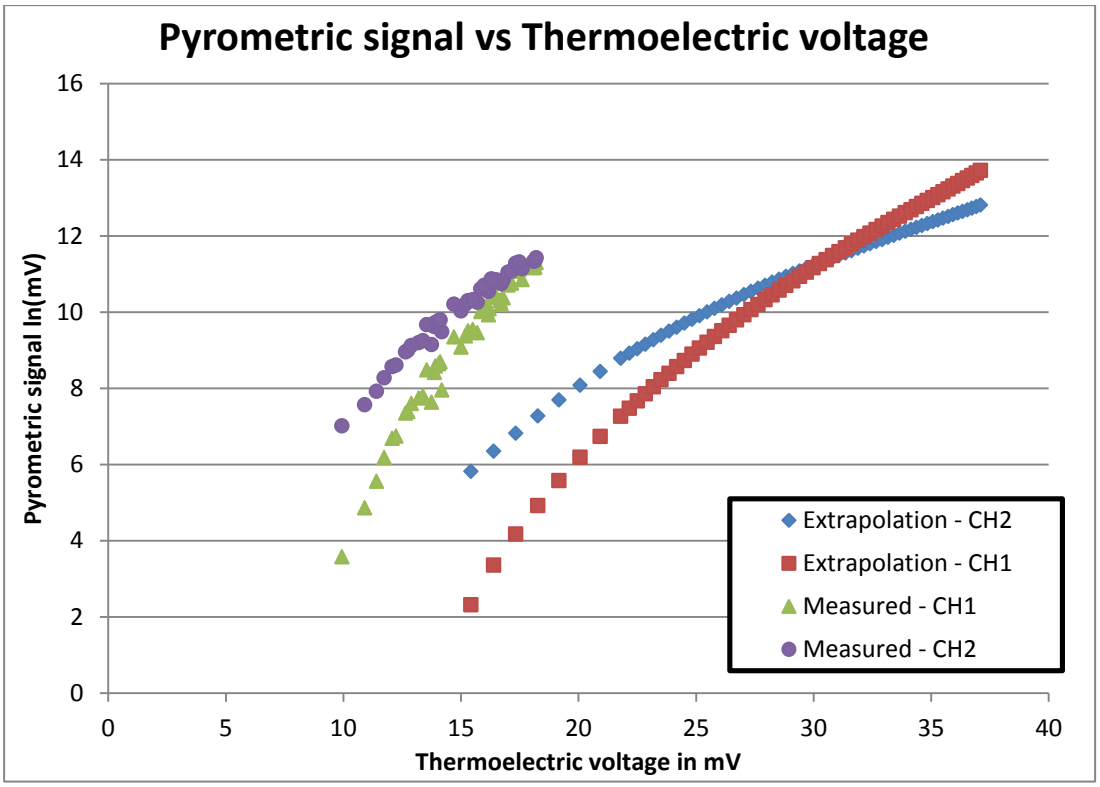

Figure 4.11 : Comparision of test results with the expected results.

It is obvious that thermocouple signals obtained from electrically heated tungsten sheet were not compatible with the reference table for type C thermocouple at all. On the other hand, a linear relation between reference table values and test results was possible to form. As a consequence of linear dependency, measured thermoelectric signals could be directly used to generate relation with average true temperature. Linear correlation was the best curve fitting option for this case. Nevertheless the precision was not sufficient for substitution of calibration function used in pyrometer software. The trial of self-design method results in the fact that using the current state of this method is not precise at this point. In conclusion, application of Wien approximation is the best approach for pyrometric measurements.

4.2.4 Error analysis

The factors that cause error in results can be classified into four subtitles. Firstly, the spectral emissivity values are not highly precise due to the fact that DeVos did not take into account light scattering factor in his calculations. As it is stated before, this may result in error not higher than 2.5 %. The other source of error may be the tungsten sheet alignment. Since it was not possible to position the tungsten sheet perpendicular to the line of fiber sight, the angle factor of 30° was already

implemented into calculation. On the other hand, due to construction of the WMR, electrodes must be bended a bit in order to be able to insert them inside the reactor. This yields non-flat tungsten surface between electrodes and displacement of thermocouple tip from the sheet center. The view angle factor was tried to be eliminated by just looking at the sheet through the observation glass and guessing the real angle value. The sheet position creates an uncertainty on the calculations. In addition to that, before inserting the electrodes with tungsten sheet in between, the thermocouple tip was placed eccentrically from the center in order to achieve to cancel out the bending effect of electrodes. Besides convective effects of Argon gas was neglected, which can also have a little effect on accuracy. For last but not least, it can be estimated that reading of signals from pyrometer and thermocouple might have brought uncertainty into the results. The most drastic part of error was caused by thermoelectric signals. They were not in the same range with the reference values. The reason beyond wrong measuring can be the old thermocouple holding claps. This may result in voltage losses during transmission of electrical signal to the computer.

5. MEASUREMENT CAMPAIGN

5.1 Reactor

The 50kWth entrained flow reactor of the TU München is schematically shown in Figure 6.1. The operation will be described briefly.

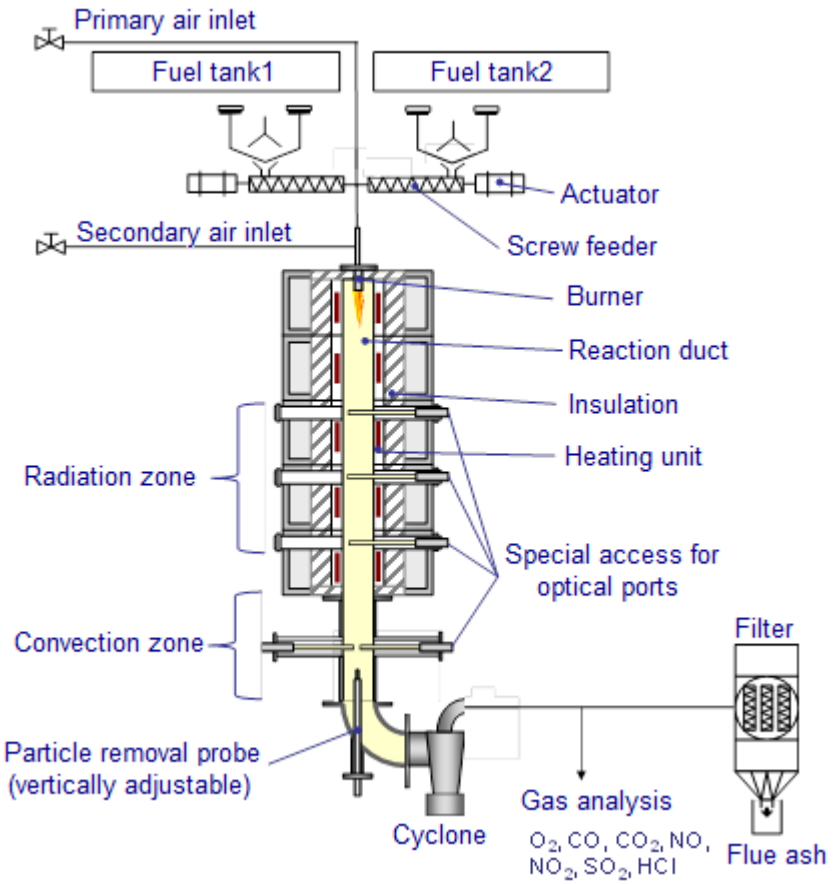

Figure 5.1 : Entrained flow reactor (TUM).

Using the entrained-flow reactor, pulverized fuels under defined combustion compounds (temperature profile, stoichiometry, gas atmosphere, etc.) are burned and the combustion behavior during combustion or fuel-characteristic properties such as slagging, pollution and high temperature corrosion are examined. Test facility consists of an upper zone (radiation zone) and a lower (convection zone), which extends through the reaction tube. In the radiation zone, the reaction tube by using

five superimposed modular-structured heating elements corresponding to a thermal heating power of 10kWth in order to be heated to a maximum temperature of 1600 ° C.

The fuels are fed from the top into the reactor with the aid of two screw feeders via the fuel feed pipe. Here, the system, which can be dosed in an arbitrarily adjustable ratio, has been designed for the simultaneous combustion of two solid fuels. Instead of a fuel, it is also possible to use solid additives such as straw. Each of the two screw feeders consists of a fuel container, a feed screw, a stirrer and optionally a vibration system in order to avoid possible bridging of the fuel particles. The fuels are injected with the aid of the primary air through the fuel feed pipe in the reaction duct. In addition, secondary air is injected perpendicular to the particle flow wise causing a swirling of the particles in order to allow them for the entry into the reaction tube. Then the particles burn during their flow through the reaction tube.

Both horizontally in the radiation zone and in the convection zone of the entrained flow reactor optical ports are arranged to provide access into the reaction tube in order to attach the measuring technique such as pyrometry. In the combustion experiments, it is possible to detect the radiation from particles in the FOV of the pyrometer and record them.

5.2 Setup

The total distance between the center of the reactor and the tip of the probe was determined as 580mm considering the required magnification ratio of 3. With respect to that specific distance, the optical probe of the 2-color pyrometer was positioned and aligned with directly the opposite aperture of the reactor. The window of aperture was cleaned in order to remove chemical salt formation over the window and provide clean sight for the optical fiber mounted at the end of the probe.

After setting the probe, the signal from the fiber was divided into two channels as main and reference. These fiber outlets were attached to the pyrometer at convenient apertures facing directly the photodiodes where electrical signals occur. Then the power source for the pyrometer was turned on.

Then the software, written in Lab-view for that sort of application, was opened. Before start, zero values and half noise amplitudes (HNA) for each channel are

acquired. Although number of samples per channel and sample recording rate are optional features, the rate is restricted with maximum rate of 83333 per channel (250000 in total for 3 channels) because of the computer card capacity.

Before the combustion reactor run, the hardware and software for pyrometric measurement must be ready in order to receive initial data for calculations. After each measurement results were documented under a file named after the date of experiment and important specifications about fuel. After combustion is over, graphs were saved and important notes such as set temperature of reactor, measured particle, experiment time, etc. were written down in a protocol file. Finally, the results were evaluated

5.3 Lab-View Code

The software consists of 10 stages including peak and valley signal finding, particle discrimination, plotting and saving results. At first, peak points are defined by the help of Savitzky-Golay (S-G) approach. In this approach, average value of samples at each channel is calculated for each cluster of data. Depending on HNA values, which are determined in the beginning, threshold coefficients are implemented in order to create criteria for peak and valley point detection at each channel. The multiplication of HNA value and the threshold coefficient is added to S-G average value. When the signal crosses the threshold line, a peak is found.

After finding peak points, the peaks are discriminated. The peaks from both Channel 1 (Visible) and Channel 2 (Infrared) are checked whether they occur in same location at both channels. They must be simultaneous within small tolerance determined. If not, these peak signals are neglected. Then valley points before and after the peaks are checked whether they have same voltage signal without any big deviation. If the peak or valley does not provide the requirements, the peak or valley is set to zero during discrimination and then discarded or cancelled out at this stage. Software accuracy settings (Table 6.1) were kept constant during all experiments.

Table 5.1 : Software settings.

AMPLIFICATION	**LOW**
WRITING INTERVAL	**600**
RATE	**50000**
SAMPLE PER CHANNEL	**5000**
ACCURACY FOR PEAK AND VALLEY DISCRIMIANTION	**--**
CHANNEL 1 (VISIBLE)	**0.1**
CHANNEL 2 (INFRARED)	**0.1**
REFERENCE	**0.05**
ITERATIVE METHOD	**--**
STEP	**0.01**
ACCURACY	**0.001**

Later, average background signals are calculated by using the samples taken for each cluster per channel. By the aid of calibration curve and S-G average values, background temperature is calculated simultaneously with respect to the signal received when no particle in the FOV. The background temperature is found by an iterative method using the ratio of signals from channel 1 and 2, which are denoted as R0i.

In case of a particle in the FOV, particle temperature is determined with an iterative method applying between 750 and 2500°C by subtracting background temperature signals (R0i) from the selected peak signals (Ri) for visible and infrared detectors and taking the ratio of them,.

The selected peak location at channel 1 and 2 must be between peak points of reference channel. The other requirement is the valley point levels before and after the selected peak signal must be close with some tolerance. When the peak satisfies

the conditions, it is detected as a particle. The pyrometric diameter of the particle is calculated by using relevant equation (eq.5.5) with recorded data at particle location.

Once the temperature and the particle is determined, the temperature, time location of the particle and signals; R1, R2, R01, R02 are recorded into a file and the name of this file ends with "_temp" for later analysis. The calculated diameters for channel 1 and 2 and velocity of particles are written into a file that has a name ending with "_diam". Meanwhile the temperature and size values of complying particles are plotted at the end to evaluate results visually.

5.4 Measurement and Results

5.4.1 Evaluation of pyrometer signals

The pyrometer measures the radiation of a particle passing through Field of View (FOV). When there is no particle in the field of view, it captures only the thermal radiation from the hot walls of the chamber of the reactor with the temperature T_b. In case there is another aperture at the opposite side, the pyrometer gets radiation from ambient background. The measured signal for the two wavelengths is denoted by R_{0i} (i = 1, 2). When a particle enters into the FOV, the emitted radiation of the particle comes with the temperature T_p and it is added to the background radiation (Fig.6.2). The signal with a particle present in the FOV is denoted by R_i (i = 1, 2). In Fig.6.3, it is showed how the measured signals are supposed to look like in principle.

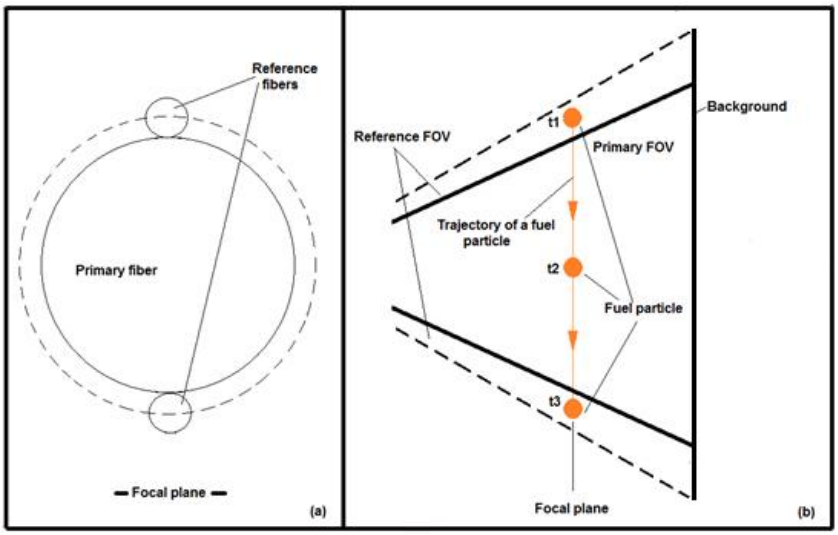

Figure 5.2 : (a) cross-sectional area of fiber bundle, (b) trajectory of a fuel particle in the FOV.

For analytical description of the pyrometer signal, the dimensionless particle area should be defined in the first place.

$$A^* = {A_p}/{A_0} \tag{5.1}$$

where, A_p: projected cross-sectional area of the particle

A_0: cross-sectional area of the FOV in the focal plane.

The signal can be determined by R_i, described as follows [40]:

$$R_i = A^*\varepsilon_P F_i(T_p) + A^*(1-\varepsilon_p)\emptyset(0,\theta_1)F_i(T_b) + A^*(1-\varepsilon_p)\emptyset(\theta_1,\theta_2)F_i(T_b) + (1-A^*)F_i(T_b) \tag{5.2}$$

The ∅ terms on the right side of equation describe the scattered radiation and they are neglected in measurements. Hence, one can write;

$$R_i - R_{0i} = A^*\varepsilon_p[F_i(T_p) - R_{0i}] \tag{5.3}$$

R_i and R_{0i} are measured by pyrometer. Then only T_p and $A^*.\varepsilon_p$ remains unknown. This is the main reason of using ratio pyrometer in our case. By taking ratio of two measurements at different wavelengths, the second unknown term can be eliminated. Therefore, the temperature can be easily calculated with the help of calibration data by leaving T_p alone in the following equation:

$$\frac{R_1-R_{01}}{R_2-R_{02}} = \frac{F_1(T_p)-R_{01}}{F_2(T_p)-R_{02}} \tag{5.4}$$

5.4.2 Particle size calculation

$A^*.\varepsilon_p$ provides the basis for determining the size of a particle. After temperature is set; $A^*.\varepsilon_p$, which gives information about emissivity and the particle size, can be evaluated. The cross-sectional area of the FOV in the focal plane, A_0, is determined via geometric optics. Emissivity is given 0.9 with 10% deviation [6]. Since the projected cross-sectional area of the particle is the only unknown, A_p is derived from eq.5.3. At the end, the diameter is found with 6% error margin by following formula:

$$D_p = 2\sqrt{A_p/\pi} = D_0\sqrt{R_i - R_{0i}/\varepsilon\left[F_i(T_p) - R_{0i}\right]} \quad \textbf{(5.5)}$$

D_0 is the diameter of the FOV.

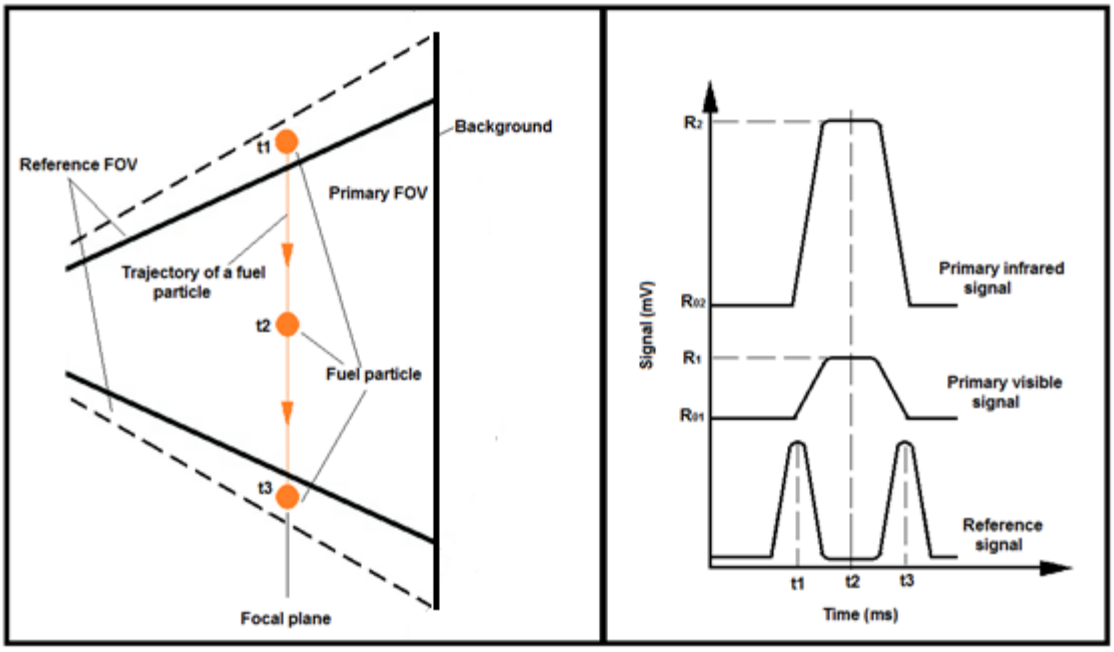

Figure 5.3 : Example of primary and reference signals while a fuel particle passing through the FOV of the optical probe.

This calculation only makes sense when the particle is completely visible in the FOV. To ensure this, reference fiber bundle is implemented into the pyrometer. Basically, this method is based on the use of reference fibers patterned around the main fiber to detect the particle before and after passing through the FOV of the main fiber. When the signals from channels look like as in the Fig.6.3, the particle is accepted to make use of it in particle size calculation. Otherwise the particle is rejected. This is how the Particle Discrimination Procedure (PDP) works.

5.4.3 Results

The straw combustion experiments were made in an entrained flow reactor. The effects of air-fuel ratio, straw type, optical port level and additive effect on temperature and size distribution of the fuel particle were investigated. As a result of first criterion, approximately 3000-4000 fuel particles were detected to determine the temperature. After second criterion (PDP), 1000-2000 of the particles were selected

and the particle size was calculated for them. All the particles which the software let through were plotted.

Following to PDP, other particle elimination was required to obtain more accurate results by eliminating faulty particles that passed both of the criteria. For example, some velocity results exceeded 10m/s, which was very unlikely for a particle to reach in reactor. Additionally, particles that have lower temperature than the set temperature of reactor were omitted. But the lower temperature limit reduced to 1000°C considering non-grayness of straw particles at current spectral ranges. That may deviate the results from real values.

5.4.3.1 Air-fuel ratio

As a fuel, two types of Caliro straw were combusted in the reactor and measurements were held. In the first test simple straw particles burned under same circumstances except air-fuel ratio. Reactor settings are tabulated in table 5.2 and following graphs are obtained.

Table 5.2 : Reactor settings for air-fuel ratio test.

COAL/FUEL	**Straw Caliro**
SET TEMPERATURE	**1100 °C**
MASS FLOW (fuel)	**1150 g/h**
LAMBDA	**1.6 / 2.0**
OPTICAL PORT LEVEL	**Upper**
ADDITIVE	**No**

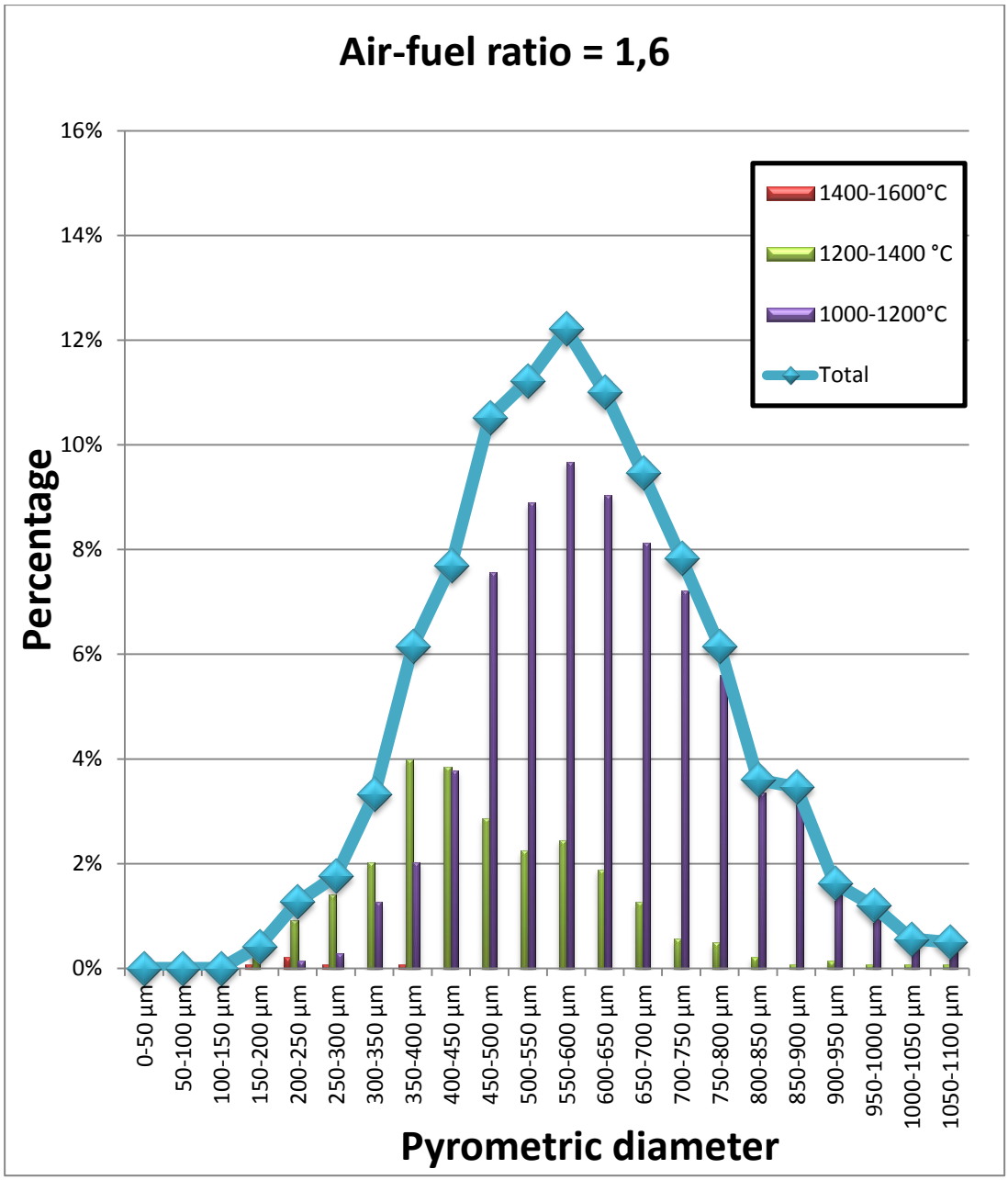

Figure 5.4 : Pyrometric particle size distribution for air-fuel ratio 1.6.

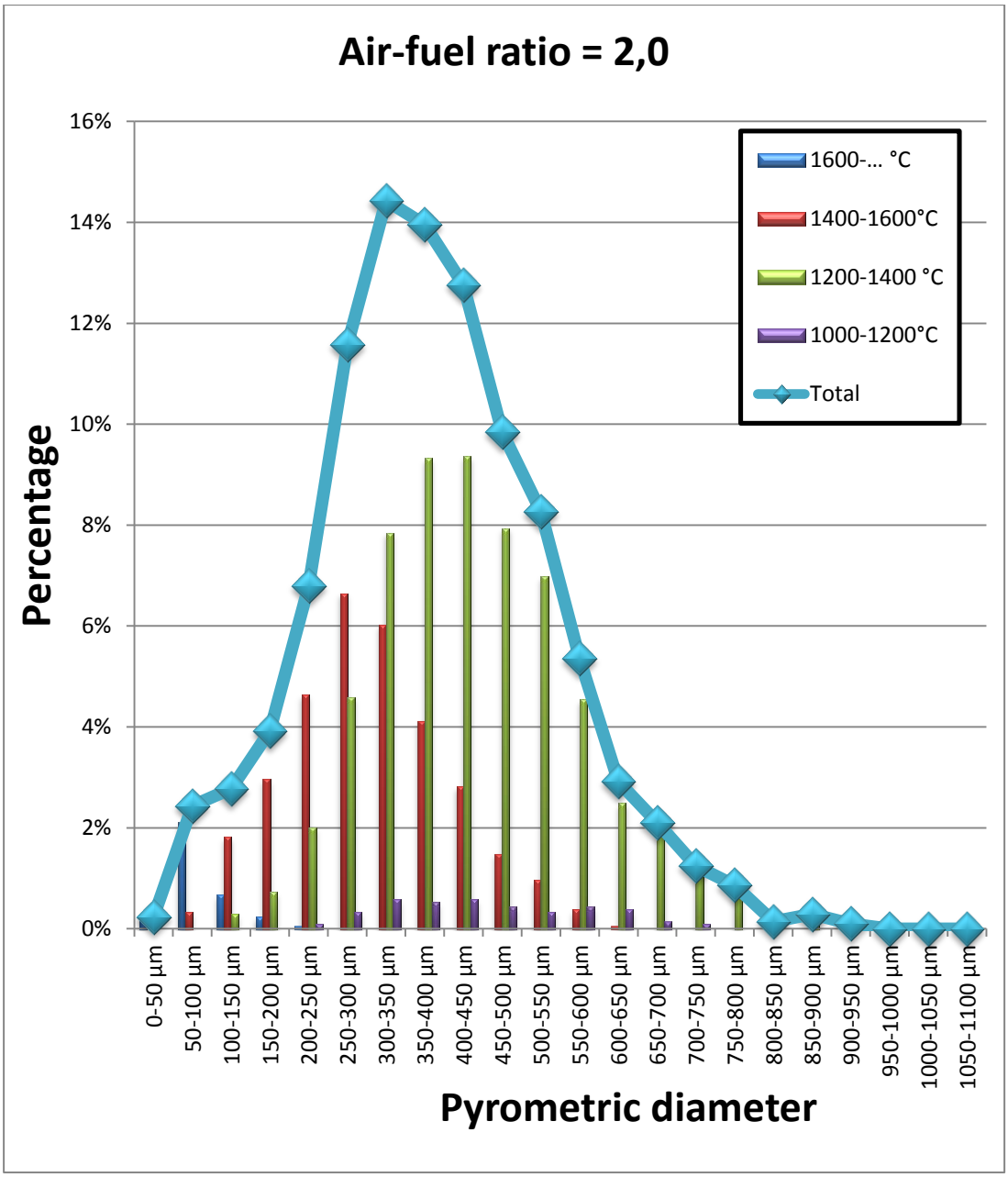

Figure 5.5 : Pyrometric particle size distribution for air-fuel ratio 2.0.

Each color represents different temperature range of particles. As it is seen in the figures above, particles combusted with less air have lower temperatures. In addition, particle size distribution shifts to the smaller diameter zone while air-fuel ratio is increasing. This can also be observed from the following table. In the experiment with less air, the ratio was set to 2.0 in the beginning. Right after start, it was dropped to 1.6. Hence it was proved that the results were reproducible by taking into account the experiment dates stated in the table 5.3.

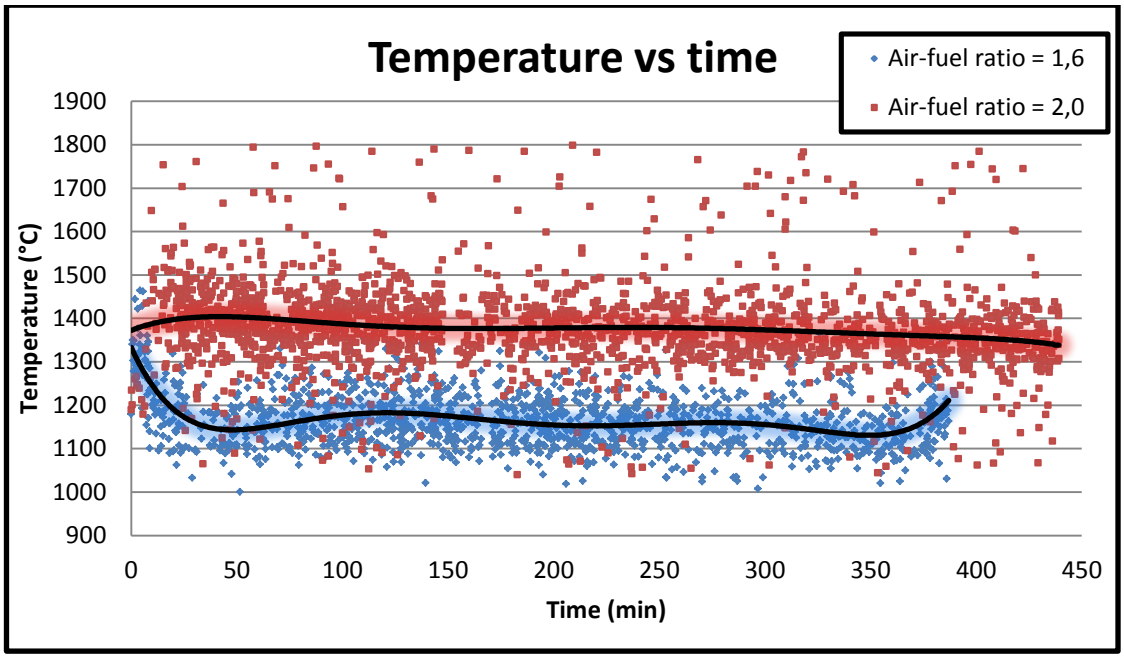

Figure 5.6 : Temperature vs time for air-fuel ratio test.

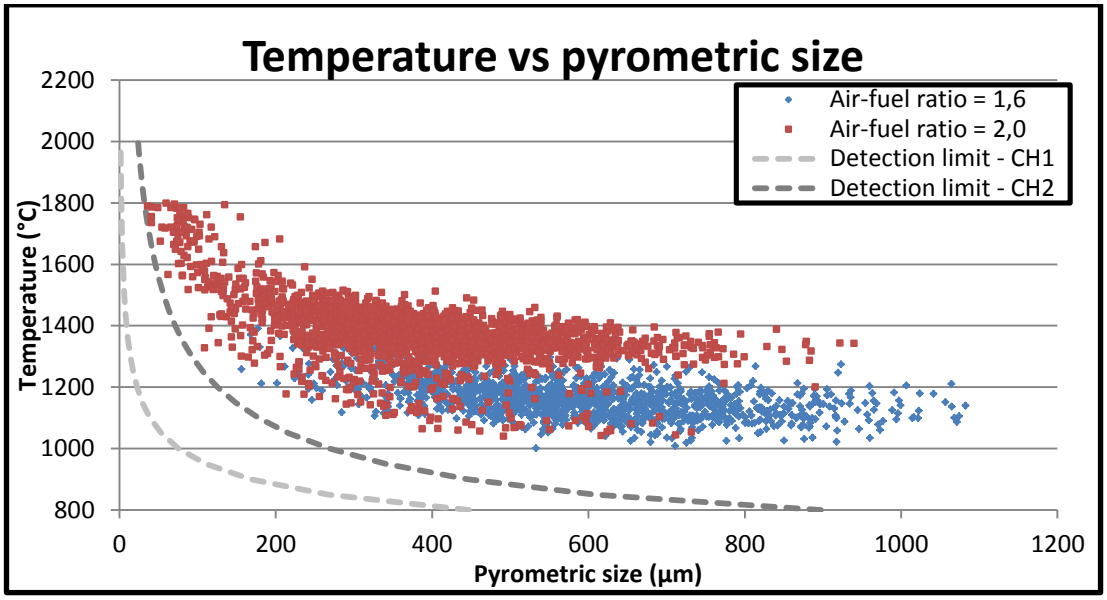

Figure 5.7 : Temperature vs pyrometric size for air-fuel ratio test.

By substituting background signals into the eq.5.3 or eq.5.5, minimum computable particle diameter can be determined at both channels. As a coalescence of the minimum pyrometric diameter values, detection limit curves are derived. Since detection limit of channel 2 is the largest in every test, detection limit curves of infrared channels are used from now on. The detection limit gets considerably affected by the background signal levels. Since background signals were close to each other for air-fuel ratio test, same detection line applied.

Table 5.3 : Results of air-fuel ratio test.

	Temperature (°C)		Pyrometric diameter (µm)		Date of test	Duration of test (min.)	Amount of detected particles
	Average	***Std. Dev.***	***Average***	***Std. Dev.***			
Air- fuel ratio = 1.6	1166.20	64.37	588.65	167.7	25.04.12	387	1416
Air- fuel ratio = 2.0	1378.52	101.15	386.74	147.1	01.05.12	439	2092

The reason behind can be that there was not enough oxygen for all the particles to burn, when the air-fuel ratio is 1.6. Therefore 74% of detected particles remained at temperature around reactor set temperature, 1100°C. Considering emission results, this inference is also valid. Although both tests lasted for approximately same duration, 25% more particles were detected in the combustion with air-fuel ratio of 2.0. That also proves the previous statement about lower reactivity of straw particles in lower oxygen case. As a result of previous test, the air-fuel ratio was fixed to 2.0 during the rest of experiments.

5.4.3.2 Optical port level

It was also tried to see the effect of optical port level on results. When the optical probe moved to the lower port, this change enabled to observe the relatively later stages of combustion and compare the results with temperature and pyrometric size distribution obtained from upper port.

Table 5.4 : Reactor settings for optical port level test.

COAL/FUEL	**Straw Caliro**
SET TEMPERATURE	**1100 °C**
MASS FLOW (fuel)	**1150 g/h**
LAMBDA	**2.0**
OPTICAL PORT LEVEL	**Lower / Upper**
ADDITIVE	**No**

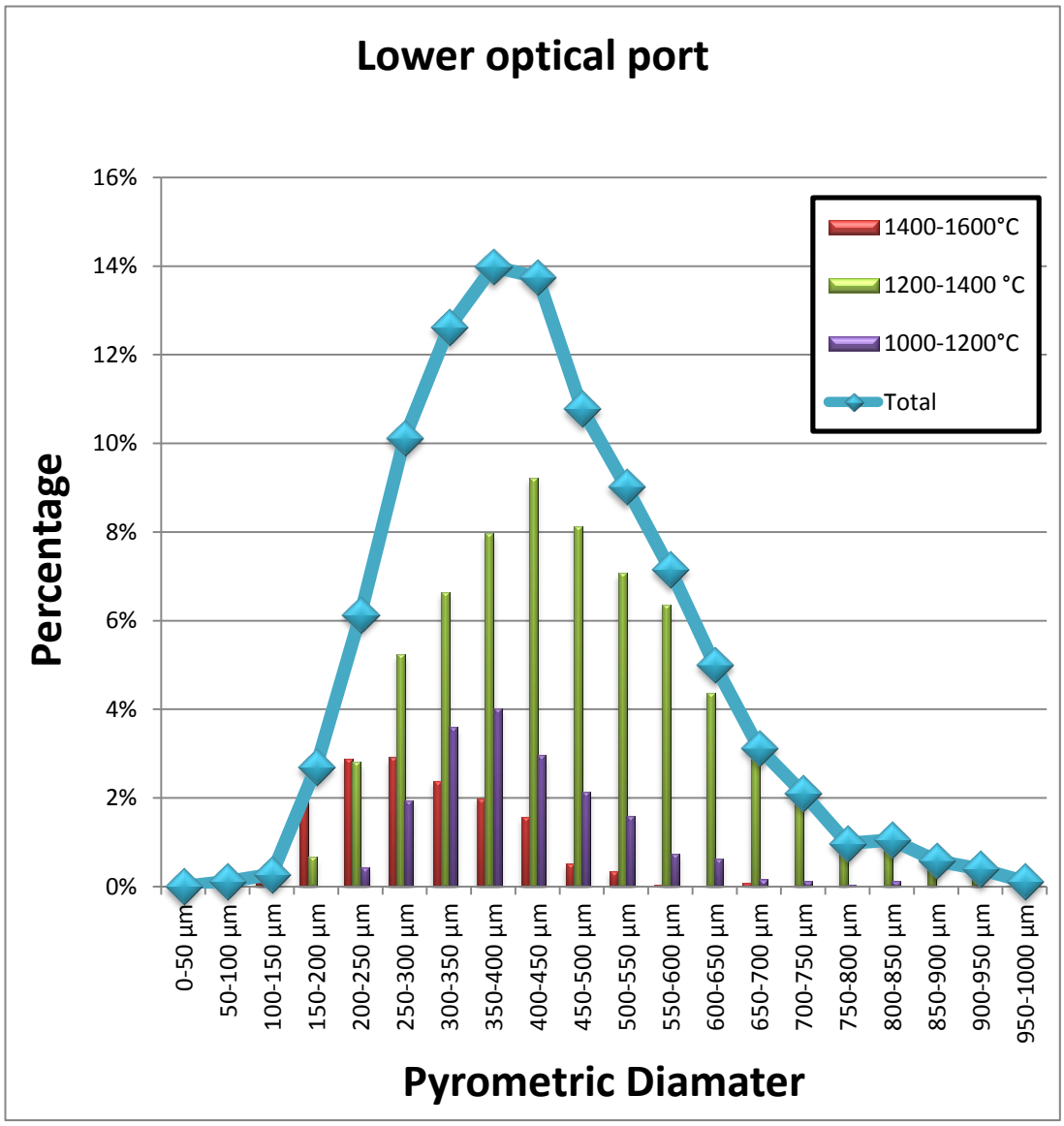

Figure 5.8 : Pyrometric particle size distribution obtained through lower optical port.

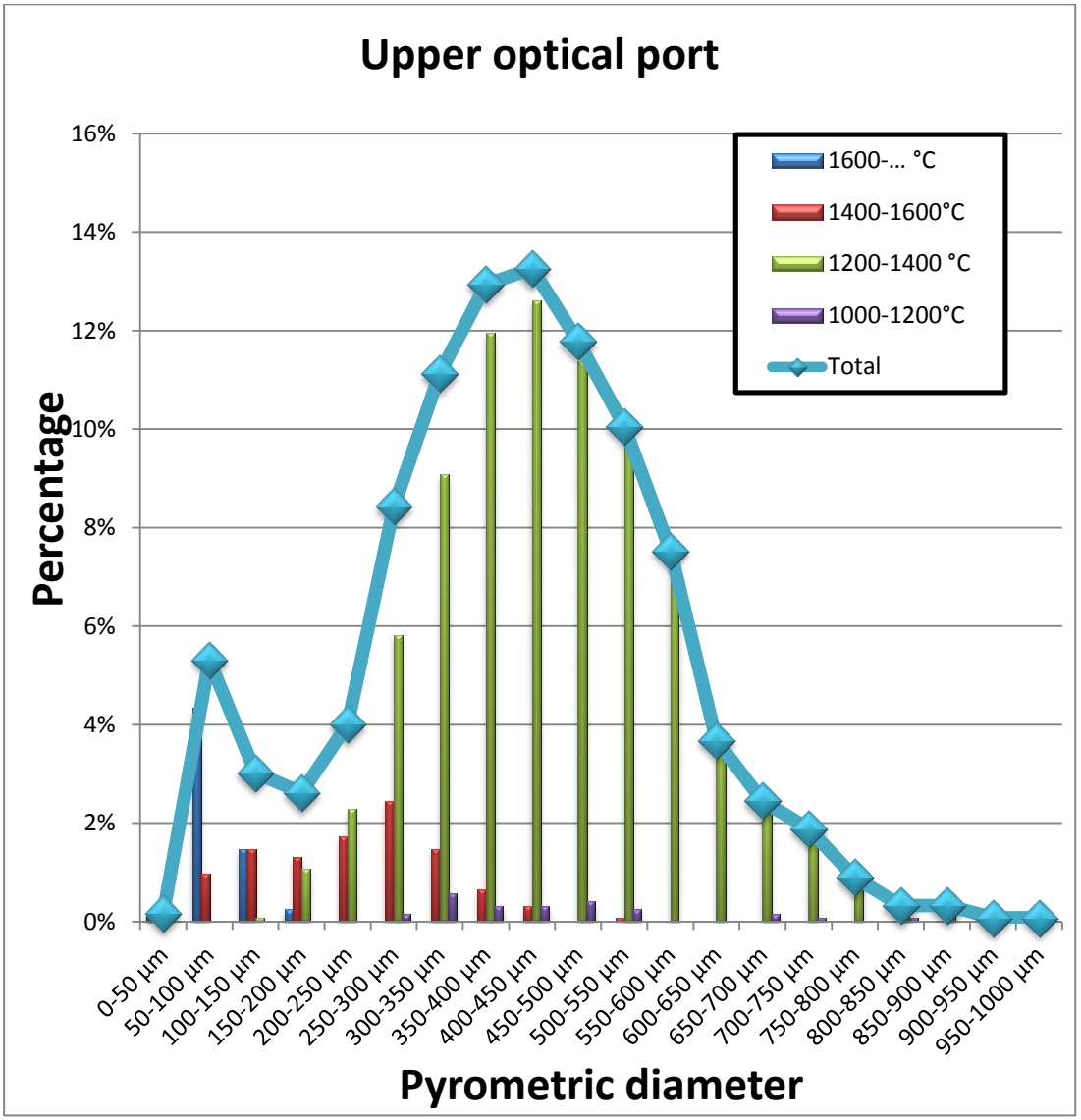

Figure 5.9 : Pyrometric particle size distribution obtained through upper optical port.

As it is seen, small particles in upper port level test do not exist in lower port level test results. That means small particles are totally burned out before reaching to the lower zones.

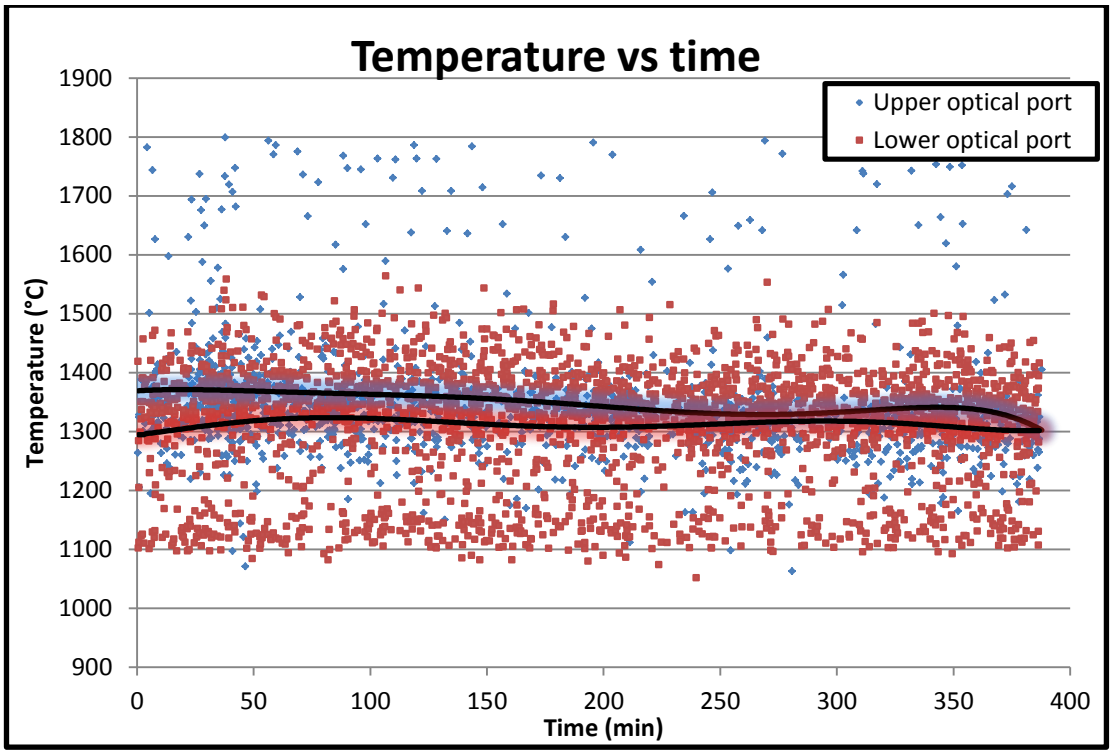

Figure 5.10 : Temperature vs time for optical port level test.

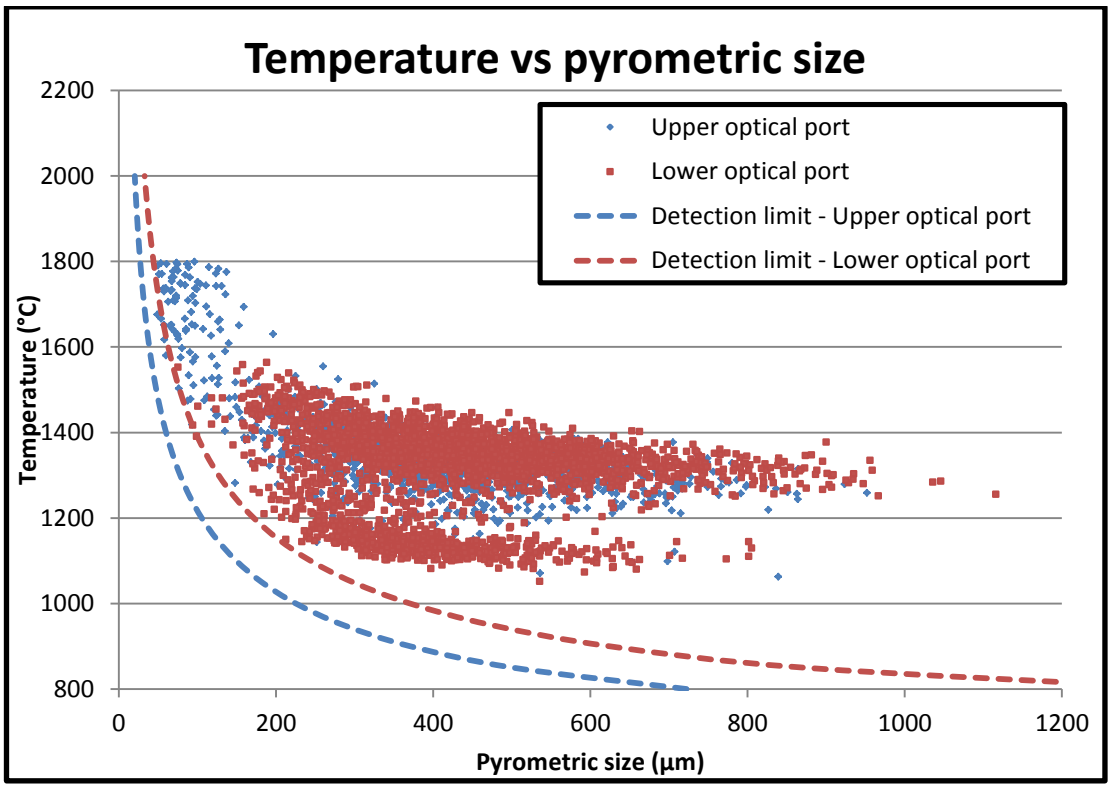

Figure 5.11: Temperature vs pyrometric size for optical port level test.

Table 5.5 : Results of optical port level test.

	Temperature (°C)		Pyrometric diameter (µm)		Date of test	Duration of test (min.)	Amount of detected particles
	Average	Std. Dev.	Average	Std. Dev.			
Lower optical port	1312.65	100.38	432.56	150.8	14.05.12	387	2564
Upper optical port	1351.65	114.37	404.99	160.8	02.05.12	388	1222

Also overall particle temperature decreases in the lower optical port test regarding the fact that later stages of combustion take place in that zone.

5.4.3.3 Fuel type

The other parameter that affects the combustion is fuel type. During experiments, the fuel used in combustion was changed with the one which contains more sulfur than previous type of straw. By adding sulfur into a fuel, it is expected that would provide less corrosive atmosphere for reactor components. Hence it was tried to see the pyrometric particle size distribution of different straw types in terms of sulfur content.

Table 5.6 : Reactor settings for fuel type test.

COAL/FUEL	**Straw Caliro / Caliro with more sulfur content**
SET TEMPERATURE	**1100 °C**
MASS FLOW (fuel)	**1150 g/h**
LAMBDA	**2.0**
OPTICAL PORT LEVEL	**Lower**

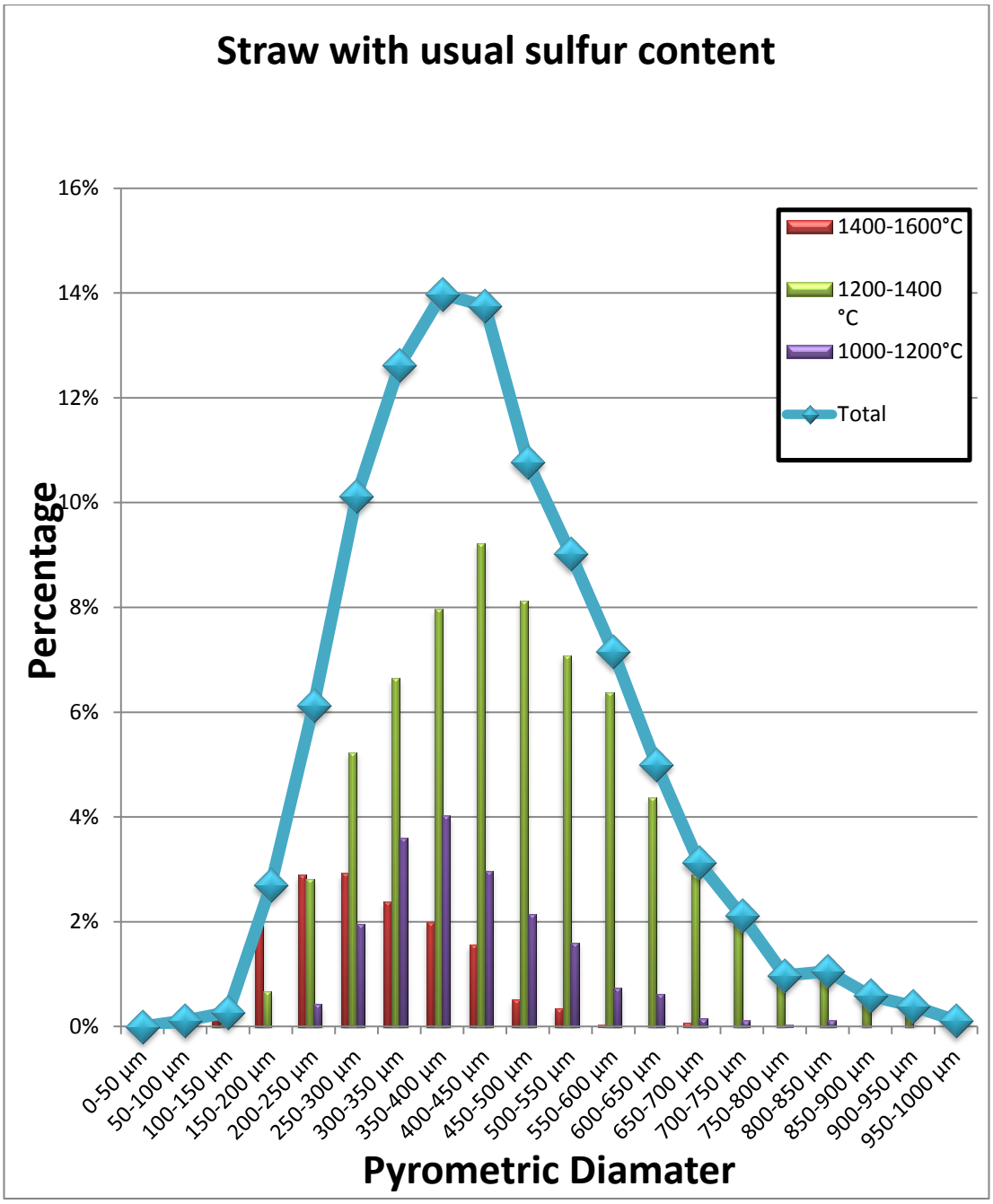

Figure 5.12 : Pyrometric particle size distribution resulting from combustion of straw with usual sulfur content.

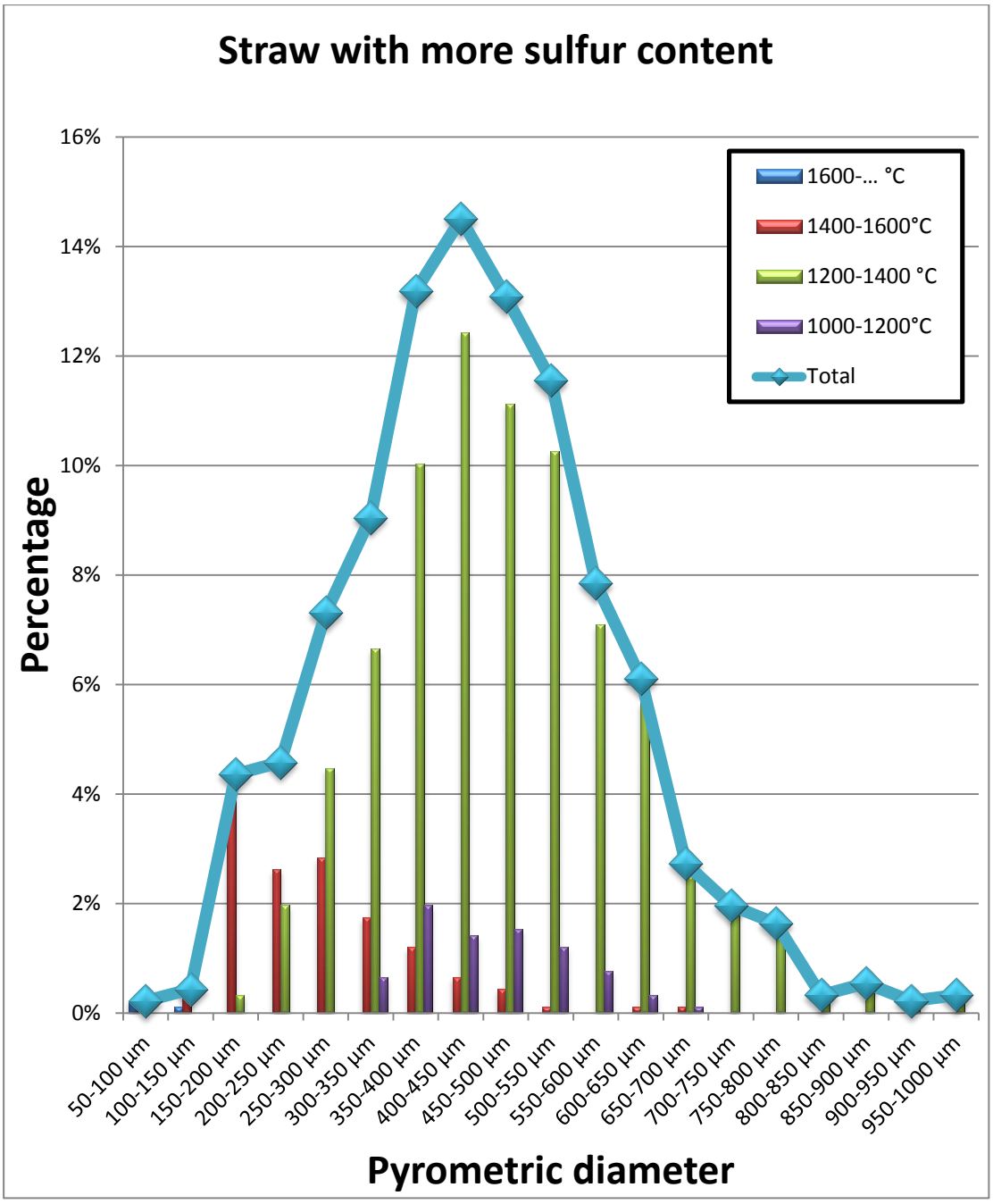

Figure 5.13 : Pyrometric particle size distribution resulting from combustion of straw with more sulfur.

According to figure above sulfur does not have big influence on combustion of straw. Particle distribution remains approximately same over temperature bands.

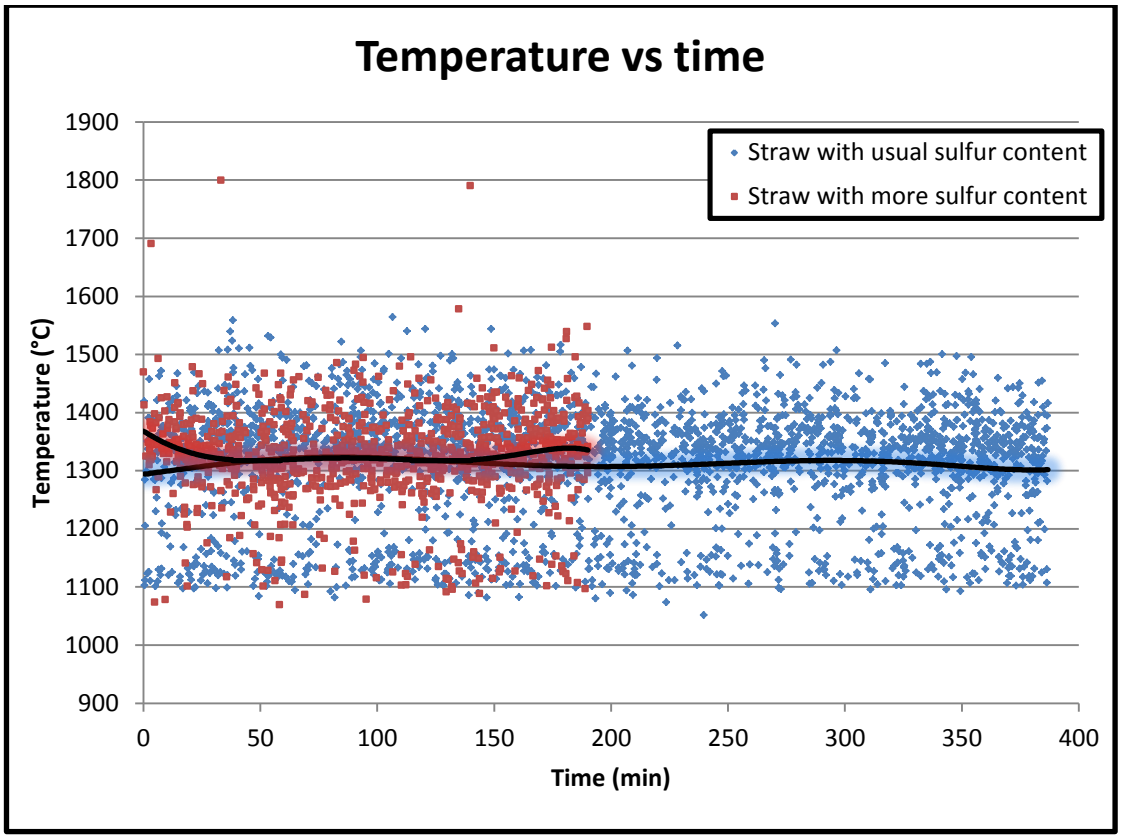

Figure 5.14 : Temperature vs time for fuel type test.

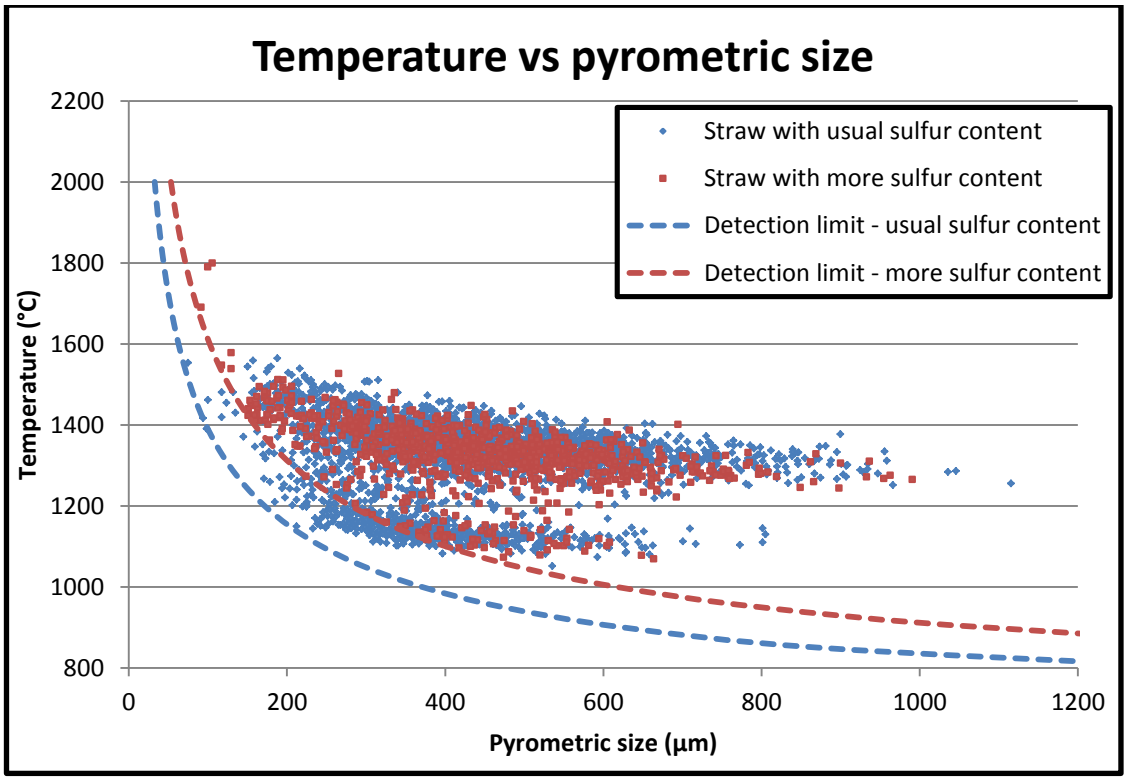

Figure 5.15 : Temperature vs pyrometric size for fuel type test.

Table 5.7 : Results of fuel type test.

	Temperature (°C)		Pyrometric diameter (µm)		Date of test	Duration of test (min.)	Amount of detected particles
	Average	Std. Dev.	Average	Std. Dev.			
Usual sulfur content	1312.65	100.3	432.56	150.8	14.05.12	387	2564
More sulfur content	1325.32	83.61	443.86	148.1	15.05.12	191	917

By examining results, it can be said that average temperatures are very close in both tests. Additionally pyrometric diameter distribution shifts to the larger sizes. On the other hand, amount of detected particle decreased 25% in combustion of Caliro straw with more sulfur content. Thus enhancement of sulfur fraction might have influence on the combustion rate of straw accounting amount of particles that react as well.

5.4.3.4 Kaolin addition

It is sometimes required to put additives into the fuel for sake of the reactor life. To prevent corrosion, Kaolin powder was added into fuel before combustion as a corrosion reducer. The measurement was held against combustion of fuel including Kaolin in order to see whether this additive would have an effect on the results. As a result following figures were derived from measurement results.

Table 5.8 : Reactor settings for effect of Kaolin test.

COAL/FUEL	**Straw Caliro with more sulfur content**
SET TEMPERATURE	**1100 °C**
MASS FLOW (fuel)	**1150 g/h**
LAMBDA	**2.0**
OPTICAL PORT LEVEL	**Lower**
ADDITIVE	**Kaolin**

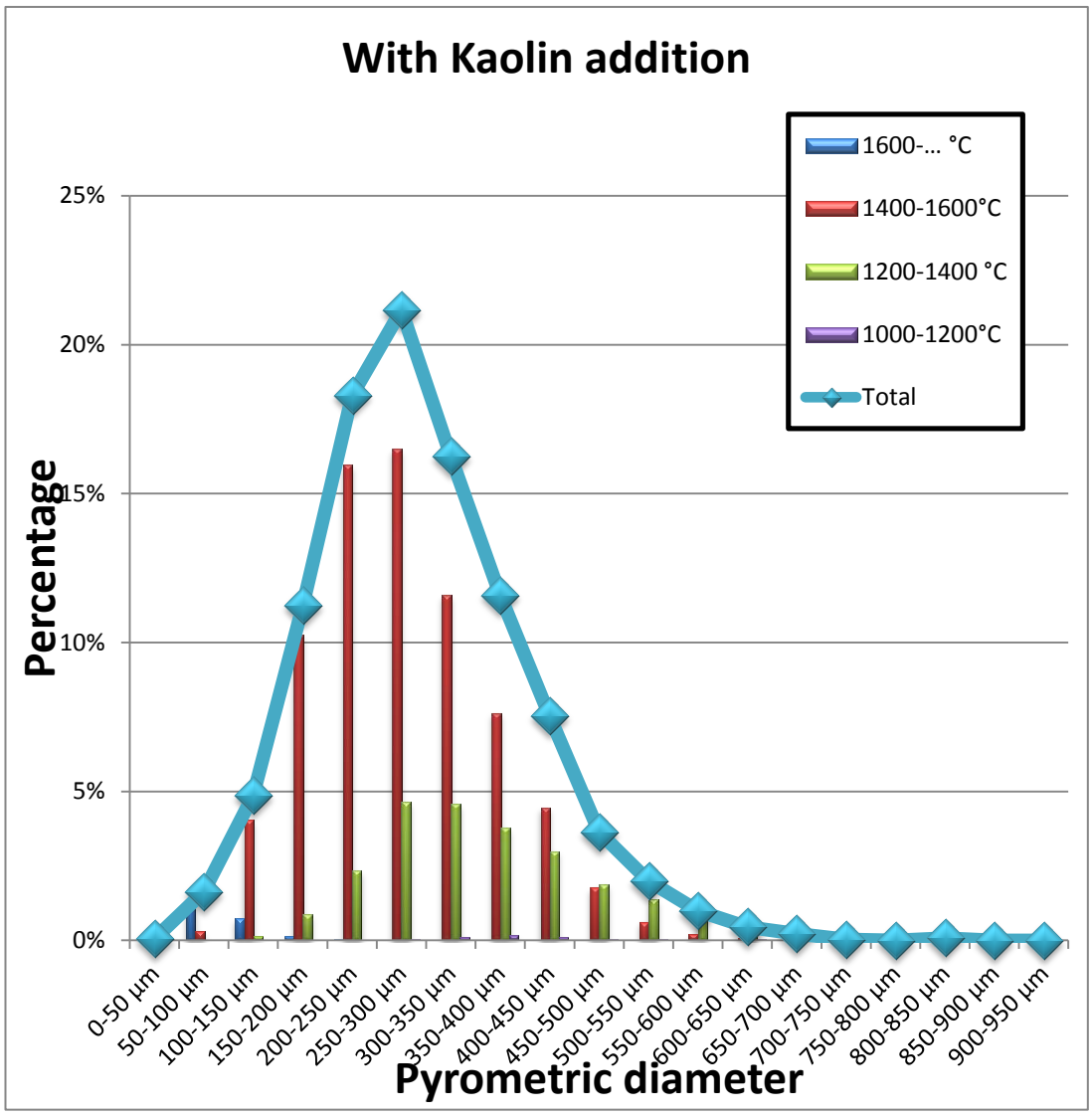

Figure 5.16 : Pyrometric particle size distribution obtained from combustion of straw particles with Kaolin additive.

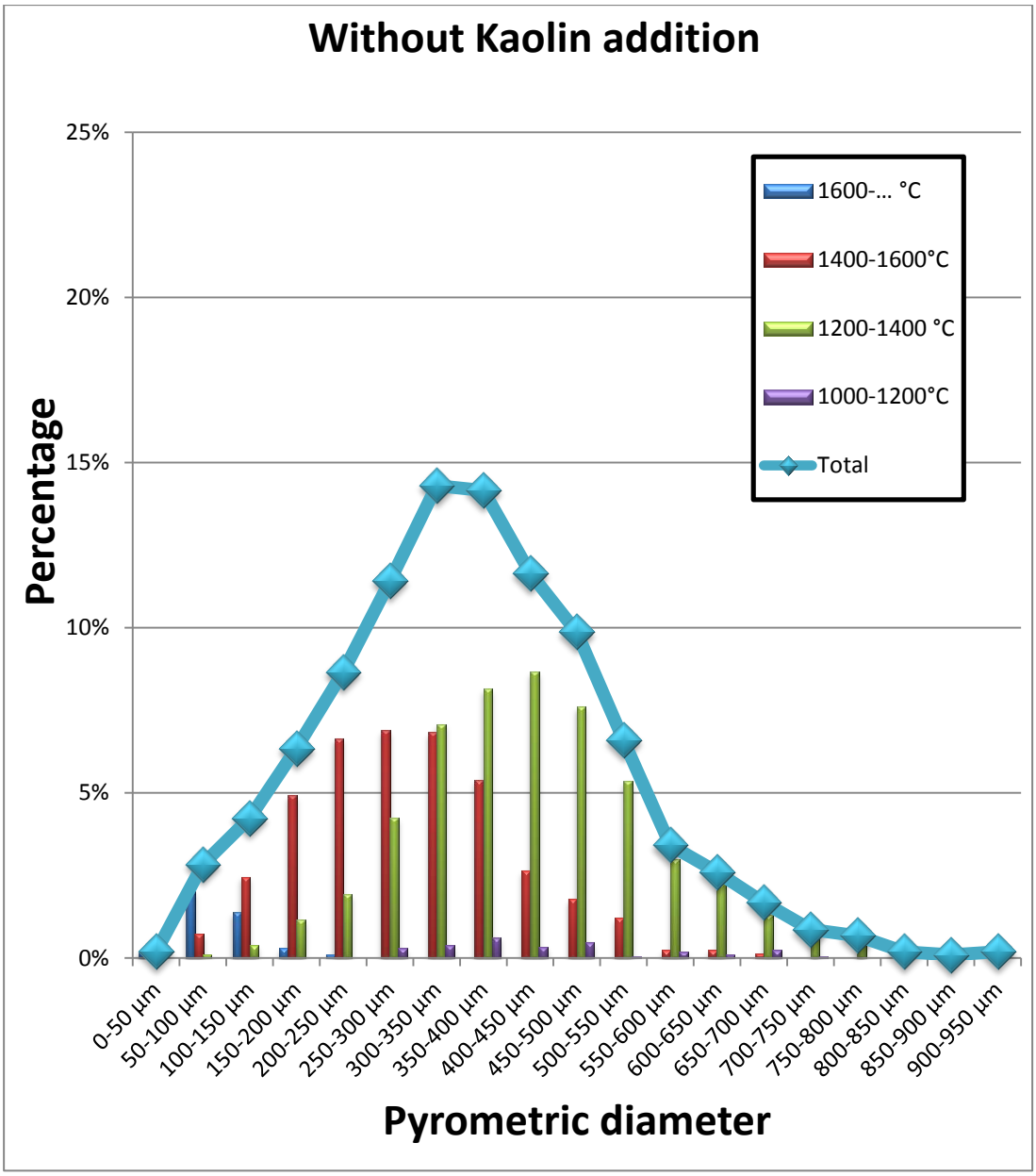

Figure 5.17 : Pyrometric particle size distribution obtained from combustion of straw particles without Kaolin additive.

Number of straw particles passed through discrimination procedure goes up with Kaolin addition. Kaolin addition doubled the detected particle amount. On the other hand, average particle diameter reduces. Particles with Kaolin may be burning later than the particles without addition. It is highly possible that some of the detected particles are Kaolin particles. Since they are not burning, they might have interacted with burning particles thermally and have reached to their temperatures. So they were detected like burning particles.

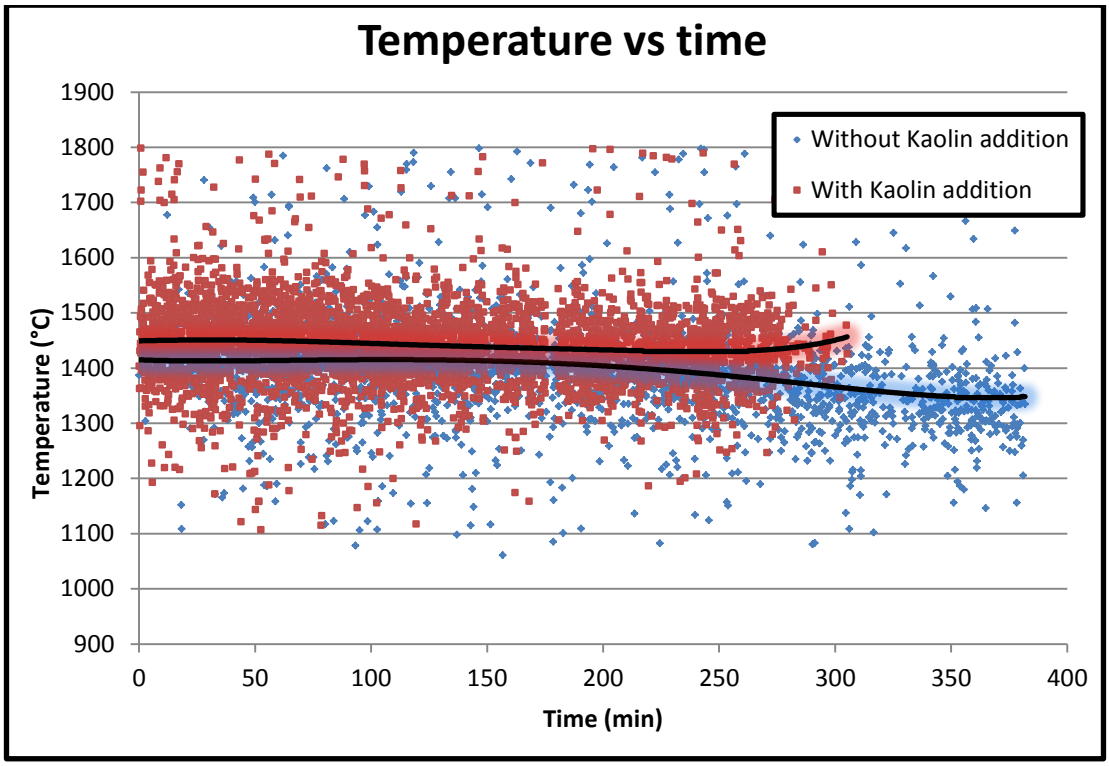

Figure 5.18 : Temperature vs time for Kaolin addition test.

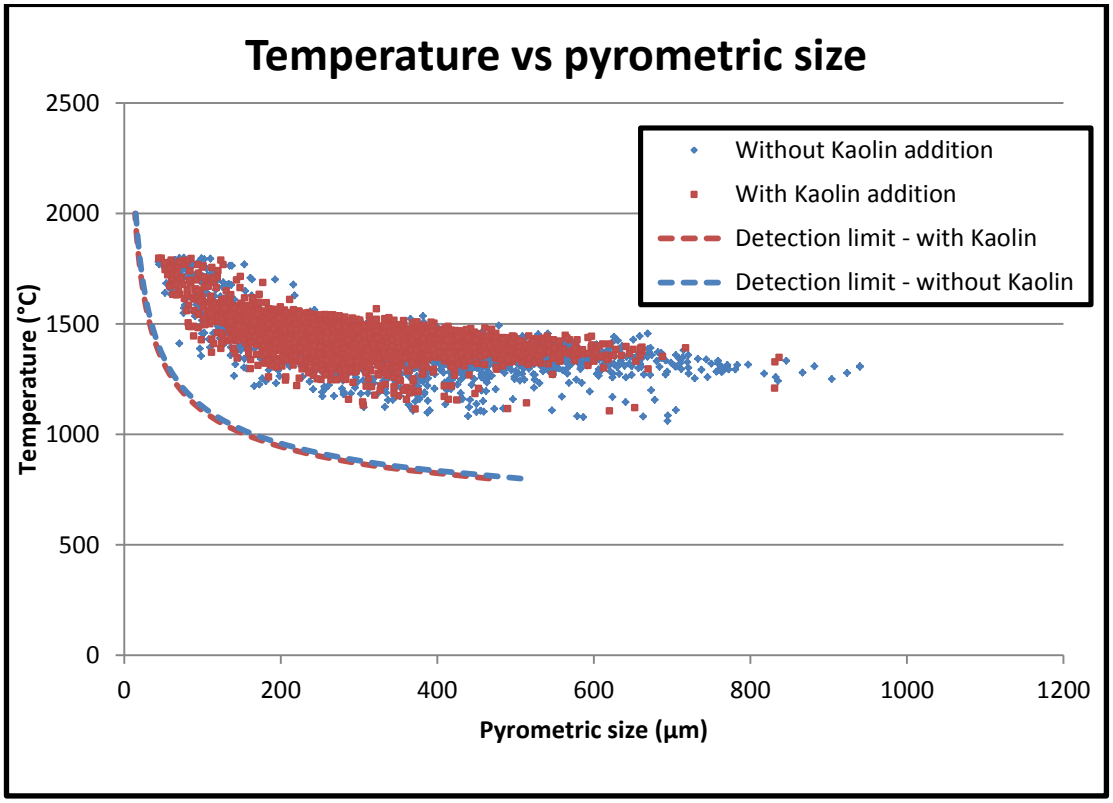

Figure 5.19 : Temperature vs pyrometric size for Kaolin addition test.

Table 5.9 : Results of Kaolin addition test.

	Temperature (°C)		Pyrometric diameter (µm)		Date of test	Duration of test (min.)	Amount of detected particles
	Average	Std. Dev.	Average	Std. Dev.			
With Kaliro addition	1441.73	74.04	293.294	104.0	24.05.12	305	4049
Without Kaliro addition	1395.11	103.68	363.30	147.3	17.05.12	382	2077

Besides the fact that Kaolin particles are detected as straw by the pyrometer, Kaolin also has an increasing effect on temperature of particles considering the measurements. Also Kaolin might be showing different emissivity characteristics. So this can lie behind the smaller pyrometric size distribution of detected particles.

5.4.3.5 Filter element cleaning

One of the most problematic issues during reactor runs was filter element. When the filter element does not provide proper suction, It directly results in performance drop of the combustion reactor. So the filter element should be cleaned in case of low suction. The combustion before and after filter cleaning was also studied to assess the importance of filtering element.

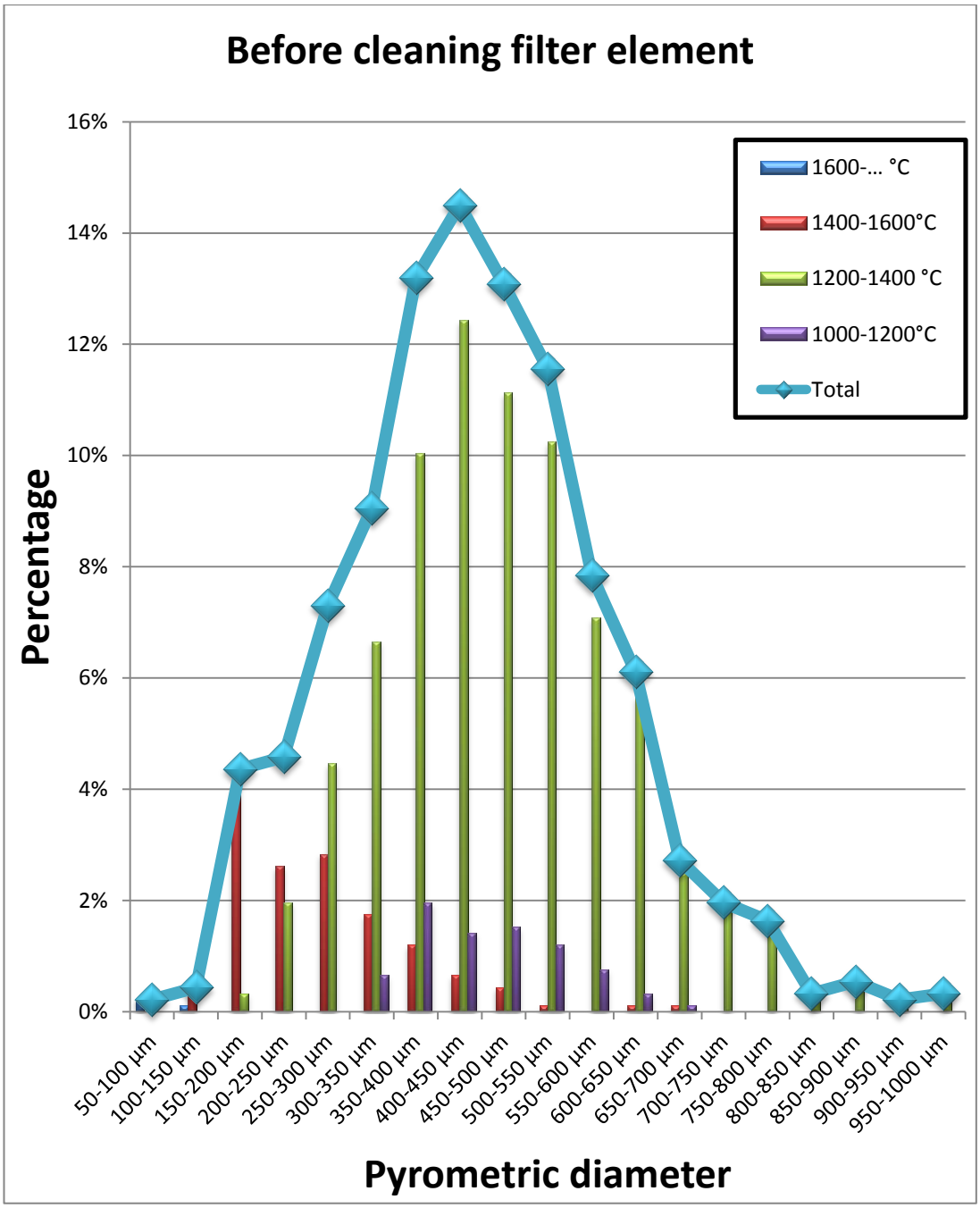

Figure 5.20 : Pyrometric particle size distribution before cleaning the filter element.

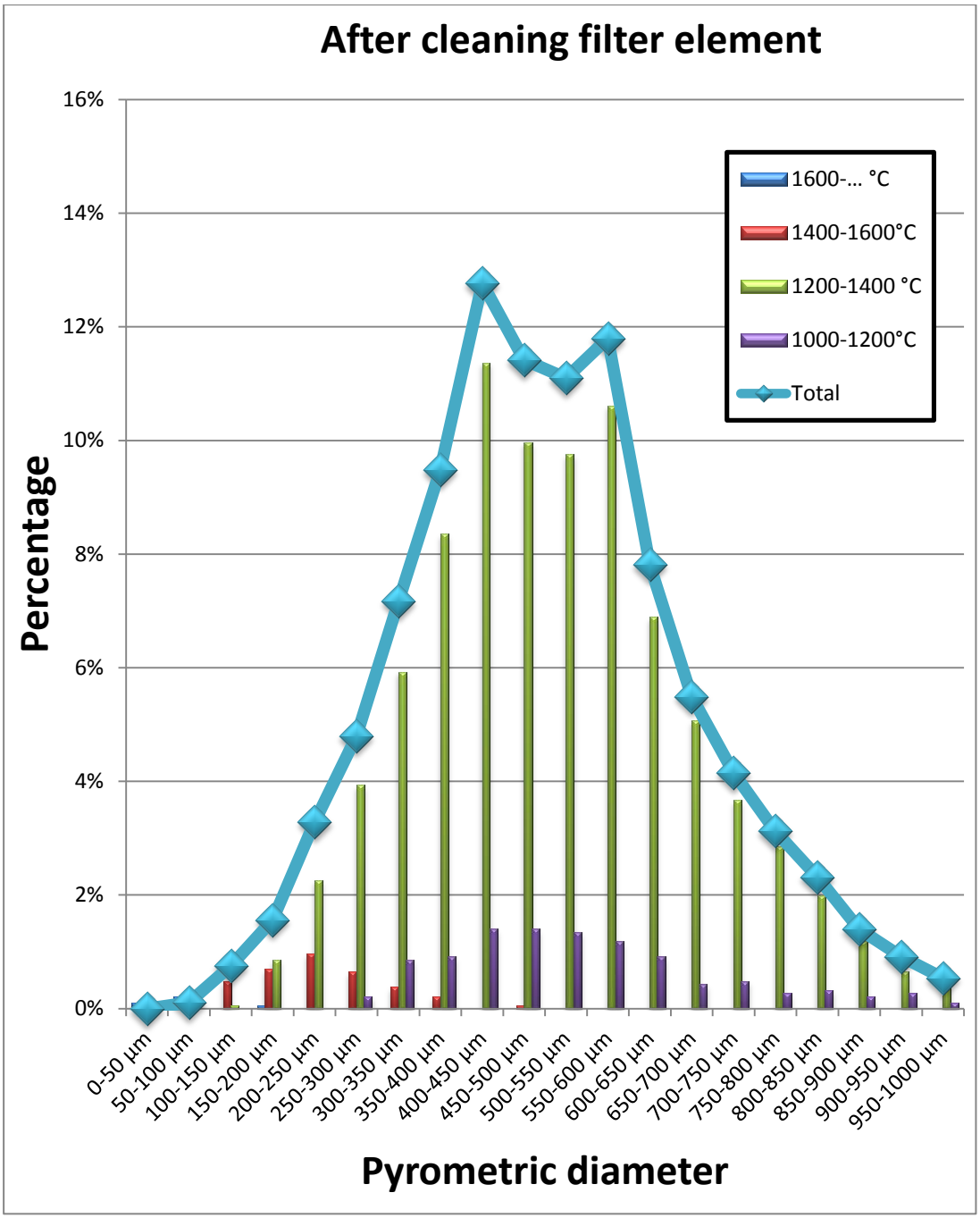

Figure 5.21 : Pyrometric particle size distribution after cleaning the filter element.

Although particle size distribution remains approximately same, detected particles 50% increased after cleaning the filter element. Cleaning filter element improves gas suction and leads to better combustion conditions.

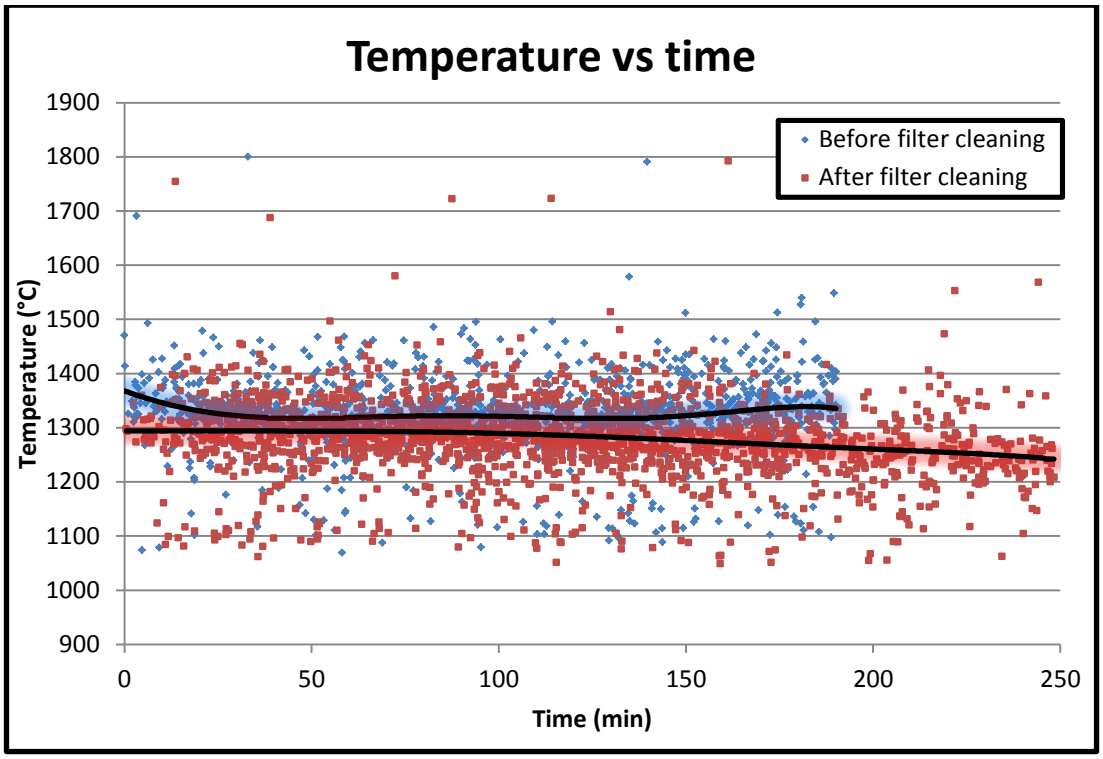

Figure 5.22 : Temperature vs time for filter element cleaning test.

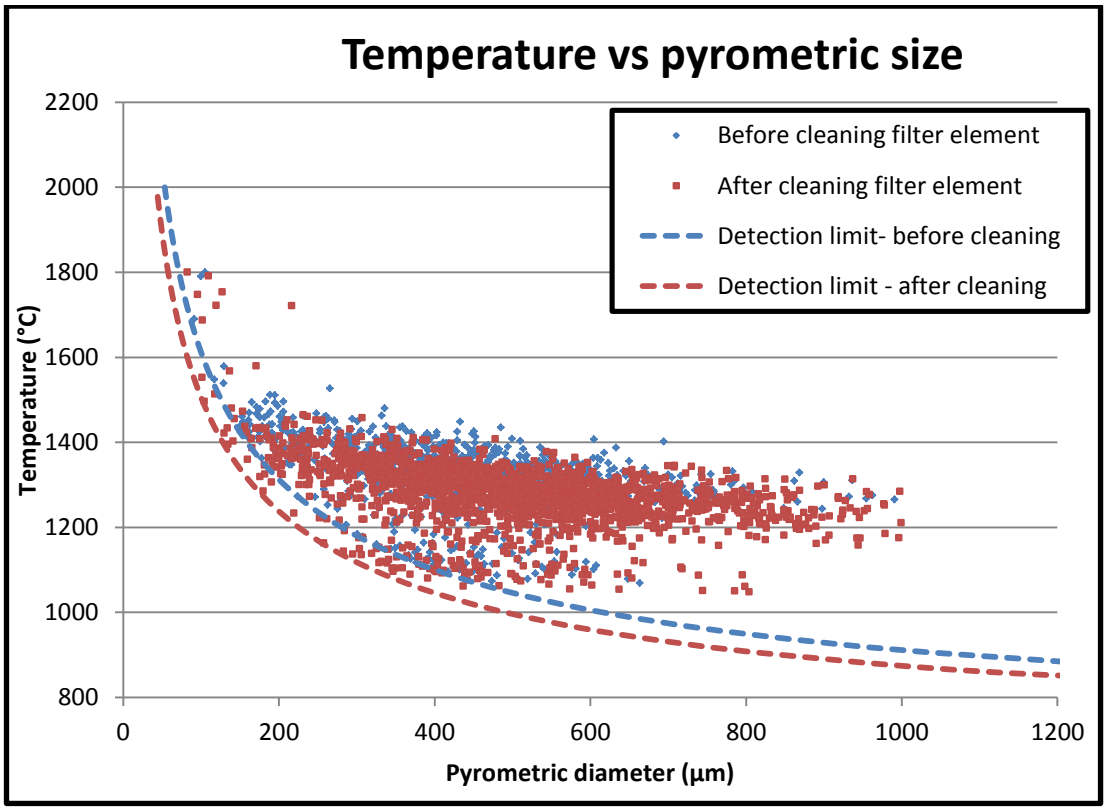

Figure 5.23 : Temperature vs pyrometric size for filter element cleaning test.

Table 5.10 : Results of filter element cleaning test.

	Temperature (°C)		Pyrometric diameter (µm)		Date of test	Duration of test (min.)	Amount of detected particles
	Average	Std. Dev.	Average	Std. Dev.			
Before filter cleaning	1325.32	83.61	443.86	148.1	15.05.12	191	919
After filter cleaning	1281.95	75.03	502.73	165.6	16.05.12	248	1856

With respect to temperature and pyrometric size change by time, Temperature level decreases 40°C, while mean particle diameter increases 60µm.

6. CONCLUSIONS AND FUTURE WORKS

A non-contact method has been developed to measure the temperature and size of an individual fuel particle with the technique of 2-color pyrometry. To be able to deliver reproducible and quantitative results, the pyrometer has to be calibrated against a black body radiator ($\varepsilon \approx 1$). The calibration was performed, due to material limitations of the radiator, up to 1200°C and recorded calibration data were extrapolated for higher temperatures by utilizing Wien's radiation law. In order to achieve calibration of the instrument for higher temperature ranges without mathematical extrapolation, which introduces errors in the measurements, a radiative calibration cell has been design. The calibration cell employs a tungsten sheet that can be electrically heated up to 2300°C. The radiative cell has been designed using an available rig (WMR) to spare time; this solution proved to be feasible but delivered too inaccurate results based on the fact that the set-up was not healthy at the time of the tests. Applying some small changes in the set-up, such as including better thermocouple holding element, proper positioning of the tungsten sheet and elimination of viewing angle factor, the radiative calibration cell can be improved to deliver proper calibration results.

The optical instrument was also successfully tested during several measurements with various combustion conditions in the entrained flow combustion reactor of Institute of Energy systems at TU München. These experiments were carried out with Caliro straws to investigate effects of combustion conditions and fuel type on fouling formation and deposition related corrosion phenomena. The results of the 2-color pyrometer are in accord to the experience; for example it has been found out that the combustion temperature of straw lowers with reduced air to fuel ratio due to the fact that less oxygen is available to complete the oxidation reaction. The measurements have also showed to be one effective monitoring tool for the overall process (velocity of the particle, irregular fuel feeding, etc.). Another interesting aspect of this technique is that, since the reactor allowed more than one level of optical access, the measurement has been carried out at different height, having the

same reactor's boundary conditions, which provided the temperature and size history of the particle population during their way through the reactor. Eventually sulfur and Kaolin addition to the fuel have been investigated showing considerable effects observed on pyrometric size and temperature distribution of burning straw particles; despite the unknown emissivity of Kaolin particles can be an uncertainty in the size determination.

It has been noticed that after prolonged measurement (several hours), the average particle temperature drops which leads to larger particle size measurement. This can be explained by the fact that the inner temperature of pyrometer is increasing (elevated room temperature due to the reactor) determining a change in the sensitivity of photodiodes. This inconvenience can be avoided by implementing a cooling system into the pyrometer.

Due to the high amplification gain, sometimes the signals were saturated at 10V, which is the limit of the digital converter. In order to fix this, the primary amplification on the detectors can be lowered. In that case, the pyrometer must be calibrated again.

Unfortunately no size distribution data of the starting fuel were available at the moment of the measurement and it is planned to run a test with an inert reference material (Al_2O_3 spheres) whose particle size distribution is known in order to validate the measurement of the pyrometer.

REFERENCES

[1] **Idris, M.** (2004). Two-Colour Pyrometer Technique for Coal-Particle Temperature Measurements in a Pulverised Coal Flame, PhD thesis, RWTH Aachen

[2] **Godoy, S. M. and Lockwood F. C.** (1998). Development of a two-colour infrared pyrometer for coal particle temperature measurements during devolatilisa-tion, Fuel Vol. 77, No. 900, pp. 995-999

[3] **Gruner, K.** (2003). Principles of Non-Contact Temperature Measurement, Rev.B, Raytek GmbH

[4] **IMPAC Infrared GmbH** (2004). *Pyrometer Handbook: Non-Contact Thermometry*

[5] **Branstetter, J. B.** (1966). Some practical aspects of surface temperature measurement by optical and ratio pyrometers, National aeronautics and space administration

[6] **Joutsenoja, T**. (1998). Pyrometric Thermometry and Sizing of Fuel Particles in Combustion, PhD thesis, Tampere University of Technology

[7] **Levendis, Y. A., Estrada, K. R., and Hottel, H. C.** (1992). Development of multicol-or pyrometers to monitor the transient response of burning carbonaceous particles. Rev. Sci. Instrum. 63 (7)

[8] **Reichelt, T., Joutsenoje, T., Spliethoff, H., Hein K. R. G., Hernber R.** (1998). Characterization of burning char particles under pressurized conditions by simultaneous in situ measurement of surface temperature and size. Twenty-Seventh Symposium (International) on Combustion/The Combustion Institute, pp. 2925–2932

[9] **Joutsenoja, T., Heino P. and Hernberg R.** (1999). Pyrometric Temperature and Size Measurements of Burning Coal Particles in a Fluidized Bed Combustion Reactor, COM-BUSTION AND FLAME 118:707–717

[10] **Macek, A. and Bulik, C.** (1984). Direct measurement of char-particle temperatures in fluidized-bed combustors, Twentieth Symposium (International) on Combustion/The Combustion Institute, pp. 1223-1230

[11] **Idris, M. and Renz, U.** (2007). Two colour pyrometer technique for coal particle temperature measurements in pressurised pulverised coal flame, Journal of the Energy Institute Vol. 80 No. 4, pp.185-191

[12] **Fu, T., Yang Z., Wang L., Cheng X., Zhong M., Shi C.** (2010). Measurement performance of an optical CCD-based pyrometer system, Optics & Laser Technology Vol. 42, pp. 586–593

[13] **Maloney D. J., Monazam E. R., Woodruff S. D., Lawson L. O.** (1991). Measurements and Analysis of Temperature Histories and Size Changes for Single Carbon and Coal Particles During the Early Stages of Heating and Devolatilization, COMBUSTION AND FLAME 84:210-220

[14] **Khatami, R., Levendis, Y. A.** (2011). On the deduction of single coal particle com-bustion temperature from three-color optical pyrometry, Combustion and Flame

[15] **Frederick, W. J., Hupa, M., Stenberg J., Hernberg R.** (1989). Optical pyrometric measurements of surface temperatures during black liquor char burning and gasification, Fuel 1994 Vol. 73, No. 12

[16] **Joutsenoja, T., Sternberg J., Hernberg R., Aho, M.** (1997). Pyrometric measurement of the temperature and size of individual combusting fuel particles, Applied optics, Vol. 36, No. 7:1525-1535

[17] **Laurila, T. Oikari R., Joutsenoja T., Mikkola P., Ranki-Kilpinen T., Taskinen P., Hernberg R.** (2005). Pyrometric Temperature and Size Measurements of Chalcopyrite Particles during Flash Oxidation in a Laminar Flow Reactor, metallurgical and materials transactions Vol. 36B, pp:201-208, 2005

[18] **Hernberg, R., Sternberg J. and Zethreus B.** (1993). Simultaneous In Situ Measurement of Temperature and Size of Burning Char Particles in a Fluidized Bed Furnace by Means of Fiberoptic Pyrometry, Combustion and Flame Vol. 95, pp.191-205

[19] **Joutsenoja, T. and Hernberg, R.** (1998). Pyrometric sizing of high-temperature particles in flow reactors, Applied optics Vol. 37, No.16, pp.3487-3493

[20] **Heino, P., Hernberg, R. and Stenberg, J.** (1997). Statistical Pyrometric Sizing of Particles in Fluidised Bed Combustion, Combustion and flame 108:315-326

[21] **Müller, B. and Renz U**. (2001). Development of a fast fiber-optic two-color pyrometer for the temperature measurement of surfaces with varying emissivities, Review of scientific instruments, Vol.72, No.8, pp.3366-3374

[22] **Incropera F. P., DeWitt D. P., Bergman T. L., Lavine A. S.** (2007). Fundamentals of Heat and Mass Transfer, 6nd ed., John Wiley & Sons, New York

[23] **Modest M. F.** (2003). Radiative Heat Transfer, 2nd ed., Academic Press, USA

[24] **Url-1** *<http://www.thomasnet.com/articles/automation-electronics/electronic-microwave-manufacturing>*, date retrieved: 06.05.2012

[25] **Url-2** *<http://faculty.virginia.edu/consciousness/new_page_6.html>, date retrieved: 06.05.2012*

[26] **Url-3** *<http://www.omega.com/techref/iredtempmeasur.html>, date retrieved: 06.05.2012*

[27] **Wieland, M.** (2011). Aufbau und Entwicklung des Zwei-Farben Pyrometers. Semester Thesis, TU Munich

[28] **De Izarra, C. and Gitton, J.** (2010). Calibration and temperature profile of a tungsten filament lamp, Eur. J. Phys., Vol.31, pp.933–942

[29] **Kostkowski, H. J. and Lee, R. D.** (1962). Theory and methods of optical pyrometry, National bureau of standards Monograph 41

[30] **De Vos, J. C.** (1954). A New determination of emissivity of the tungsten ribbon, Physica Vol.20, pp.669-690

[31] **Larrabe, R. D.** (1959). Spectral Emissivity of Tungsten, Journal of the optical society of America, Vol.49, No.6

[32] **Ferronato, J. L., Bauer, B.** (2010). Pyrolysis investigation of solid fuels in a pressurized wire-mesh reactor. Diploma Thesis, TU Munich

APPENDICES

APPENDIX A: The emissivity of tungsten ribbon as a function of λ and T [22]
APPENDIX B : Comparison of the emissivity of tungsten at 2900 K, obtained by other investigators [22]
APPENDIX C : Comparison of the emissivity of tungsten at 2900 K, used by the standard laboratories [22]
APPENDIX D : The spectral emissivity of tungsten by Larrabee and DeVos [23]
Appendix E : Spectral emissivities of Tungsten for different temperatures provided by the NASA Astrophysics Data System

APPENDIX A

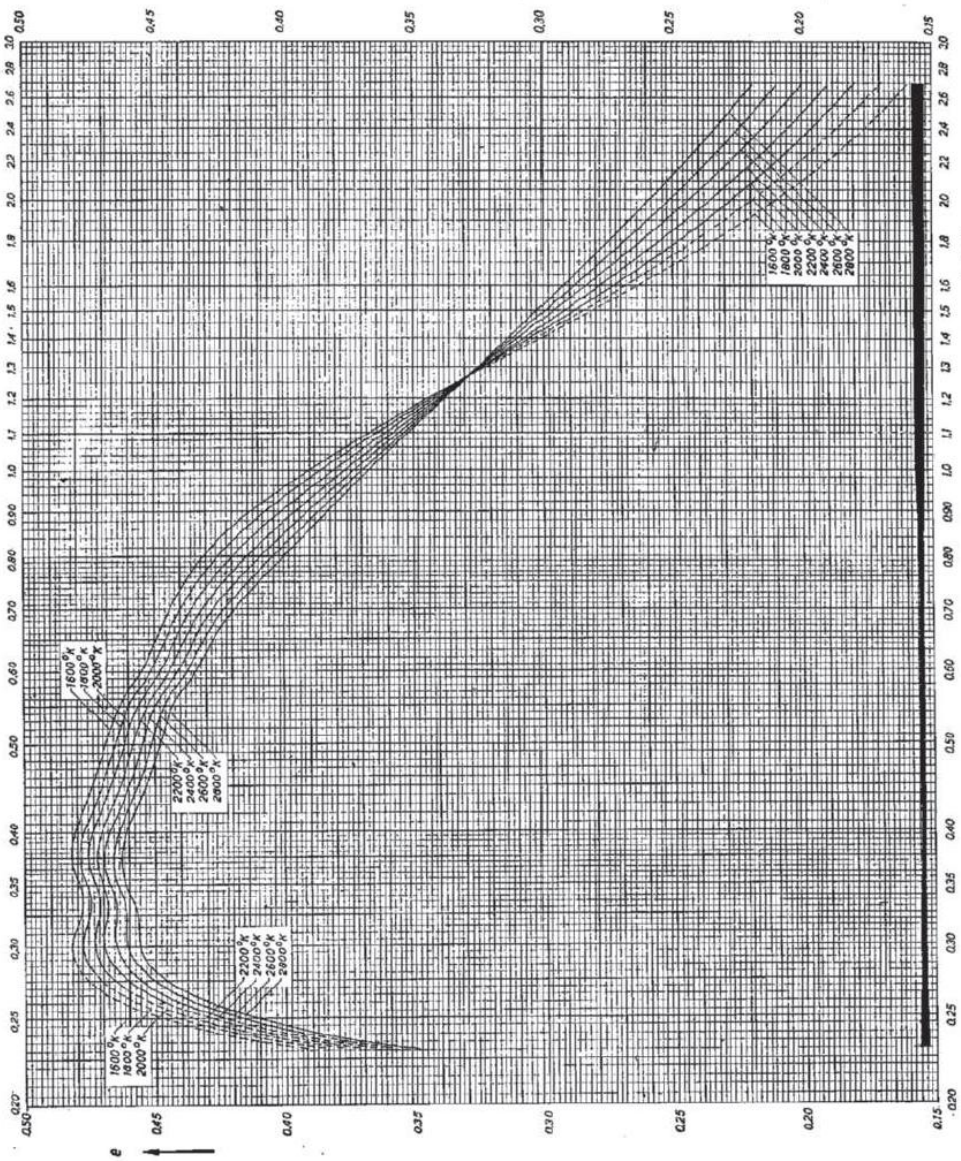

Fig. 6. The emissivity of well-defined tungsten ribbon as a function of wavelength at temperatures between 1600°K and 2800°K. The dotted parts of the curves are obtained by extrapolation. The accuracy attained in the measurements, is indicated by the line at the bottom of the figure. The width of this line is equal to the mean square error of the average of a set measurements.

APPENDIX B

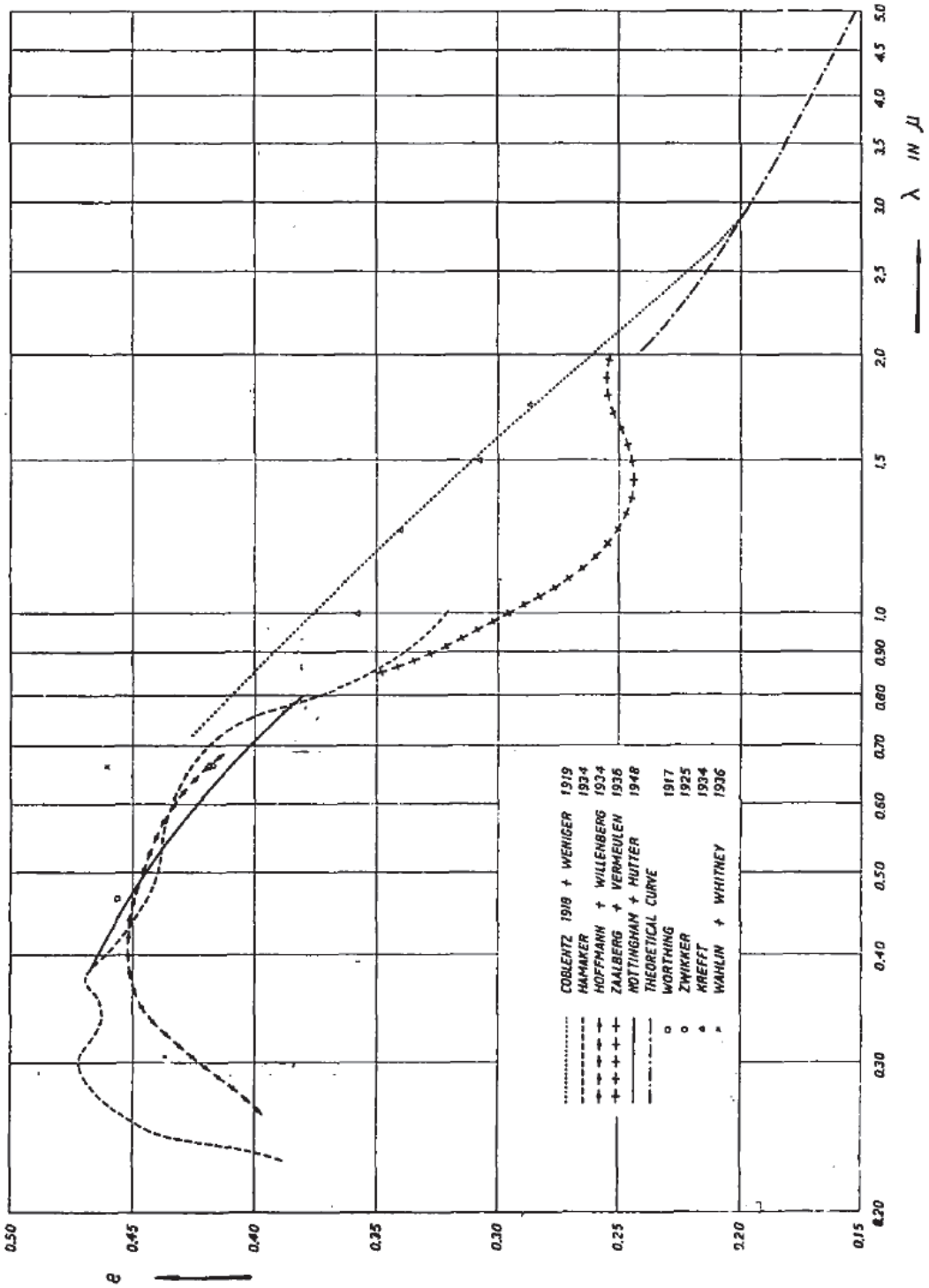
COBLENTZ 1919 + WENIGER 1919
HAMAKER 1934
HOFFMANN + WILLENBERG 1934
ZAALBERG + VERMEULEN 1936
NOTTINGHAM + HUTTER 1948
THEORETICAL CURVE
WORTHING 1917
ZWIKKER 1925
KREFFT 1934
WAHLIN + WHITNEY 1936
ε
λ IN μ
0.50
0.45
0.40
0.35
0.30
0.25
0.20
0.15
0.20
0.30
0.40
0.50
0.60
0.70
0.80
0.90
1.0
1.5
2.0
2.5
3.0
3.5
4.0
4.5
5.0

APPENDIX C

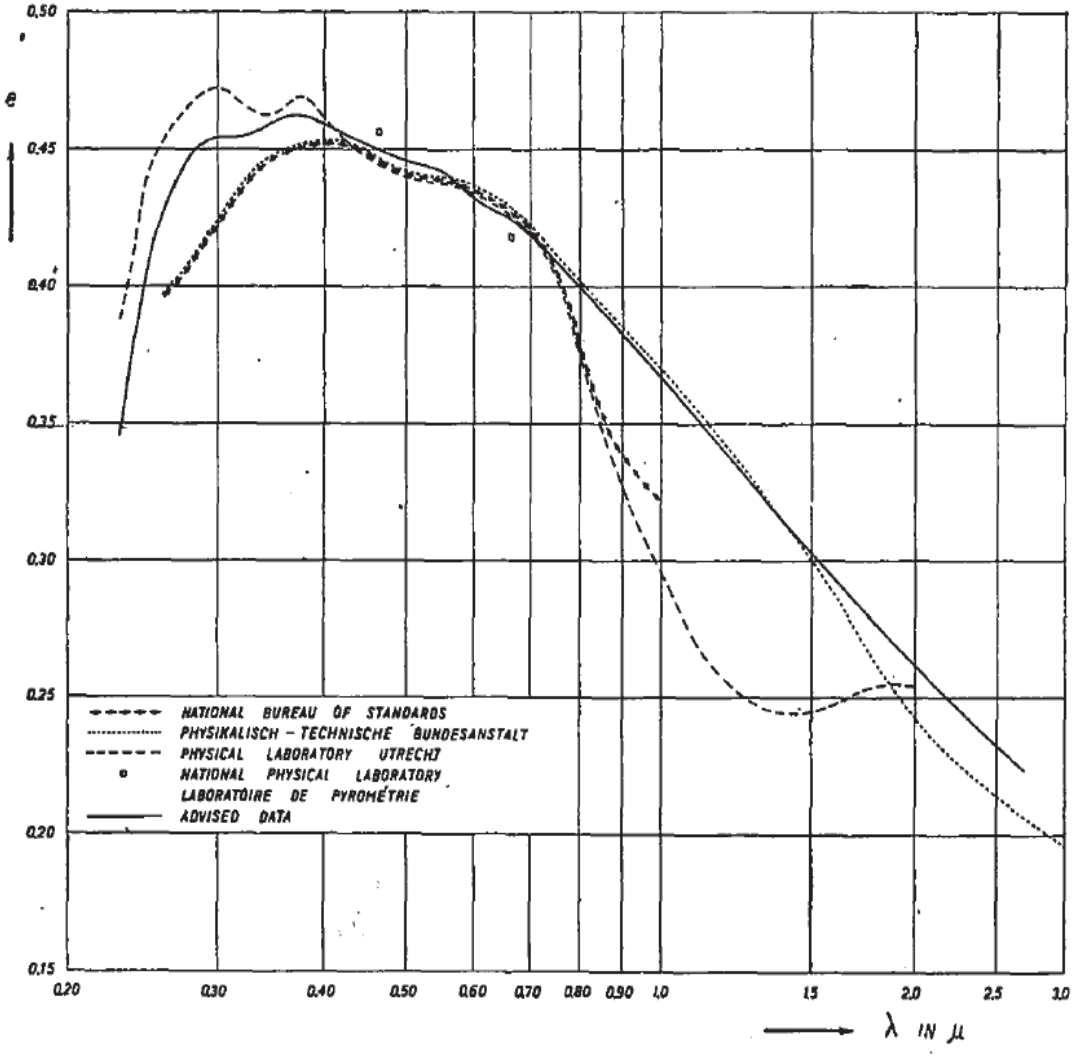
0.50
0.45
0.40
0.35
0.30
0.25
0.20
0.15
0.20
0.30
0.40
0.50
0.60
0.70
0.80
0.90
1.0
1.5
2.0
2.5
3.0
λ IN μ
NATIONAL BUREAU OF STANDARDS
PHYSIKALISCH – TECHNISCHE BUNDESANSTALT
PHYSICAL LABORATORY UTRECHT
NATIONAL PHYSICAL LABORATORY
LABORATOIRE DE PYROMÉTRIE
ADVISED DATA

APPENDIX D

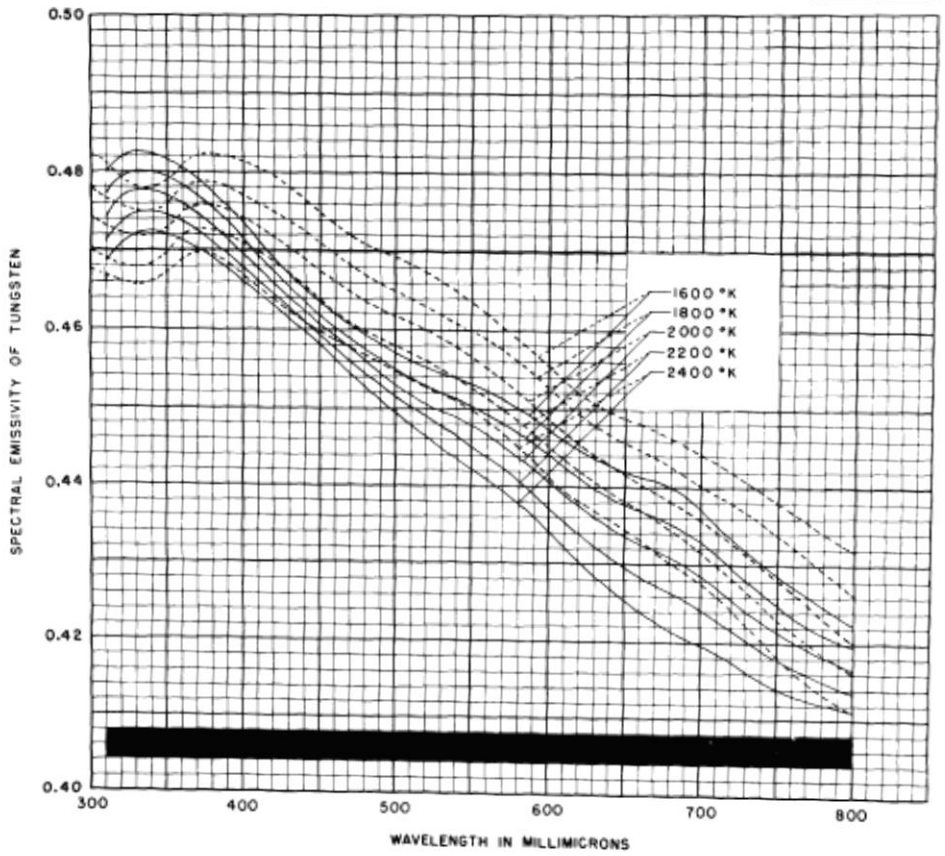

Fig. 31. The spectral emissivity of tungsten
— present experiment
-- J. C. De Vos, Physica 20, 690 (1954)

APPENDIX E

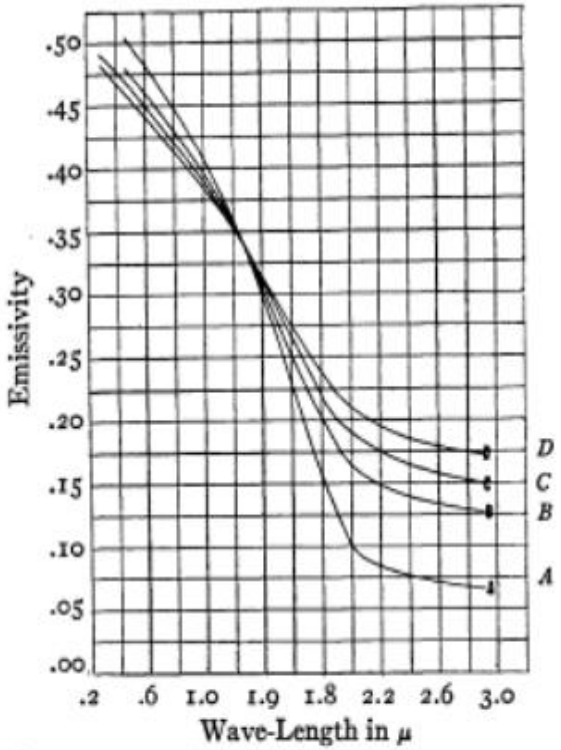

FIG. 3.—Spectral emissivities for different temperatures as a function of the wave-length over a wide range. Curve A, $T=300°$ K. Curve B, $T=1300°$ K. Curve C, $T=1700°$ K. Curve D, $T=2100°$ K.

CURRICULUM VITAE

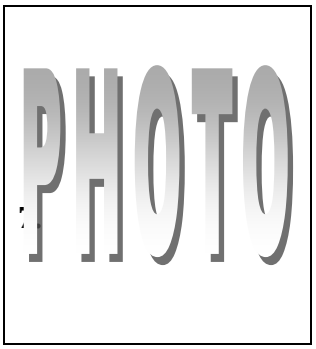

Name Surname:	Kaan Erdem
Place and Date of Birth:	Bandırma, 02.10.1988
Address:	Hükümet Cad. No:62/16 Erdek/Balıkesir
E-Mail:	kaanerdeme@gmail.com
B.Sc.:	Mechanical Engineering